UNIVERSITY OF SOUTHAMPTON

Repetitive Control for FES-based Tremor Suppression

by

Engin H. Copur

A thesis submitted in partial fulfillment for the
degree of Doctor of Philosophy
in the
Faculty of Physical Sciences and Engineering
Electronics and Computer Science

January 2017

UNIVERSITY OF SOUTHAMPTON

ABSTRACT

FACULTY OF PHYSICAL SCIENCES AND ENGINEERING
Electronics and Computer Science

Doctor of Philosophy

REPETITIVE CONTROL FOR FES-BASED TREMOR SUPPRESSION

by Engin H. Copur

Tremor is an involuntary, rhythmic movement of one or more body parts which prevents patients from performing activities of daily living (ADL), thereby greatly diminishing quality of life. Although there are various methods to suppress tremor, each is limited by either cost, ability to produce sufficient tremor suppression (TS) or interference with voluntary action. Functional electrical stimulation (FES) has attracted significant research attention as a novel approach for TS, and has substantial potential advantage in terms of cost, convenience and size. Results from previous studies have demonstrated that FES controlled by classical control methods is unable to produce satisfactory TS, while also producing intense interference with voluntary action. Thus their performance is inherently limited by the drawbacks of conventional feedback design.

Since repetitive control (RC) is able to reject a periodic disturbance completely and tremor can be regarded as a periodic disturbance, RC may have more potential for TS than other classical feedback control techniques. This thesis thus provides the first thorough implementation and assessment of RC for TS by means of FES in order to establish its feasibility and performance advantages compared to the conventional filter techniques (FT) that have so far been employed. Due to the importance of the wrist joint in ADL, wrist movement in flexion/extension is targeted within this programme of research. First, simulations are performed using a previously validated linear model of tremulous wrist dynamics to evaluate the feasibility of applying linear RC for TS, and results show that RC is able to produce complete tremor suppression but incurs a severe interference with voluntary action. Since this linear model does not account for the critical properties of the dynamics and RC requires a reliable knowledge of the plant dynamics to guarantee the stability of RC and improve its performance, this thesis then proposes a nonlinear model structure with an identification procedure that maintains the balance between the accuracy and the needs of the clinical domain. Then a linearising control approach is undertaken to enable linear RC design and a mechanism is proposed to preserve the voluntary action which is restricted by applying RC. Analysis confirms that the proposed mechanism can significantly reduce the undesirable interference of RC with voluntary action. Finally, two separate experimental studies are conducted using a test platform. The former is performed to fix the order of the model components in advance to reduce the computational effort of the identification procedure. The response of the wrist joint to FES signals applied to the flexion/extension muscles of each participant is collected. Using these input/output data sets, different models are identified for a number of different orders. Then the fitting accuracies of all models with the same order are averaged

and an order is selected with maintaining the balance between model accuracy and simplicity. The second experimental study is to confirm the higher potential of the proposed RC compared with FT for FES-based TS. A mechanical system is introduced to the existing test platform to induce tremor artificially since the participants are unimpaired. The participants are asked to complete three consecutive tests to examine the effect of induced tremor on the ability of patients to perform voluntary task, the capability of FES to suppress the induced tremor and the effect of FES on the voluntary motion.

The results indicate that the proposed RC approach with the developed model identification procedure can suppress tremor more effectively than FT and leads to a minimal interference with voluntary motion. This research therefore has established the feasibility of RC for TS by validating the model accuracy, the identification procedure, and the control performance. It has therefore potential for future exploration to provide more effective solutions for patients.

Contents

List of Figures

List of Tables

Declaration of Authorship

I, **Engin H. Copur**, declare that the thesis entitled

Repetitive Control for FES-based Tremor Suppression

and the work presented in the thesis are both my own, and have been generated by me as the result of my own original research.

I confirm that:

- this work was done wholly or mainly while in candidature for a research degree at this University;
- where any part of this thesis has previously been submitted for a degree or any other qualification at this University or any other institution, this has been clearly stated;
- where I have consulted the published work of others, this is always clearly attributed;
- where I have quoted from the work of others, the source is always given. With the exception of such quotations, this thesis is entirely my own work;
- I have acknowledged all main sources of help;
- where the thesis is based on work done by myself jointly with others, I have made clear exactly what was done by others and what I have contributed myself;
- parts of this work have been published as: (Copur et al., 2014), (Copur et al., 2015), (Copur et al., 2016a) and (Copur et al., 2016b).

Signed:.....

Date:.....

Acknowledgements

I would like to express my special appreciation and thanks to my supervisors Dr Bing Chu, Dr Chris Freeman and Dr Dina Shona Laila for their support, help and patience throughout my PhD. I could not have succeeded this challenging journey without their continuous guidance and immense knowledge. I am also deeply indebted to Prof. Dr. Metin Uymaz Salamci for his encouragement and help. Everything I learnt from him will always continue to light my way in my future career and my life. I would like to thank all of my friends who have greatly aided in my success, have given me good advice and have made every moment here memorable and enjoyable. Special thanks to my friends Ahmet Gelgec, Berak Genc, Halil Yetgin, Bunyamin Yildiz, Mehmet Emin Erendor, Mustafa Cagri Kutlu and Dr. Oliver Brend who helped me by participating in my experiments. I would also like to thank my beautiful girlfriend. She has been always there for me when I needed her no matter what, and she has always made me smile, even in tough times of my PhD. Finally, I would like to thank my family, especially my dad and mom, for always believing in me. All the support they have provided me over the years was the greatest gift anyone has ever given me. I owe all my success to them.

List of Symbols

L	Length of a set of frequencies
$M(\omega)$	Magnitude response of wrist model
N	Length of acquired data
f	Frequency in Hz
i	Square root of -1
s	Complex frequency variable
$\overline{y}$	Mean value of y
$\varphi_P(\omega)$	Phase response of the wrist model
ω	Frequency in rad

Gains and Parameters

K	State feedback gain
N_H	Finite length of ZPHP filter
N_p	Number of samples in a period of periodic disturbance
T_s	Sampling period
W_j	Weighting factor
a_1,a_2,...,a_{l_P}	Coefficients of $A_P(q)$
$a_1^\star$,$a_2^\star$,...,$a_{l_P}^\star$	Coefficients of the desired characteristic polynomial $\Upsilon(q)^\star$
b_0,b_1,...,b_{n_P}	Coefficients of $B_P(q)$
f_N	Nyquist frequency in Hz, $f_N = 0.5/T$
f_p	Frequency of a periodic signal in Hz
f_0,f_1,...,f_{2N_H}	Filter coefficients of ZPHP filter
$h_0, h_1, h_2, \ldots$	Markov parameter sequences of impulse response of $P(q)$
l_p	Number of poles order of $P(q)$
m_p	Number of time delay order of $P(q)$
n	Order of high-pass or band-pass filter
n_p	Number of zeros order of $P(q)$
$u_{c,fcr}$ and $u_{c,ecr}$	Levels of co-activation for the FCR and ECR
$\alpha - 1$	Order of the numerator of $F(q)$
$\alpha - \beta$	Order of the denominator of $F(q)$
γ	Positive scalar

$\hat{\theta}$	Parameter vector estimate
θ_d	Parameter vector of $d(k)$
θ_{a_P}	Linear parameter vector including the coefficients of $A_P(q)$
θ_{b_P}	Linear parameter vector including the coefficients of $B_P(q)$
θ_{l_P}	Linear parameter vector including the coefficients of $A_P(q)$ and $B_P(q)$
θ_n	Nonlinear parameter vector including the coefficients of $h_{IRC}(u)$
$\kappa_1, \kappa_2, \ldots, \kappa_n$	Coefficients of $F(q)$
$\mu_1, \ldots, \mu_{m-1}, \mu_m$	Coefficients of $h_{IRC}(u)$
ξ	Gain to adjust learning rate, $0 < \xi < 1$
σ	Positive gain to amplify stimulation input in FBC
ϕ	Parameter vector comprising of coefficients of $F(q)$
ω_c	Boundary frequency separating the regions of voluntary and involuntary frequencies

Matrices, Vectors, Sets and Spaces

$\mathbb{R}$	Real space
Z^N	Input/output data set
x	State vector of the state space format of $P(q)$
Θ	Output vector of the state space format of $P(q)$
Ξ	System matrix of the state space format of $P(q)$
Ψ	Input vector of the state space format of $P(q)$
$\mathbf{0}_{i\times j}$	Zero matrix of a dimension $i \times j$

Signals

$d(k)$	Tremulous motion of joint
$\tilde{d}(k)$	Abnormal muscle activation signal or disturbance signal
$\tilde{d}_{ecr}(k)$	Involuntary muscle torque to ECR muscle
$\tilde{d}_{fcr}(k)$	Involuntary muscle torque to FCR muscle
$e(k)$	Error signal, $e = y_{ref} - y$
$u(k)$	Control action
$u_{fcr}(k)$	FES signal of the FCR muscle
$u_{ecr}(k)$	FES signal of the ECR muscle
$w(k)$	Zero mean white noise
$v(k)$	Voluntary muscle activation signal
$y(k)$	Joint position
$y_{ref}(k)$	Reference signal
$\hat{y}(k\|k-1)$	One-step-ahead predicted output
$\hat{y}_s$	Simulated output of the identified model
$\varepsilon(k)$	Difference between measured and predicted outputs

$\nu(k)$	External disturbance
$\tau(k)$	Summed steady-state torque
$\tau_{fcr}(k)$ and $\tau_{ecr}(k)$	Output torques produced by FCR and ECR muscles
$\tau_{ss,fcr}(k)$ and $\tau_{ss,ecr}(k)$	Steady-state output torques produced by FCR and ECR muscles
$\tau_{ss}(k)$	Stedy-state output torque

Transfer Functions and Operators

$\|\cdot\|_\infty$	Infinity norm of a system
$\|\cdot\|_2$	2−norm of a system
$A_P(q)$	Denominator of $P(q)$
$B_P(q)$	Nominator of $P(q)$
$C(q)$	Compensator
$F(q)$	Finite impulse response filter
$F_B(q)$	Filter model
$F_H(q)$	Zero-phase high-pass (ZPHP) filter
$H(q)$	Linear transfer function of the RBD of the joint
$H_{LAD,fcr}(q)$	LAD for the FCR muscle
$H_{LAD,ecr}(q)$	LAD for the ECR muscle
$IM(q)$	Internal model
J	Cost function
J_1	Performance indicator to quantify voluntary distortion
J_2	Performance indicator to quantify tremor suppression
$P(q)$	Wrist model
$P^*(q)$, $P(q^{-1})$	Complex conjugate of $P(q)$
$S(q)$	Relationship from v to y and from $\tilde{d}$ to y
$h_{IRC}(u)$	Combined IRC
$h_{IRC,ecr}(u_{ecr})$	IRC of the ECR muscle
$h_{IRC,fcr}(u_{fcr})$	IRC of the FCR muscle
Δy_v	Measure to quantify voluntary distortion for $\omega \in [0, \omega_c]$
Δy_t	Measure to quantify tremor suppression for $\omega \in [\omega_c, 2\pi]$
$\Upsilon(q)_c$	Characteristic polynomial of the closed-loop system
$\Upsilon(q)^\star$	Desired characteristic polynomial

Ancronyms

ADL	Activities of daily living
ARX	Autoregressive Exogenous
BPF	Band-Pass Filter
CV	Cross-Validation
DBS	Deep Brain Stimulation
DC	Direct Current
DOF	Degree-of-freedom
ECR	Extensor Carpi Radialis
ED	Extensor Digitorum
EKF	Extended Kalman Filter
EMG	Electromyography
FBC	Filter Based Compensator
FCR	Flexor Carpi Radialis
FCU	Flexor Carpi Ulnaris
FES	Functional Electrical Signal
FIR	Finite Impulse Response
FL	Force-Length
FLC	Fuzzy Logic Control
FMI-RC	Frequency Modified Repetitive Control
FT	Filtering Technique
FV	Force-Velocity
GB-RC	Gradient Based Repetitive Control
HPF	High-Pass Filter
ILC	Iterative Learning Control
IMP	Internal Model Principle
IRC	Isometric Recruitment Curve
LAD	Linear Activation Dynamics
LTI	Linear Time- Invariant
MS	Multiple Sclerosis
MSIF	Multiple Sclerosis International Federation
NCC-CC	The National Collaborating Centre for Chronic Conditions
PD	Proportional-Derivative Controller

PI	Proportional-Integral Controller
PID	Proportional-Integral-Derivative Controller
PL	Palmaris Longus
PWM	Pulse Width Modulation
RBD	Rigid Body Dynamics
RC	Repetitive Control
RHP	Right Hand Plane
rTMS	Repetitive Transcranial Magnetic Stimulation
SISO	Single-input single output
ST	Stereotactic Thalamotomy
TMS	Transcranial Magnetic Stimulation
TS	Tremor Suppression
V	Validation
WHO	World Health Organization
ZPHP	Zero Phase High Pass

Chapter 1

Introduction

Tremor presents as a rhythmic, approximately periodic and involuntarily oscillation of a body part and manifests as a symptom of neurological disorders, occurring in over 50% of Multiple Sclerosis (MS) and 75% of Parkinson's disease cases. Intention tremor is frequently diagnosed within MS patients and occurs in the distal joints of the upper limb such as the wrist or fingers, and typically has a frequency between 2-5 Hz (Deuschl et al., 1998; Koch et al., 2007). In ballistic movements, it is caused by delayed activation of the antagonist muscle to decelerate the initial agonist movement, causing overshoot, followed by delay in the activation of the second agonist to correct movement, thereby causing over-correction. This leads to serious impairment of functional abilities which may contribute to social isolation and depression. Due to its prevalence and impact, suppression of tremor has been a popular research area for many years.

1.1 Research Motivation and Methodology

Invasive interventions to suppress tremor have inherent risks and are expensive (Schuurman et al., 2000; Yap et al., 2007; Hassan et al., 2012), while medication has not provided effective treatment (Heenan et al., 2014). Other non-pharmacological methods include tremor suppressing orthoses (Pledgie and Barner, 2000; Rocon et al., 2012), limb cooling (Feys et al., 2005), vibration therapy (Feys et al., 2006) and adding limb weights (Hawes et al., 2010). However they also give rise to significant difficulties and adverse effects. For example, slowness and fatigue in performing the task are inevitable outcomes of limb cooling due to the slowing down of nerve conduction and muscle spindle activity. Moreover, such methods also cause a decrease in maximum achievable voluntary forces. Adding weights to the body part also leads to faster muscle fatigue. Tremor suppressing orthoses are electromechanical systems comprised of actuators and sensors. The presence of these devices is extremely inconvenient when performing daily life activities, causing

fatigue, obstructing range of movement, and generating feelings of self-consciousness due to their large size. Hence this integration into patients' daily lives is challenging.

An alternative approach is to use functional electrical stimulation (FES) to suppress tremor. FES provides muscle contraction through artificial excitation of nerves. This contraction is triggered by low-level electrical impulses that are transmitted through surface electrodes placed in contact with the skin over the relevant muscles. This technique is generally applied in a closed-loop feedback arrangement where the electrical stimulation input stimulates muscles in anti-phase with respect to the tremulous motion. This stimulation input is manipulated by a controller in response to the measured output comprising the angular position of the relevant joint. Thus effective suppression depends strongly on how accurately the level and timing of FES applied to the appropriate muscles are regulated by the controller. However a highly effective control algorithm has not so far been proposed. All classical feedback systems have been found to cause undesirable distortion below 1 Hz which interferes with the patient's voluntary motion, as well as introducing large high-frequency stimulation transients which cause significant discomfort (Prochazka et al., 1992a). Additionally, they are incapable of producing complete tremor suppression.

To enforce complete tremor suppression necessitates embedding an internal model of the periodic disturbance within the control structure prior to ensuring closed-loop asymptotic stability (Francis and Wonham, 1975). This is the motivation behind a technique termed repetitive control (RC) which is hence the only approach capable of completely eliminating a general form of repetitive disturbance. Thus this study aims to develop a rigorous, general framework for implementing RC action for complete tremor suppression by means of FES. This framework includes a transparent control design procedure to suppress tremor, and a mechanism to preserve the patient's voluntary motion. Within this framework, a general class of RC is harnessed to eliminate distortion of voluntary intention at low frequencies and prevent FES from producing large high-frequency stimulation transients. Therefore the controller is guaranteed to not interfere with voluntary motion or cause discomfort.

The proposed control structure is applied to suppress tremor at the wrist via FES regulated co-contraction of wrist extensors/flexors. The wrist is targeted due to its importance in performing daily life activities and the stronger influence of intention tremor on distal joints than proximal joints. To demonstrate the ability of RC algorithms to suppress tremor, the simulation study is firstly performed and the results are bench-marked against a classical feedback control employing a filter to suppress tremor. Since RC requires a model of the underlying dynamics of the wrist joint, this study then provides a system identification procedure that is suitable for clinical application. This procedure eliminates the limitations of the existing methods and also enables a linear control design to be adopted to suppress tremor. Then experiments are carried out to validate

the simulation results. For experiments, ethical approval is obtained from the University of Southampton (ERGO Ref: 16530).

1.2 Contribution and Thesis Organisation

The main contributions of this thesis can be summarised as follows:

- A rigorous comparison between the proposed RC scheme and the existing filtering technique mentioned previously is performed to establish the feasibility of the RC scheme in tremor suppression (Chapter 3).
- A model of the tremulous wrist and accompanying identification procedure is proposed to address the significant limitations of existing methodologies (Chapter 4). These include model structures that (i) neglect critical features, and (ii) restrict the range of admissible control schemes, together with identification procedures that (iii) employ stimulation inputs that are uncomfortable for patients, (iv) are overly complex and time-consuming for clinical use, and (v) cannot be automated.
- A novel framework for implementing RC based FES tremor suppression is developed (Chapter 5). This framework includes a linearising procedure to enable linear tremor suppression control design, and a mechanism to preserve the patients voluntary motion. Performance properties are rigorously derived leading to a transparent design procedure.
- As the feasibility tests are conducted with unimpaired participants, it is necessary to induce tremor artificially at realistic frequencies. This is done by designing and introducing a mechanical activation system to an existing testing apparatus (Chapter 6). This is the first platform for simultaneously applying artificial tremor and quantifying the characteristics of wrist movement.
- Experimental results from a study with unimpaired participants confirm the efficacy of the proposed identification procedures, and show that high levels of accuracy can be achieved in a short identification time using test procedures that are suitable for future transference to the clinical domain. They also confirm that RC can suppress tremor more efficiently than conventional filtering techniques and the implementation of the mechanism leads to minimal interference of RC with voluntary motion. The latter shows that RC does not impair the functional activities of participants.

The following papers have been generated based on the above contributions:

- Copur, E. H., Freeman, C.T.and Chu, B., and Laila, D. (2014). Repetitive control based tremor suppression using electrical stimulation. In UKACC 10^{th} International Conference on Control, Loughborough, UK, pages 585-590.

- Copur, E. H., Freeman, C.T.and Chu, B., and Laila, D. (2015). FES based tremor suppression using repetitive control. In 54^{th} IEEE Conference on Decision and Control, Osaka, Japan, pages 6023-6028.

- Copur, E. H., Freeman, C. T., Chu, B. and Laila, D. S. (2016). System identification for FES-based tremor suppression. *European Journal of Control*, 27:45–59.

- Copur, E. H., Freeman, C. T., Chu, B. and Laila, D. S. (2016). Repetitive Control of Electrical Stimulation for Tremor Suppression. *IEEE Transactions on Control Systems Technology.* [Submitted in July 2016]

Chapter 2

An Overview of Tremor Suppression

Multiple sclerosis (MS) is an inflammatory demyelinating disease of the central nervous system (CNS) and is one of the most diagnosed neurological disorders (Nakahara et al., 2012). According to a study prepared by The National Collaborating Centre for Chronic Conditions (NCC-CC) in 2003, between 1,820 and 3,380 new people each year in England and Wales suffer from MS (NCC-CC, 2003). Another wide-ranging study published by the Multiple Sclerosis International Federation (MSIF) in 2013 provides an overview of MS on a global scale, including epidemiology, and the resources available for diagnosis and treatment. This states on the basis of data gathered from 92 countries that approximately 2 million people are diagnosed with MS, and its prevalence in Europe is 108 people per 100,000 (MSIF, 2013). According to these statistics, MS is one of the most prevalent disorders in the world. A common symptom of MS is tremor, which appears in between 25 and 60 percent of patients with MS (Koch et al., 2007; Mehanna and Jankovic, 2013). This means that worldwide 575,000 to 1,380,000 people with MS suffer from this movement disorder. This fact has meant research into tremor has received significant attention in the research community.

2.1 Types of Tremor

Tremor is a functional movement disorder that can be described as an involuntary, approximately rhythmic and roughly sinusoidal movement which may occur in any human body part (Elble and Koller, 1990). MS is not the only cause of tremor, and it can also be caused by the use of drugs, alcohol or neurological disorders such as stroke, traumatic brain injury or Parkinson's disease. Tremor can be generally subdivided into two major categories: i) physiological tremor, ii) pathological tremor. Physiological tremor can appear in every unimpaired human being without any clinical manifestations. A shaking body due to a fever or cold is an example of physiological tremor. On the other

hand, pathological tremors are usually caused by neurological diseases. However the mechanisms underlying physiological tremor and pathological tremor are similar.

There are four physiological basic mechanisms underlying tremor. These mechanisms can be regarded as: i) mechanical factors, ii) reflex oscillations, iii) central oscillations, iv) oscillations from distorted feedforward loops. To discuss the effects of mechanical factors on tremor, a limb can be simply considered as a mass-spring system with a natural frequency of $\frac{1}{2\pi}\sqrt{K/J}$ where K and J are the stiffness and inertia of the limb, respectively. Any change in these properties produces a shift in the natural frequency. Therefore, pre-existing oscillations in a limb, like breathing-induced oscillations, may cause to induce a shaking movement of a limb at its natural frequency. Oscillatory reflex loops may also cause tremulous motion, and are produced when there are inherent delays in the feedback from muscles. This loop resembles a servo mechanism oscillating at a particular frequency related to the delay. The third mechanism is the central oscillation in which tremor is generated by the abnormal rhythmic activation of a group of neurons in a nucleus or neural circuits between different nuclei or different populations of neurons (Dewey, 2013). One example of tremor arising from central oscillation is essential tremor whose origin is unknown (Deuschl et al., 1998). It is defined as a bilateral, largely symmetric tremor of the hands and forearms (Zeuner and Deuschl, 2012). The last mechanism causing tremor is a malfunction of feedforward loops within the CNS, especially the cerebellum. This mechanism usually causes intention tremor, a symptom of MS. Due to the frequent diagnosis of MS mentioned previously, intention tremor is one of the most widely diagnosed tremor types. Thus, this study focuses specifically on suppressing intention tremor.

2.1.1 Intention tremor

In ballistic movements intention tremor is caused by delayed activation of the antagonist muscle to decelerate the initial agonist movement, causing overshoot, followed by delay in the activation of the second agonist to correct movement, thereby causing over-correction. Intention tremor usually manifests itself in the upper limb joints (Bain, 2002; Koch et al., 2007) as an involuntary rhythmic 2-5 Hz oscillation (Deuschl et al., 1998; Elble and Koller, 1990). Its dramatic effect increases visibly when the patient wants to perform a voluntary motion, as its amplitude increases when approaching the target (Alusi et al., 2001). Therefore patients have difficulty in performing an intended movement, such as writing, pressing a button, turning a key or reaching for an object. These challenges in performing daily life activities may hence lead to embarrassment and even social isolation. Tremor can hence significantly degrade the patient's quality of life (Koch et al., 2007; Zhang et al., 2011). Due to its prevalence and impact, tremor has become a very popular research area, with a primary focus on effective methods to suppress

tremor. These methods can be separated into invasive and non-invasive approaches, as discussed next.

2.2 Invasive Methods for Intention Tremor Suppression

There are two main invasive methods: the first is stereotactic thalamotomy (ST) and the second is deep brain stimulation (DBS). ST for relief of tremor in MS patients was first reported by Cooper (1960), in which it was proposed that the intention tremor could be relieved by a surgical lesion placed in the ventrolateral nucleus of the thalamus (Samra et al., 1970). This neurosurgical technique for the treatment of intention tremor was used for over 30 years, but unfortunately there was little consensus among researchers about its success because of the variable healing rate (Matsumoto et al., 2001). Because of the uncertain results of ST, researchers sought another effective surgical treatment, and recently significant interest has focused on DBS. The first studies to reduce tremor using DBS date back to the 1960s, and DBS has been used for the treatment of several types of tremor since 1987 (Kringelbach et al., 2007). With DBS, a pulse generator, referred to as brain pacemaker, is implanted to send electrical impulses through electrodes implanted into a specific part of the brain, as shown in Figure 2.1. This electrical impulses block the neural signals which cause tremor. For the suppression of intention tremor, this specific area, termed the 'target', is usually the lateral thalamus (Vim nucleus) (Deuschl et al., 2009).

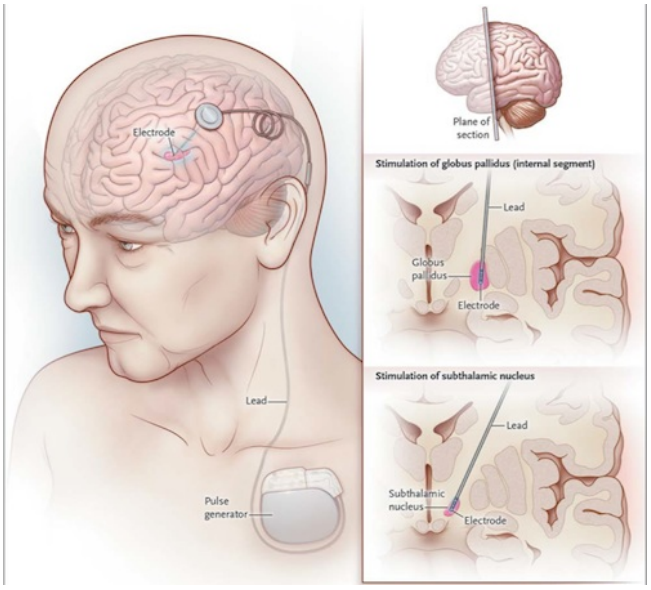

Figure 2.1: Schematic representation of electrode placement in DBS. This illustration is taken from Mckelvey (2014).

Although these two surgical therapies are widely used, there is no universal agreement on which method is more effective than the other in terms of risk and benefit ratios

(Schuurman et al., 2000; Yap et al., 2007). Furthermore, many adverse effects are reported after surgery and during long-term follow-up observations. These complications include confusion, a prickling or burning sensation of skin and ataxia, termed as a group of disorders affecting speech, co-ordination or balance. Additionally, these adverse effects may be permanent or sporadic (Hassan et al., 2012; Schuurman et al., 2000; Tasker, 1998; Yap et al., 2007). Another problem is the cost of these surgeries. According to a report in 1999, patients had to pay between £6,740 and £11,000 for ST, and £12,740 to £14,450 for DBS (Nicholson and Milne, 1999). In spite of these disadvantages, research into invasive methods is still in progress.

2.3 Non-invasive Methods for Intention Tremor Suppression

Non-invasive methods are used as widely as invasive methods. In general, invasive methods are prescribed for patients who do not respond well to non-invasive methods and are suitable for the surgical procedures involved. Non-invasive treatments can be classified into two categories, according to whether drugs are used.

2.3.1 Pharmacological Treatment

The first category comprises pharmacological treatment that involves medication only. In discussing this area, it is important to note that the drugs used in the treatment of essential tremor also address intention tremor; but that the resulting clinical outcomes can vary from patient to patient after the drug use (Elble, 2009). Toparimate (Sechi et al., 2003), isoniazid in combination with pyridoxine (Hallett et al., 1985) and carbamazepine (Sechi et al., 1989) are leading examples of drugs which are used to treat intention tremor. In particular, 4-aminopyridine (Schniepp et al., 2012), primidone (Naderi et al., 2012) and levetiracetam (Feys et al., 2009) have also been investigated to determine their efficacy. However none of these pharmacotherapeutic strategies can provide effective treatment for intention tremor or essential tremor.

2.3.2 Non-pharmacological Treatment

The second category of non-invasive treatment is termed non-pharmacological treatment, and covers several different methods. In 2011, a literature search was performed to define the primary research studies focusing on non-pharmacological treatments (O'Connor and Kini, 2011). Within this study, 460 articles were investigated and 19 articles were selected based on a combination of keywords and a publishing date prior to November 2010. Using these results, different non-pharmacological treatments were defined, which can

be categorized as tremor-suppressing orthoses, physical therapy, limb cooling, functional electrical stimulation, vibration therapy, limb weights and transcranial magnetic stimulation. However no studies employing physical therapy for the treatment of intention tremor could be found, although there were some studies which evaluated the effect of physical therapy on multiple sclerosis patients with ataxia, which is also a symptom of intention dysfunction (Armutlu et al., 2001; Jones et al., 1996). For this reason, physical therapy was removed from the list of non-pharmacological treatment methods.

2.3.2.1 Limb Cooling

The method of limb cooling was used in (Feys et al., 2005) and its aim was to examine the effect of peripheral sustained cooling on intention tremor. This method is based on cooling the limb of patients using a cooling pad wrapped around the forearm for a specified duration with a cooling fluid circulated through the cooling pad by an electromechanical device, as shown in Figure 2.2.

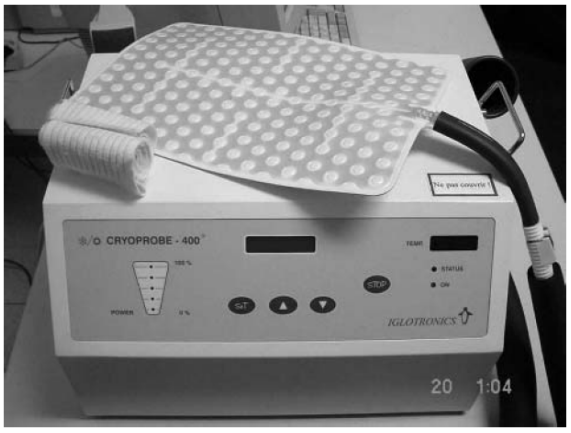

Figure 2.2: The cooling device and pad. This illustration is taken from Feys et al. (2009).

In (Feys et al., 2005), the cooling proceeded until the skin temperature reduced to 18°C or 25°C to examine the effects of the cooling intensity on tremor suppression and voluntary action. Then patients with intention tremor performed a finger tapping test and a wrist step tracking test. During each test, physiological variables such as skin temperature at the wrist and elbow, heart rate and body temperature were acquired before and up to 30 minutes after cooling with time intervals of 10 minutes. The results showed that cooling was able to suppress tremor but this effect was temporary and also caused a decrease in the nerve conduction velocity and muscle spindle activity. Moreover, it also caused changes in muscle properties, leading to a decrease in maximum voluntary muscle forces if the arm was cooled deeply. Therefore cooling impaired the voluntary actions of patients.

2.3.2.2 Vibration Therapy

A further method is to apply vibration to the wrist extensor muscle of MS patients with intention tremor by means of a cylindrical tendon vibrator. This was studied in (Feys et al., 2006), and the patients taking part were asked to perform a step-tracking task using a motion tracking device. The accuracy of the tracking task was used to determine whether or not the tendon vibration was effective in reducing the amplitude of tremor. The results of the tests showed that the amplitude of the tremor was able to be decreased by 28%. However the results of Feys et al. (2006) were later interpreted by O'Connor and Kini (2011) who stated that the patient experiences of the method were not explored, nor was there any information about whether this method was applicable to clinical situations.

2.3.2.3 Transcranial Magnetic Stimulation

One additional method with which to suppress tremor was the use of repetitive transcranial magnetic stimulation (rTMS). In this technique, a stimulation coil is positioned on the patient's scalp and generates electrical current in specific regions of brain by means of magnetic induction (Chalah et al., 2015). Its application is illustrated in Figure 2.3. It

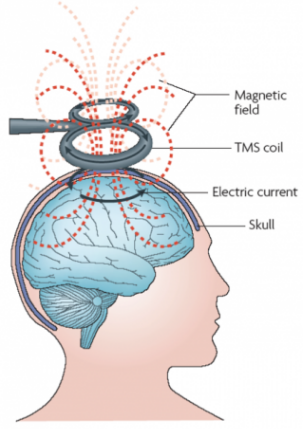

Figure 2.3: Schematic representation of the application of rTMS. This illustration is taken from Archer (2014).

has been developed for stimulating the motor cortex, recording motor evoked potentials from peripheral muscles, or for modulating the excitability of other non-motor areas in order to establish their necessity for a given task (Oliveri et al., 2007). This method was also used to induce an intention tremor in healthy people artificially and then the data from experiments were used to simulate intention tremor for modelling purposes (Topka et al., 1999). Additionally, rTMS has recently attracted attention as a recent non-invasive method for the treatment of tremor. The use of rTMS for tremor suppression was investigated in Rogasch and Todd (2013). However, Chalah et al. (2015) stated

that only preliminary data were available for rTMS techniques and its performance has therefore not yet been confirmed.

2.3.2.4 Biomechanical Loading

Another method comprises biomechanical loading, in which the stiffness, damping and mass properties of the upper limb are altered using mechanical components (Rocon et al., 2006). This method is hence an application of passive control techniques for tremor suppression. For example, one type of biomechanical loading takes the form of adding weights to the distal upper extremity. In 2010, an experimental study was conducted with 6 patients with MS suffering from intention tremor (Hawes et al., 2010). To investigate the effect of this treatment on tremor suppression, a stepwise system was created which included techniques such as the hand-over-hand technique, the weighted wrist, and the weighted tool, splint or coupling. These are illustrated in Figure 2.4.

The participants were asked to test these techniques during the activities of handwriting and eating finger food. In the hand-over-hand technique, the participants tried to use

Figure 2.4: The biomechanical loading techniques investigated in Hawes et al. (2010). (a) hand-over-hand technique, (b) weighted wrist, (c) weighted tool with a commercially available 1/2-lb weighted pencil, (d) weighted tool with a 1/4-lb soft weighted pen wrap, (e) splint and (f) coupling. The figures are taken from Hawes et al. (2010).

their unaffected hand to support the other hand, for instance, while they were writing something using their affected hand. In the weighted wrist technique, participants wore wrist straps attached with weights ranging from 1/2 to 2 lbs on their dominant arm. According to the observations of participants, the most helpful technique was the hand-over-hand technique. However, the authors of this study stated that the number of participants was insufficient to make general conclusions about the efficacy of this form of occupational treatment. In addition, there were limitations to the study due to an unpredictable bias of the patient and participant baseline data. Therefore, this method cannot be considered to be a suitable treatment method for intention tremor.

2.3.2.5 Tremor-suppressing Orthoses

Rehabilitation robotics are electro-mechanical systems that have gained widespread acceptance as an effective treatment for patients suffering from motor impairments. In the case of tremor, the operation of the robot is based on actuators generating the opposite dynamic forces to the tremulous motion. Such robotic systems have existed from the early 1980s (Adelstein, 1981; Feys et al., 2006). A type of rehabilitation robotics which is widely used to reduce tremor is the exoskeleton design. This is a mechatronic system as shown in Figure 2.5.

Some exoskeletons are commercially available. These robotic systems can be categorized into the following three types according to Rocon et al. (2012): 1) non-ambulatory, 2) wheelchair-mounted and 3) ambulatory-oriented. All of these systems consist of actuators, control architecture and sensors to measure position, velocity, acceleration and force. In (Pledgie and Barner, 2000), a non-ambulatory system was implemented by means of a

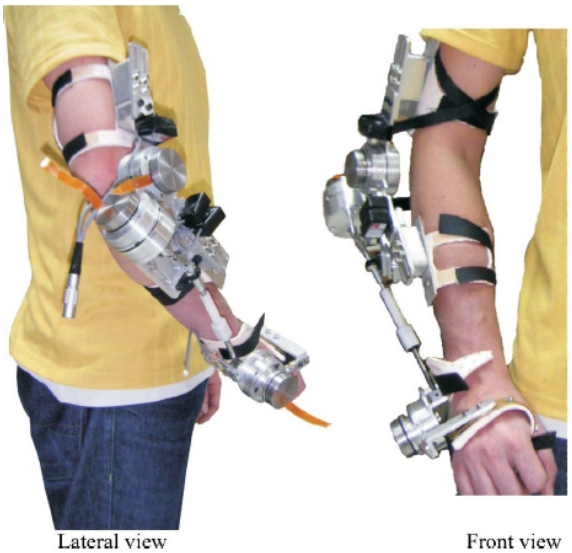

Figure 2.5: A exoskeleton design for tremor suppression. The figure is taken from Rocon et al. (2007).

second-order negative feedback system designed with two different sets of feedback coefficients to produce -10 dB and -20 dB attenuation at the tremor frequency. Measurements were taken from 5 subjects who had different tremor severity, but only in one case was the desired attenuation able to be obtained. Moreover, the human-machine system was assumed to adequately be represented by a second-order linear model; but the authors stated that to achieve the desired attenuation at the tremor frequency, a more accurate human-machine model may have been required. This is because a second-order linear model cannot represent a combination of biological and mechatronic systems with close accuracy. On the other hand, the ambulatory-oriented system employs a different structural design from the non-ambulatory system even though both of them can use the same actuation or sensing mechanism. An ambulatory-oriented system can also be described as a wearable orthosis; because patients wear these devices on their affected limbs. By means of this feature, which does not exist in other systems, the ambulatory-oriented system gives patients with tremor great mobility. In reality, all these systems are able to suppress tremor significantly (Manto et al., 2007; Pledgie and Barner, 2000; Rocon et al., 2012); but their integration into patients' daily life is very difficult. This is because the presence of actuators and sensors on their affected limb is extremely inconvenient when performing daily life activities, causing fatigue, obstructing range of movement, and generating feelings of self-consciousness due to their large size.

2.4 Functional Electrical Stimulation

An alternative non-pharmological method to those mentioned above is functional electrical stimulation (FES), an approach developed in the early 1960s (Liberson et al., 1961; Long and Masciarelli, 1963; Vodovnik et al., 1965) and used to suppress tremor since the 1990s. FES provides muscle contraction through artificial excitation of nerves. This contraction is triggered by low-level electrical impulses that are transmitted through electrodes. These conductors can be placed on the skin surface or into muscles or on the muscle's surface or wrapped around the nerve stimulating the relevant muscle (Lynch and Popovic, 2008). To suppress tremor, this technique is generally applied in a closed-loop feedback arrangement where the electrical impulses stimulates muscles in anti-phase with respect to the tremulous motion. However effective tremor suppression depends strongly on how accurately the level and timing of FES applied to the appropriate muscles is regulated by the controller.

The early studies on designing an effective controller for FES based tremor suppression date back to the 1990s. In 1992, two different filters were implemented in the feedback path of the closed-loop system and used to suppress tremor at the wrist or elbow joint. These filters were designed using simulations of the closed-loop system which employed a model of the relevant limb dynamics. The design requirement was that the system had a maximum gain in the range of 2 - 5 Hz to suppress tremor and had a minimum gain with

a minimum phase lag in the 0 - 1 Hz range to preserve the voluntary action of patients (Prochazka et al., 1992a,b). Then this control structure was applied to three different groups comprising essential, Parkinsonian and intention tremor associated with MS. The results showed that the three types of tremor could be reduced by 73%, 62% and 38%, respectively (Prochazka et al., 1992b). The authors stated that this technique had two definite advantages: 1) no need of mechanical loading causing muscle fatigue and 2) no need of electromechanical devices like the one used in orthoses. However, Prochazka et al. (1992a) reported that it was fairly difficult to maintain the balance between performance and stability. Furthermore, the model used to design the filters was not identified for each patient individually, resulting in poor control performance, particularly in intention tremor. Additionally, these filters were analog and this type of filter may be difficult to implement using hardware. For this reason, another study was made in 1999 to resolve the aformentioned issue (Gillard et al., 1999). In this experimental study, digital filters were used instead of analog filters to suppress Parkinsonian tremor. The experiments were performed with three patients with Parkinsonian tremor. The authors found that the digital system gave better results than the analog system in terms of amount of tremor attenuation. A mean tremor attenuation of 61% was obtained using the analog system, and a mean attenuation of 85% was obtained in the digital system. However the digital filters were designed using the limb model derived by Prochazka et al. (1992a) instead of individually obtaining a model for each patient. Thus the reliability of the results significantly decreased.

In 2006, a 1-DOF dynamical model of the elbow joint was developed comprising a pair of antagonist muscles and a skeleton segment (Zhang and Ang, 2006). Unlike the previous studies described above, a different type of controller combining a fuzzy logic control (FLC) using a logical system to manipulate the control input, a compensator and a PD controller was used to tune the electrical pulses generated by the functional electrical stimulator in (Zhang and Ang, 2006). FLC was used to regulate the electrical pulses of the stimulation and was considered as the primary controller, while the others were supportive controllers. The aim of the use of a compensator was to reduce the effect of control effort on the voluntary motion as the PD controller was employed to stabilize the control process and enhance the control performance. Here, the compensator consisted of two gains multiplied by the output of FLC. The simulation results of this study showed that the pathological tremor could be reduced by 85%. However, these results were only based on simulations and no experimental studies were performed to support these simulation results.

Another study used an artificial neural oscillator as an adaptive feedforward controller to regulate the electrical impulses generated by FES (Zhang et al., 2011). The neural oscillator was combined with a feedback controller, in this case, a PD controller, to reduce the effect of unexpected disturbances, i.e. noise from imperfect sensors, because the neural oscillator is sensitive to such disturbances. Using simulations, it could be seen

clearly that the tremor could be attenuated significantly. The average tremor suppression was indicated to be around 90% in this study. However the simulation results have not been confirmed experimentally.

Another control strategy is based on the modification of joint stiffness using FES controlled by a PI controller with anti-windup, which is used to deal with actuator saturation limiting control inputs (Bo et al., 2011a). In this study, an online tremor estimation algorithm was first used to separate the tremor signal from the voluntary motion signals and then the signals of voluntary motion were filtered. Finally, using the information extracted from tremor, the FES was tuned to attenuate the tremor. This control strategy was also tested on 4 healthy subjects and 1 tremor patient. The experimental results showed that the amplitude of the tremor could be reduced, but its level of suppression was not as significant as that of the previous studies mentioned here.

In addition to the aforementioned drawbacks, classical feedback approaches have well-known performance limitations, including a decrease in robust stability margins as suppression increases over the required frequency range, together with an increase in undesirable low frequency distortion. These characteristics explain the limited ability of previous closed-loop FES controllers to suppress higher frequencies (Bo et al., 2011a). The difficulty in designing a stable feedback system with sufficient suppression is highlighted in (Prochazka et al., 1992a), together with the tendency of the feedback system to produce large high-frequency stimulation transients which cause significant discomfort to patients. Additionally, these classical approaches are never able to produce complete tremor suppression.

In control theory, the internal model principle (IMP) states that a model of the reference or disturbance system must be included in the controller to ensure either perfect reference tracking or complete disturbance rejection in a stable feedback system. For example, to track an unit step reference input with zero steady-state error, the controller must include a model of the unit step function, i.e. $1/s$ where s is complex frequency variable. This equates to integral control action with an integral gain of 1. Thus an alternative control methodology is repetitive control (RC) since it is based on the IMP. The first RC applications were studied in 1981 by Inoue et al. (1981b,a), and this control technique has been examined both theoretically and experimentally in wide-ranging studies for many years (Inoue et al., 1981b; Hara et al., 1985; Tomizuka et al., 1989; Van den Eerenbeemt, 2003; Kalyanam and Tsao, 2012; Wang et al., 2012; Houtzager et al., 2013). The first study on RC design for tremor suppression was proposed by Verstappen et al. (2012) but it was not compared with a classical feedback control design such as filter-based methods mentioned above and there was no examination of whether RC interfered with voluntary effort. Because of its success in rejecting periodic disturbances, the RC controller structure may be used to suppress tremor whilst avoiding limitations associated with classical techniques. However RC requires a model of the underlying limb dynamics and a large

amount of uncertainty in the model makes it difficult or impossible to guarantee stability of the RC system.

2.5 Summary

According to the studies reviewed in this section, FES has strong potential for suppressing tremor: it does not have any side effects like drugs, and is not expensive and invasive like surgical treatment. Furthermore, the usage of FES does not make life difficult for patients unlike rehabilitation robots. Despite all the advantages of FES, its potential has not been realised. A review of the literature has established several studies investigating classical feedback control for FES based tremor suppression which reveal that all classical feedback systems cause undesirable interference with the patient's voluntary motion, as well as introducing large high-frequency stimulation transients which cause significant discomfort. To evaluate the inherent limitations of classical feedback systems and confirm the ability of RC to address these drawbacks, a number of simulation studies will be performed in Chapter 3.

Chapter 3

A Comparison of Conventional Filtering and Repetitive Control

The aim of this chapter is to undertake a rigorous comparison of existing filter based tremor suppression technique with RC in order to establish the potential of RC. This chapter begins by introducing a general closed-loop FES system suitable for tremor suppression. Next, the required specifications of closed-loop characteristics to suppress tremor will be introduced and two measures will be described to quantify if the closed-loop characteristics satisfy these requirements. Then a conventional filtering method previously used in this control structure will be introduced. Simulations will be performed to investigate its efficacy and limitations which will be evaluated using the defined measures. To address these limitations, the RC framework will be proposed and to establish the feasibility of RC for tremor suppression, it will be lastly compared against the conventional filtering technique using the same key performance indicators.

3.1 Tremor Suppression Using Feedback Control

As previously addressed, filtering methods have been the predominant focus of research on suppression of tremor (Liu et al., 2011), estimation of tremor frequency and amplitude (Riviere et al., 1997; Bo et al., 2011b), or removal of tremor signals from measurements (Zhang et al., 2009; Mellano et al., 2011) since the 1990s. In the study conducted by Liu et al. (2011), an adaptive filter was proposed to suppress physiological tremor in the hand by means of a motor-driven system in order to improve the positional accuracy in robot-assisted microsurgery. A filtering method to suppress pathological tremor by means of FES was first demonstrated experimentally by Prochazka et al. (1992a) and Prochazka et al. (1992b). They built the first reliable linear model representing tremulous limb dynamics combined with electrical stimulation of relevant muscles. The authors then used it to design effective filters to suppress tremor within a closed-loop feedback

system. The results of experiments with a dozen patients proved that the filters achieved a reduction of between 38% and 68% in amplitude of the intention tremor. Because of these findings, Prochazka et al. (1992a) and Prochazka et al. (1992b) are without doubt the leading studies in the field of FES based tremor suppression. For this reason, a comparison of RC with the filtering technique proposed by Prochazka et al. (1992a) and Prochazka et al. (1992b) has been chosen on the basis to establish the feasibility of RC for tremor suppression. Due to its reliability and simplicity for simulation, the model proposed by Prochazka et al. (1992a) will be used in the simulations conducted throughout this chapter.

The closed-loop system employed in Prochazka et al. (1992a) is next described and generalised to enable it to also be used within an RC framework.

3.1.1 Feedback Control Structure

Neural signals causing intention tremor are usually generated by the brain and then transmitted to muscles by the central nervous system. Since it is impossible to eliminate these abnormal signals driving tremor through this transmission, an appropriate compensator should be embedded in the feedback path of a control architecture to suppress tremor. This can be achieved by the basic feedback structure shown in Figure 3.1. This closed-loop system includes a model of limb dynamics $P(q)$, mapping the muscle activation signal to the angular position $y(k)$. Here the muscle activation is due to both tremor and voluntary activation. The problem considered here is to manipulate control action $u(k)$ using a compensator $C(q)$ to suppress tremor in response to abnormal muscle activation $\tilde{d}(k)$ while preserving the natural wrist response to voluntary muscle activation $v(k)$.

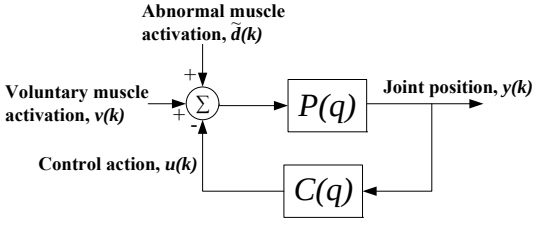

Figure 3.1: Block diagram of closed-loop system with compensator.

3.1.2 Specification of Closed-Loop Characteristics

As mentioned in Chapter 2, intention tremor occurs at a frequency range between 2-5 Hz (Deuschl et al., 1998; Koch et al., 2007; Elble, 2009) and studies have shown that the activities of daily living (ADL) are usually generated at a frequency below 1 Hz (Mann et al., 1989; Stiles and Hahs, 1991). Hence, compensator $C(q)$ should be designed to

suppress tremor in the frequency range of 2 to 5 Hz while preserving voluntary action of the targeted limb below 1 Hz.

Without loss of generality, let the sampling period be $T_s = 1$. With $q = e^{j\omega}$, the relationships from v to y and from $\tilde{d}$ to y can both be expressed in the frequency domain by

$$S(e^{j\omega}) = P(e^{j\omega}) \left(1 + P(e^{j\omega})C(e^{j\omega})\right)^{-1}. \tag{3.1}$$

Now suppose ω_c denotes the boundary frequency separating the regions of the voluntary and involuntary frequencies. In line with the aforementioned purpose, the closed-loop system must satisfy:

$$\left|S(e^{j\omega})\right| = \left|P(e^{j\omega})\right| \text{ and } \angle S(e^{j\omega}) = \angle P(e^{j\omega}) \; ; \; \forall \omega \in [0, \omega_c] \tag{3.2}$$

in order to preserve voluntary action below 1 Hz. Similarly, in order to suppress the involuntary frequency region between 2 and 5 Hz, it must satisfy

$$\left|S(e^{j\omega})\right| = 0 \; ; \; \forall \omega \geq \omega_c. \tag{3.3}$$

To satisfy (3.2) and (3.3), $C(e^{j\omega})$ must, respectively, hold the following response characteristics

$$\left|C(e^{j\omega})\right| = 0 \text{ and } \angle C(e^{j\omega}) = 0 \; ; \; \forall \omega \in [0, \omega_c] \, , \tag{3.4}$$

and

$$\left|C(e^{j\omega})\right| = \infty \; ; \; \forall \omega \geq \omega_c \tag{3.5}$$

Assuming that (3.2) and (3.3) are approximately satisfied, the desired frequency response of closed-loop system is schematically depicted in Figure 3.2.

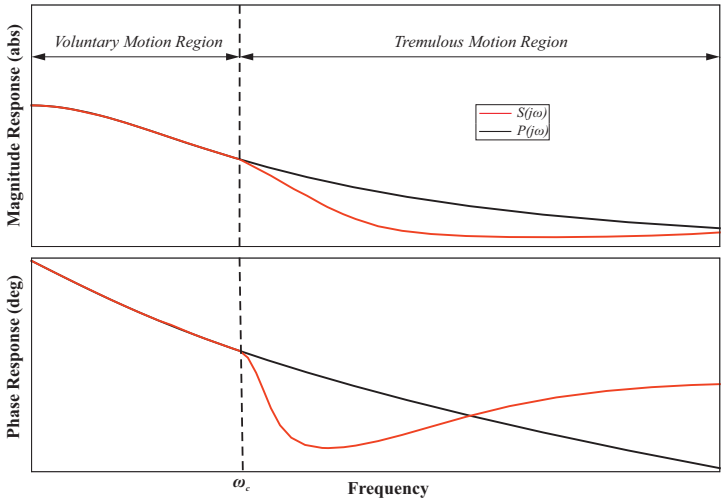

Figure 3.2: Schematic frequency response of wrist model (black line) and closed-loop system (red line).

3.1.3 Quantification of Measures

The notation used in this section is as follows. The $\mathcal{H}_2$-norm of operator P is denoted by $\|P\|_2$. The $\mathcal{H}_\infty$-norm of P is denoted by $\|P\|_\infty$ and defined by $\|P\|_\infty = \sup \left|P(e^{j\omega})\right|$. For a specific frequency range $[\omega_1, \omega_2]$, the $\mathcal{H}_\infty$-norm of P is denoted by $\left\|\overset{\omega}{P}\left(e^{j\omega}\right)\big|_{\omega\in[\omega_1,\omega_2]}\right\|_\infty$. A signal including only components over the specific frequency range $[\omega_1, \omega_2]$ is denoted by $\cdot\big|_{\omega\in[\omega_1,\omega_2]}$. The response of $P(q)$ to the input v is defined by $y_v \coloneqq P(q)\, v$. The response of the closed-loop system to the input v and $\tilde{d}$ is defined by $y \coloneqq P(q)\left(1 + P(q)\, C(q)\right)^{-1}(v + \tilde{d})$.

Suppose the control action u is applied to suppress tremor $\tilde{d}$ while voluntary action v is also exerted by the patient. To quantify the degree of preservation of voluntary intention, the following measure can be used over the voluntary frequency range, and is denoted by

$$J_1 = \left\|\left(P\left(e^{j\omega}\right) - S\left(e^{j\omega}\right)\right)\big|_{\omega\in[0,\omega_c]}\right\|_\infty = \sup_{\omega\in[0,\omega_c]} \left|P\left(e^{j\omega}\right) - S\left(e^{j\omega}\right)\right|. \tag{3.6}$$

To satisfy (3.2), measure J_1 (3.6) should be kept as small as possible. Now recall that complete tremor suppression equates to $y\big|_{\omega>\omega_c} = 0$, and also $y_v\big|_{\omega>\omega_c} = 0$ since voluntary action has only low frequency components by definition. To quantify tremor suppression, the following measure can therefore be defined over the involuntary frequency range, and is denoted by

$$J_2 = \left\|(y_v - y)\big|_{\omega\geq\omega_c}\right\|_2 = \left\|y\big|_{\omega\geq\omega_c}\right\|_2 \tag{3.7}$$

and should be kept as small as possible to satisfy (3.3).

In the next section, simulations will be performed using a previously validated and widely-accepted model in order to first evaluate the efficacy and limitations of the filtering technique, and second to establish the feasibility of RC for tremor suppression. The simulation results of both control methods will be compared in terms of the measures (3.6) and (3.7).

3.1.4 Limb Dynamics Specification

As stated in Section 3.1.3, to design $C(s)$ satisfying (3.2) and (3.3) requires a model of the limb dynamics. Thus, a model of the limb of interest is needed for use in simulations. The wrist joint was here targeted due to its importance within voluntary movements performed by the hand and the prevalence of intention tremor in the wrist joint. The leading experimental study on modelling the tremulous limb (Prochazka et al., 1992a) proposed a linear model of the wrist joint that was obtained from experimental data. This model was defined by

$$P(q) = \frac{1.567q^4 + 1.463q^3 + 11.4q^2 + 1.456q + 0.032}{100q^5 - 97.34q^4 + 24.98q^3 - 0.293q^2 + 0.179q - 0.005} \tag{3.8}$$

which is sampled with a sampling time of 0.05 second and will be used throughout this section to design the compensator $C(q)$ evaluated. Lenz et al. (2002) found that the power spectrum of EMG signals measured from patients with intention tremor usually contains a significant and single peak in the frequency range of intention tremor from 2 to 5 Hz, as shown in Figure 3.3. For simulations, the following assumptions have been made:

- These findings mean tremor can be assumed to take the form of an approximately sinusoidal movement at a frequency between 2 and 5 Hz. In simulation, a sinusoidal input $\tilde{d}$ of frequency $f_p = 2$ Hz will therefore be applied to the system shown in Figure 3.1.
- It will also be assumed that voluntary muscle activity is absent, thereby giving $v = 0$.

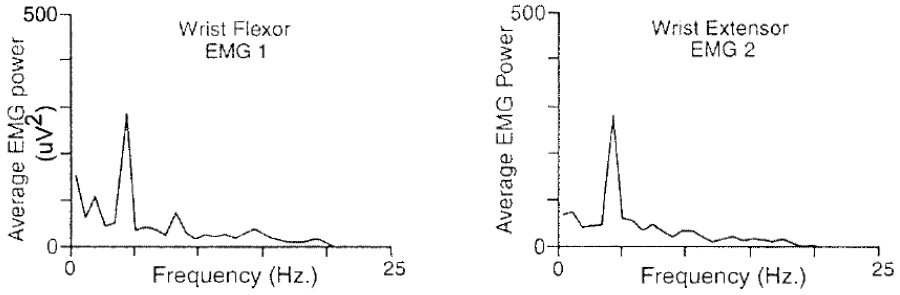

Figure 3.3: Spectral power from EMG signal of (a) wrist flexor and (b) wrist extensor muscles. These figures are taken from Lenz et al. (2002).

3.2 Filter Based Compensation Technique

In this section the conventional filter based approach to tremor suppression is examined. Here a high-pass filter (HPF) or a band-pass filter (BPF) followed by a positive gain σ can be implemented in the feedback path to satisfy the desired frequency response characteristics of (3.4) and (3.5). With $F_B(q)$ denoting the filter, $C(q)$ is replaced by $\sigma F_B(q)$, as shown in Figure 3.4. Since a Butterworth filter has a smooth frequency response and is easily implementable, Butterworth-type HPF and BPF will be employed in this section. These designs also correspond to those previously employed for tremor suppression in (Prochazka et al., 1992a). The design of these filters requires the estimation of several parameters: 1) a filter order n, and 2) a cut-off frequency for the HPF case, or a lower and a higher cut-off frequencies for the BPF case. J_1 and J_2, measures defined respectively by (3.6) and (3.7), will next be evaluated to estimate the parameters that best enable the designed filters to satisfy requirements (3.2) and (3.3).

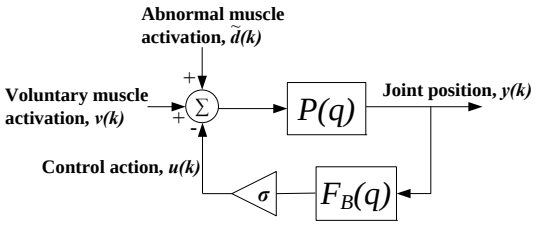

Figure 3.4: Block diagram of closed-loop system with filter.

The following sections will first introduce suitable ranges for the design parameters of HPF and BPF, which are cut-off frequency f_c and filter order n of $F_B(q)$, and gain σ in $C(q)$ defined as $C(q) \coloneqq \sigma F_B(q)$. Next, the effects of changing these design parameters on the measures J_1 and J_2 will be discussed. Then the limitations of the proposed filtering technique will be investigated. Lastly, to assess the accuracy and reliability of the simulation-based results, they will be compared with the findings of Prochazka et al. (1992b).

3.2.1 High-Pass Filter Case

In this section, Butterworth-type high-pass filters were designed using a broad range of design parameters comprising cut-off frequency f_c, filter order n and gain σ. Since the lower limit of the frequency range of the intention tremor is 2 Hz and the upper limit of the frequency range of the voluntary movement is 1 Hz, four cut-off frequencies, f_c, were selected within the range of 1 to 2 Hz. Then HPFs with different filter order, n, were designed for each cut-off frequency. For each design a different gain, σ, ranging from 2.6 to 3.8, was applied to produce compensator $C(q) = \sigma F_B(q)$. This was then applied to produce the closed-loop dynamics $S(e^{j\omega})$ given by (3.1). To estimate whether σ resulted in a stable system, root locus analysis was performed. For each stable system (3.1), J_1 and J_2 were calculated. Then the filters which closely satisfied (3.2) and (3.3) were established. The results are given in Table 3.1.

From these results, it can be seen that smaller cut-off frequencies lead to higher values of J_1, indicating a higher interference in voluntary motion since a part of the frequency range associated with voluntary motions remains in the transition region of the filter response for cut-off frequencies close to 1 Hz. This makes it difficult to satisfy (3.2) in this low frequency part of the transition region. On the other hand, if a cut-off frequency is selected to be close to 2 Hz, then J_2 is necessarily increased, and so the amount of tremor suppression is decreased. Thus there is an inherent trade-off between tremor suppression performance and the distortion in voluntary motion. This trade-off is illustrated in Figure 3.5(a).

In the cases with low gain σ and cut-off frequencies higher than 1.2 Hz, a filter with high order produces a decrease in J_1. However, this result is reversed when using high gains,

Table 3.1: Changes in measures J_1 and J_2 with varied HPF design parameters. *uns* denotes unstable closed-loop system.

		J_1							J_2						
f_c	$n \backslash \sigma$	2.6	2.8	3.0	3.2	3.4	3.6	3.8	2.6	2.8	3.0	3.2	3.4	3.6	3.8
1.2 Hz	2	0.5776	0.6032	0.6279	0.6517	0.6747	*uns*	*uns*	0.0690	0.0658	0.0630	0.0604	0.0589	*uns*	*uns*
	3	0.8249	0.8873	0.9514	1.0172	1.0850	1.1549	*uns*	0.0596	0.0570	0.0546	0.0525	0.0506	0.0491	*uns*
	4	1.9423	2.2985	2.7425	3.3121	4.0709	5.1317	*uns*	0.0550	0.0529	0.0511	0.0496	0.0484	0.0475	*uns*
1.5 Hz	2	0.4835	0.5059	0.5275	0.5484	0.5687	0.5883	*uns*	0.0653	0.0625	0.0600	0.0577	0.0556	0.0540	*uns*
	3	0.5944	0.6353	0.6766	0.7184	0.7607	0.8038	*uns*	0.0561	0.0538	0.0517	0.0498	0.0481	0.0465	*uns*
	4	0.7041	0.8058	0.9210	1.0525	1.2040	1.3803	*uns*	0.0527	0.0508	0.0490	0.0474	0.0459	0.0447	*uns*
	5	0.2963	0.3208	0.3454	0.3699	*uns*	*uns*	*uns*	0.0548	0.0542	0.0550	0.0589	*uns*	*uns*	*uns*
1.8 Hz	2	0.4073	0.4270	0.4461	0.4645	0.4824	0.4998	*uns*	0.0646	0.0620	0.0597	0.0576	0.0556	0.0537	*uns*
	3	0.4070	0.4418	0.4766	0.5113	0.5456	0.5796	*uns*	0.0571	0.0549	0.0530	0.0511	0.0495	0.0479	*uns*
	4	0.2340	0.2568	0.2804	0.3050	0.3305	0.3570	*uns*	0.0569	0.0548	0.0530	0.0512	0.0496	0.0482	*uns*
	5	0.1028	0.1107	0.1185	0.1263	0.1341	0.1419	*uns*	0.0639	0.0619	0.0601	0.0587	0.0576	0.0570	*uns*
2 Hz	2	0.3635	0.3823	0.4001	0.4171	0.4336	0.4496	*uns*	0.0654	0.0630	0.0608	0.0587	0.0568	0.0550	*uns*
	3	0.2934	0.3198	0.3468	0.3741	0.4019	0.4301	*uns*	0.0605	0.0584	0.0564	0.0546	0.0529	0.0513	*uns*
	4	0.1364	0.1483	0.1606	0.1730	0.1857	0.1987	*uns*	0.0654	0.0632	0.0611	0.0592	0.0574	0.0557	*uns*
	5	0.0581	0.0625	0.0669	0.0712	0.0756	0.0800	*uns*	0.0848	0.0821	0.0795	0.0772	0.0750	0.0731	*uns*

since a higher gain σ causes more tremor suppression and this results in an amplification in the low frequency range due to the *waterbed* effect, as shown in Figure 3.5(b). The *waterbed* effect describes an inherent trade-off that arises when an attenuation in some frequency range occurs. It states that an attenuation in some frequency range of each transfer function from each input to the error of the closed-loop system results in an amplification in an other frequency range of these transfer functions (Songchon and Longman, 2000). The *waterbed* effect is also explained mathematically in Appendix A. Table 3.1 shows the minimum value of J_2 is 0.0447 and the minimum value of J_1 is 0.0581. This shows clearly that HPF leads to an inevitable interference with voluntary

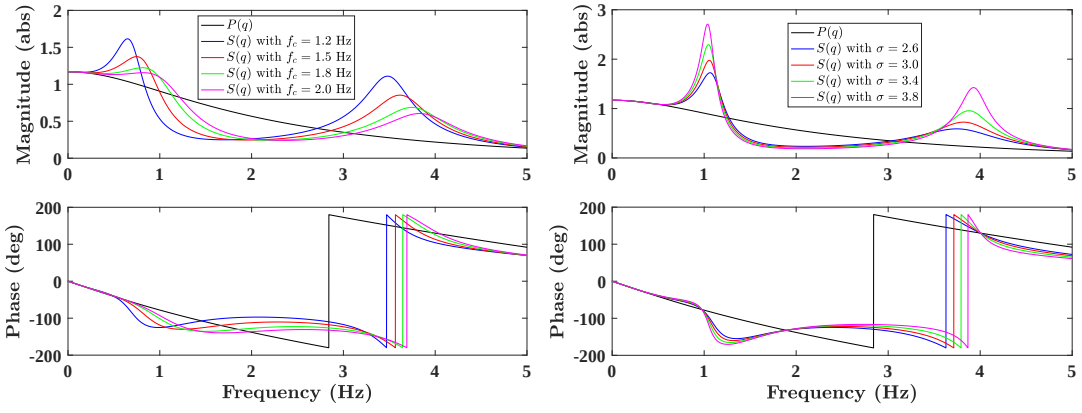

(a) (b)

Figure 3.5: Bode plots of closed loop system $S(q)$ a) with 3^{rd} order HPF of $\sigma = 2.8$ and various cut-off frequencies, b) with 4^{th} order HPF of $f_c = 1.5$ Hz with various gain values.

motion.

Figure 3.6 shows the wrist position in the flexion/extension direction and compares the responses of $P(q)$ and $S(q)$ with various gain values in response to a sinusoidal tremor signal $\tilde{d}$ of 2 Hz frequency. The measure J_2 is calculated to be 0.12 without tremor suppression when $\tilde{d}$ is applied to $P(q)$. Then HPF is able to suppress tremor by between 29.3% and 62.8%. However the maximum tremor suppression raises J_1 by 96%, thereby increasing interference in voluntary motion. Additionally, HPF is incapable of achieving complete tremor suppression.

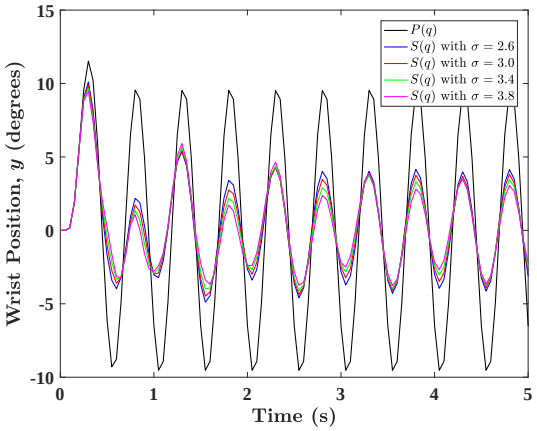

Figure 3.6: Comparison of the responses of $P(q)$ and $S(q)$ with 4^{th} order HPF of 1.5 Hz cut-off frequency and various gain values.

3.2.2 Band-Pass Filter Case

In the previous section, a HPF has been employed to control stimulation input, u, thereby suppressing tremor in the frequency range of 2-5 Hz. Due to the necessity of suppressing tremor in this frequency range, an alternative filter based controller to the HPF case is a band-pass filter. For this reason, in this section, a Butterworth-type BPF will be employed instead and different closed-loop systems will again be constructed by changing the order and the frequency band of the band-pass filter. As before, the gain, σ, attached to the filter will also be varied. The resulting closed-loop systems will be driven by the same tremor input $\tilde{d}$ applied previously and the effects of changing these design parameters on tremor suppression and distortion in voluntary action will be investigated in terms of J_1 and J_2.

Results using frequency bands of [1.2 5.8] Hz, [1.5 5.5] Hz, [1.8 5.2] Hz, [2.0 5.0] Hz, orders of $n = 4, 6, 8, 10$ and gains of $\sigma = 1.2, 1.4, 1.6, 1.8, 2.0, 2.2, 2.4$ are given in Table 3.2. Since gains higher than 2.4 produce unstable systems, only values between 1.2 and 2.4 are considered here. In some cases, choosing the lower limit of the frequency band close to 1 Hz increases J_1. Table 3.2 also indicates that higher σ value cause lower values of J_2 with higher values of J_1, thereby showing more tremor suppression with more interference

in voluntary action. A way to reduce this interference is to increase the order n of the BPF without changing the frequency band.

Table 3.2: Changes in measures J_1 and J_2 with varied HPF design parameters.

		J_1							J_2						
f_c	n \ σ	1.2	1.4	1.6	1.8	2.0	2.2	2.4	1.2	1.4	1.6	1.8	2.0	2.2	2.4
[1.2 5.8] Hz	4	0.3416	0.3762	0.4071	0.4357	0.4628	0.4886	0.5132	0.1143	0.1095	0.1043	0.0990	0.0939	0.0891	0.0849
	6	0.3891	0.4395	0.4884	0.5369	0.5853	0.6340	0.6830	0.1014	0.0964	0.0915	0.0868	0.0824	0.0783	0.0749
	8	0.5088	0.6313	0.7654	0.9091	1.0591	1.2223	1.4080	0.0918	0.0869	0.0824	0.0782	0.0743	0.0709	0.0681
	10	0.3882	0.4786	0.5783	0.6876	0.8067	0.9348	1.0704	0.0849	0.0803	0.0762	0.0726	0.0695	0.0673	0.0667
[1.5 5.5] Hz	4	0.2495	0.2810	0.3101	0.3371	0.3621	0.3853	0.4069	0.0993	0.0945	0.0899	0.0854	0.0812	0.0773	0.0739
	6	0.2029	0.2396	0.2770	0.3147	0.3527	0.3908	0.4288	0.0866	0.0819	0.0775	0.0735	0.0699	0.0666	0.0638
	8	0.1219	0.1454	0.1700	0.1957	0.2227	0.2509	0.2806	0.0791	0.0746	0.0705	0.0669	0.0637	0.0608	0.0583
	10	0.0629	0.0735	0.0841	0.0947	0.1053	0.1159	0.1265	0.0751	0.0708	0.0670	0.0638	0.0609	0.0584	0.0564
[1.8 5.2] Hz	4	0.1641	0.1882	0.2114	0.2336	0.2550	0.2754	0.2951	0.0902	0.0859	0.0818	0.0780	0.0745	0.0713	0.0684
	6	0.0844	0.0996	0.1152	0.1310	0.1473	0.1639	0.1808	0.0794	0.0751	0.0712	0.0677	0.0646	0.0618	0.0593
	8	0.0352	0.0413	0.0474	0.0536	0.0599	0.0662	0.0726	0.0760	0.0718	0.0680	0.0647	0.0617	0.0591	0.0568
	10	0.0146	0.0171	0.0195	0.0219	0.0243	0.0267	0.0291	0.0786	0.0744	0.0707	0.0673	0.0644	0.0617	0.0594
[2 5] Hz	4	0.1183	0.1367	0.1548	0.1724	0.1896	0.2064	0.2228	0.0887	0.0847	0.0809	0.0775	0.0743	0.0714	0.0688
	6	0.0466	0.0548	0.0631	0.0715	0.0800	0.0887	0.0975	0.0826	0.0786	0.0750	0.0717	0.0688	0.0661	0.0636
	8	0.0161	0.0188	0.0216	0.0243	0.0271	0.0299	0.0326	0.0879	0.0840	0.0804	0.0771	0.0741	0.0713	0.0687
	10	0.0057	0.0066	0.0075	0.0085	0.0094	0.0104	0.0113	0.1074	0.1043	0.1011	0.0979	0.0948	0.0918	0.0889

Additionally, Figure 3.7 shows clearly the increasing undesired amplifications due to the *waterbed* effect when σ is increased to obtain more suppression. From Table 3.2, the maximum and minimum values of J_2 are 0.1074 and 0.0564, repectively. Having J_2 of 0.12 without tremor suppression, BPF can suppress tremor by 10.5% to 53.0%. This is illustrated in Figure 3.8 where the wrist joint positions in the flexion/extension direction are plotted for both cases. The minimum value of J_1 in Table 3.2 is 0.0057. This shows that BPF can have a minimal interference with voluntary action but produces an insufficient tremor suppression in return. Comparison with the results of HPF reveals that more suppression with a reasonable interference can be obtained with HPF. Comparing Figure 3.7 with Figure 3.5 shows BPF leads to more amplification in other frequencies than HPF due to the *waterbed* effect.

3.2.3 Limitations of Filtering Technique

The simulation results confirm that high-pass and band-pass filters are able to suppress tremor by up to 62.8% and 53.0%, respectively. These results coincide with those proposed in (Prochazka et al., 1992b) where intention tremor was able to be suppressed by up to 68%. However, results also clearly illustrate inherent limitations on performance in the closed-loop system structure, such as the *waterbed* effect and regions of stability. The *waterbed* effect causes substantial increases in amplitudes at a few frequencies around the tremor frequency, leading to interference in voluntary action, when tremor

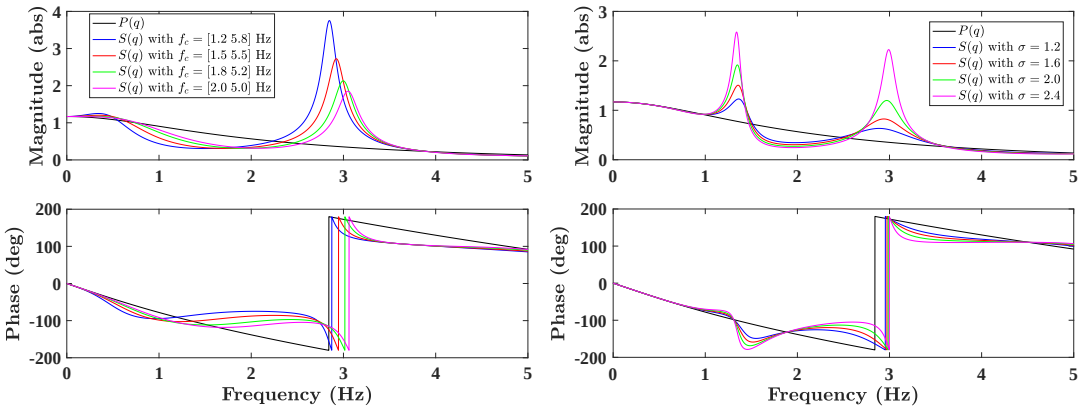

(a) (b)

Figure 3.7: Bode plots of closed loop system a) with 4^{th} order BPF of $\sigma = 2.4$ and various cut-off frequencies, b) with 10^{th} order BPF of $f_c = [1.5\ 5.5]$ Hz with various gain values.

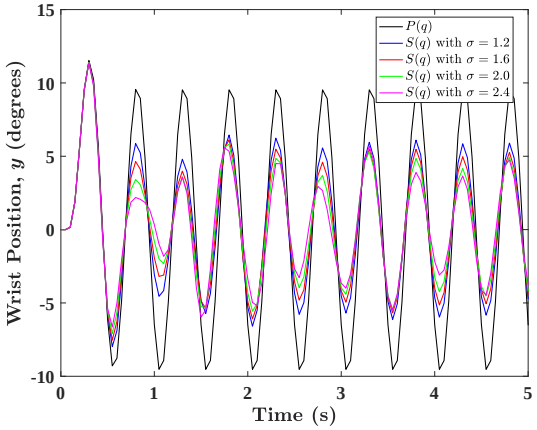

Figure 3.8: Comparison of the responses of $P(q)$ and $S(q)$ with 10^{th} order BPF of $f_c = [1.5\ 5.5]$ and various gain values.

suppression is increased. Moreover, the stability is very sensitive to any change in n and σ. These parameters must therefore be tuned within extremely narrow limits to avoid the closed-loop system from becoming unstable. Finally, none of these filters are capable of suppressing tremor completely.

Next, two RC algorithms will be introduced in Section 3.3. Then simulation results will be presented and quantified using the measures of (3.6) and (3.7) to examine whether RC can address the limitations of the conventional filtering technique.

3.3 Repetitive Control

As mentioned in Chapter 2, an internal model of the periodic disturbance, here tremor, must be included in the control structure to enable complete disturbance rejection (Francis and Wonham, 1975). Since repetitive control (RC) was formulated based on this internal model principle, it enables tremor to be suppressed completely. Repetitive control fits with the general component structure of Figure 3.1. In particular, RC has the form shown in Figure 3.9 where $IM(q)$ is the internal model which takes the form of $\left(q^{N_p}-1\right)^{-1}$ and can generate any N_p-periodic signal with suitable initial conditions. Here, N_p is defined as $N_p \coloneqq 1/f_pT_s$ in which f_p is the frequency of the periodic signal and T_s is the sampling time.

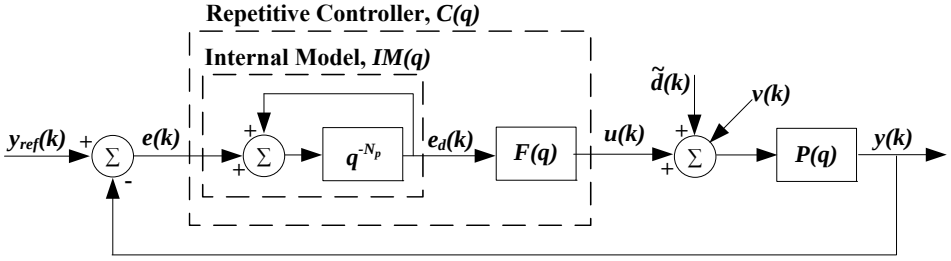

Figure 3.9: Standard repetitive control scheme.

The repetitive control action is generally considered to have the structure

$$u(k) = F(q)\left(q^{N_p}-1\right)^{-1} e(k) \tag{3.9}$$

with $F(q)$ taking the form

$$F(q) = \kappa_1 q^{\beta-1} + \kappa_2 q^{\beta-2} + \cdots + \kappa_\beta q^0 + \cdots + \kappa_{\alpha-1} q^{-(\alpha-\beta-1)} + \kappa_\alpha q^{-(\alpha-\beta)} \tag{3.10}$$

where α, β are positive integers and is applied to the system $P(q)$. Using this structure, any N_p-periodic disturbance $\tilde{d}(k)$ is completely rejected if and only if transfer function $F(q)$ is chosen such that the roots of

$$1 - q^{-N_p}\left(1 - P(q)F(q)\right) = 0 \tag{3.11}$$

are all inside the unit circle. A sufficient condition for this is given by the induced norm condition

$$\left\|1 - P(q)F(q)\right\|_\infty < 1 \tag{3.12}$$

or equivalently, in the frequency domain by

$$\sup_{\omega\in[0,2\pi]} \left|1 - P(e^{j\omega})F(e^{j\omega})\right| < 1, \tag{3.13}$$

assuming that $1 - P(q)F(q)$ is internally stable. The system model $P(q)$ and control action (3.9) result in the system shown in Figure 3.9. Note that here $y_{ref}(k)$ is N_p-periodic signal, and can be chosen as $y_{ref} = 0$ if no tracking is specified.

In the necessary condition for monotonic convergence (3.13), the term $\left|1 - P(e^{j\omega})F(e^{j\omega})\right|$ dictates how rapidly frequency component $\omega \in [0, 2\pi]$ of the error diminishes to zero. Hence to obtain the fastest learning rate, $F(q)$ should be selected as the right inverse of the linear dynamics $P(q)$. However, this design choice is often infeasible due to the instability that occurs when the true plant differs from $P(q)$ due to the presence of effects such as fatigue and spastacity (Longman, 2010).

In practice, choosing $F(q)$ to satisfy (3.12) or (3.13) is challenging, especially if the system has zeros outside the unit circle. The following methods, namely frequency modified inverse RC (FMI-RC) and gradient based RC (GB-RC), have been selected from the many available RC variants because of their track record in experimental effectiveness, their attractive robustness properties, and their ease of implementation (Longman, 2010; Hatonen et al., 2006a). Both approaches start with the designer selecting parameters α and β which determine the order of $F(q)$ via its definition (3.10).

3.3.1 Frequency Modified Inverse RC (FMI-RC) Algorithm

Condition (3.13) can be addressed pragmatically by selecting $F(q)$ as an approximation of $P^{-1}(q)$ through suitable choice of parameters $\phi = [\kappa_1 \ \kappa_2 \ \cdots \ \kappa_\alpha]^\top$ appearing in $F(q)$ definition (3.10). This is achieved by minimising the cost function

$$J = \sum_{i=0}^{L} [1 - P(e^{j\omega_i})F(e^{j\omega_i})][1 - P(e^{j\omega_i})F(e^{j\omega_i})]^* \tag{3.14}$$

where $\omega_i = 2\pi f_i T_s$ in which $\{f_i\}_{i=0,\ldots,L}$ is an appropriate set of frequencies selected from 0 to $f_N = 1/2T_s$. The solution, ϕ^*, to (3.14) is given by $\phi^* = \Gamma^{-1}\Phi$ where

$$\begin{aligned}
\Gamma &= \sum_{i=0}^{L} M^2(\omega_j) \begin{bmatrix} 1 & \cos(\omega_i) & \cdots & \cos((\alpha-1)\omega_i) \\ \cos(\omega_i) & 1 & \cdots & \cos((\alpha-2)\omega_i) \\ \vdots & \vdots & \ddots & \vdots \\ \cos((\alpha-1)\omega_i) & \cos((\alpha-2)\omega_i) & \vdots & 1 \end{bmatrix}, \\
\Phi &= \sum_{i=0}^{L} M(\omega_j) \begin{bmatrix} \cos((\beta-1)\omega_i + \varphi(\omega_i)) \\ \\ \vdots \\ \\ \cos((\beta-\alpha)\omega_i + \varphi(\omega_i)) \end{bmatrix}
\end{aligned} \tag{3.15}$$

in which $M(\omega)$ and $\varphi(\omega)$ are the magnitude and phase of $P(q)$, respectively.

3.3.2 Gradient-based RC (GB-RC) Algorithm

Condition (3.13) is satisfied by choosing $\alpha = \beta = N_p$ in (3.10), together with

$$\kappa_i = \gamma h_{N_p - i}, \quad i = 1, \ldots, N_p, \tag{3.16}$$

in which h_i are the Markov parameters of $P(q)$ with $h_i = 0 \ \forall i > N_p$, and γ selected as

$$0 < \gamma < \frac{2}{\sup\limits_{\omega \in [0,2\pi]} \left|P(e^{j\omega})\right|^2}. \tag{3.17}$$

This range is derived by substituting $F(q) = \gamma P^*(q)$ into the left-hand side of (3.13) to yield

$$\sup_{\omega \in [0,2\pi]} \left|1 - P(e^{j\omega})F(e^{j\omega})\right| = \sup_{\omega \in [0,2\pi]} \left|1 - \gamma P(e^{j\omega})P^*(e^{j\omega})\right| = \sup_{\omega \in [0,2\pi]} \left|1 - \gamma \left|P(e^{j\omega})\right|^2\right| \tag{3.18}$$

and it follows that selection (3.17) satisfies (3.13).

3.3.3 Evaluation of RC Algorithms

To enable fair comparison between RC and the conventional filter appraoch of Section (3.2), the same plant model of (3.8) is used for evaluation. In particular, the sampling time T_s was selected to be 0.05 s for simulation. To simulate the tremulous motion, the same sinusoidal input $\tilde{d}$ of $f_p = 2$ Hz ($N_p = 1/T_s f_p = 20$) was applied to the closed-loop system of Figure 3.9. To suppress the tremor in the absence of voluntary action $v = 0$, y_{ref} was chosen to be 0. Then $\beta \leq N_p = 10$, (in which β appears in (3.10)), was selected and RC forms were designed to satisfy either (3.12) or (3.13). Introducing $q = e^{j\omega T_s}$ and then replacing (3.1) with

$$S(q) = P(q)\big(1 + P(q)F(q)(q^{N_p} - 1)^{-1}\big)^{-1}, \tag{3.19}$$

the simulation results were evaluated using the measures J_1 and J_2 given by (3.6) and (3.7) to examine whether the designed RC forms were able to satisfy the low and high frequency characteristics of the closed loop system, defined by (3.2) and (3.3).

Table 3.3 shows the effects of varying α and β in $F(q)$ (3.10) to design different FMI-RC forms on J_1 and J_2. Having $J_2 = 0.12$ for the case without tremor suppression, FMI-RC can suppress tremor by up to 81.8%. Increasing α reduces the magnitude of $1 - P(e^{j\omega})F(e^{j\omega})$, leading to shorter transient response for the FMI-RC application. This is illustrated in Figure 3.10(b) and Figure 3.10(c). The values of J_2 in Table 3.3 shows clearly that FMI-RC affects the voluntary action significantly. This can be seen in the low frequency region of Figure 3.10(a).

Table 3.3: Changes in the measures with varied control parameters of FMI-RC.

α/β	6/6	8/6	10/6	12/6	14/6	16/6
J_1	1.4429	1.2590	1.19033	1.1706	1.1677	1.1665
J_2	0.0227	0.0222	0.0220	0.0219	0.0218	0.0218

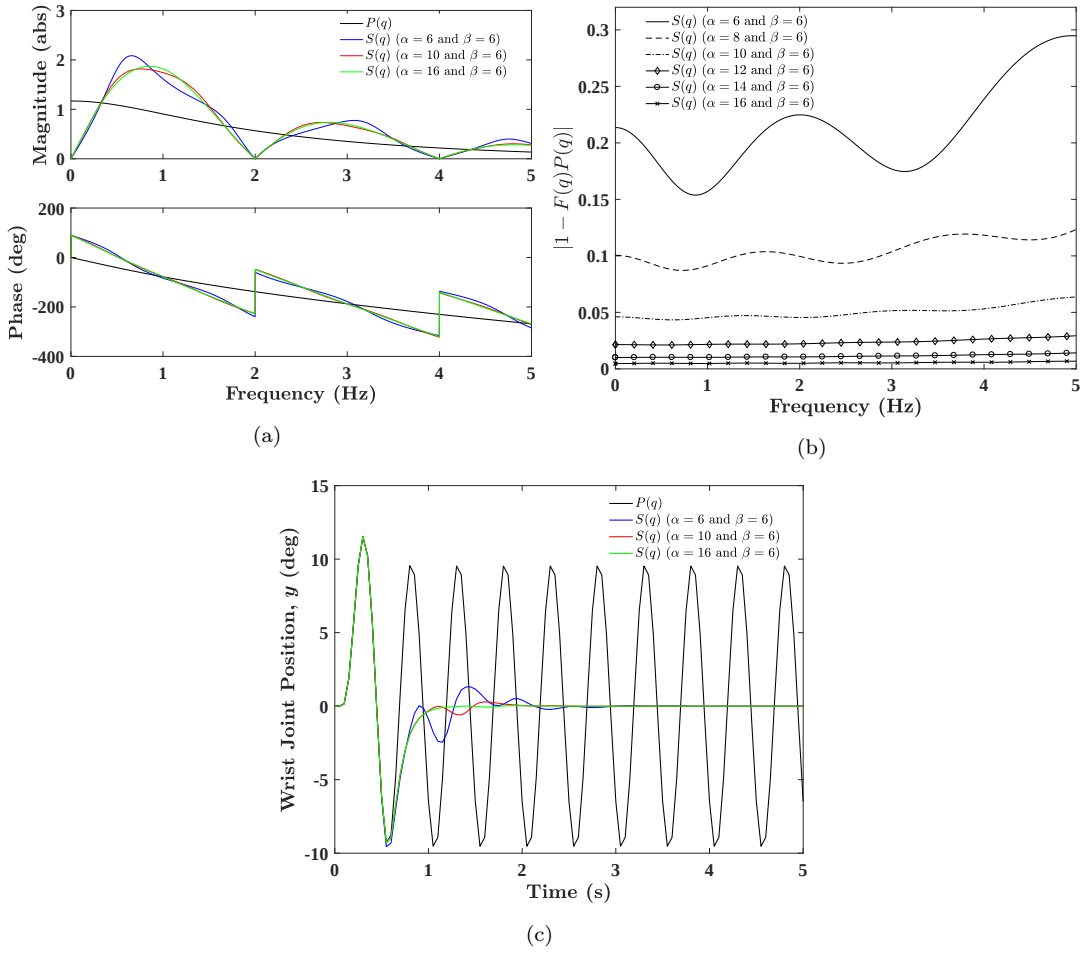

Figure 3.10: The effects of varying control parameters α and β of FMI-RC on a) frequency responses, b) convergence and c) time responses of $S(q)$ driven by $\tilde{d}$.

Table 3.4 gives the results for GB-RC algorithm. The minimum J_2 is calculated to be 0.0278. Comparison of the case without tremor suppression reveals that GB-RC can suppress tremor by up to 76.8% with a significant increase in J_1 in return, leading to more interference in voluntary action since J_1 increases to 3.2954 in the case where maximum suppression is obtained. Additionally, Figure 3.11(b) shows that increasing γ reduces the magnitude of $1 - P(e^{j\omega})F(e^{j\omega})$, thereby shortening the transient response. This decrease in settling time is also illustrated in Figure 3.11(c).

Table 3.4: Changes in the measures with varied control parameters of GB-RC.

γ	0.1	0.2	0.3	0.4	0.5	0.6	0.7	1.7
J_1	1.1688	1.1688	1.1688	1.1688	1.1688	1.1688	1.1688	3.2954
J_2	0.0825	0.0634	0.0528	0.0462	0.0418	0.0386	0.0362	0.0278

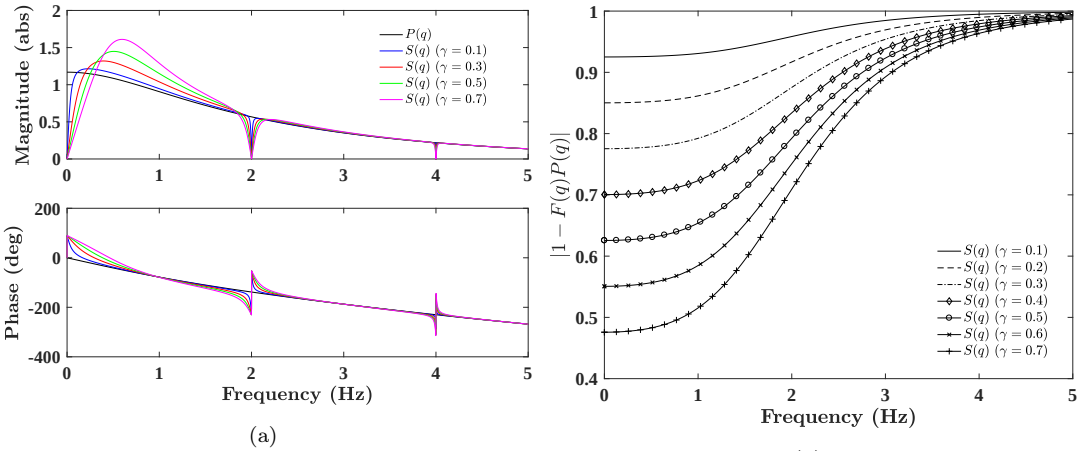

(a) (b)

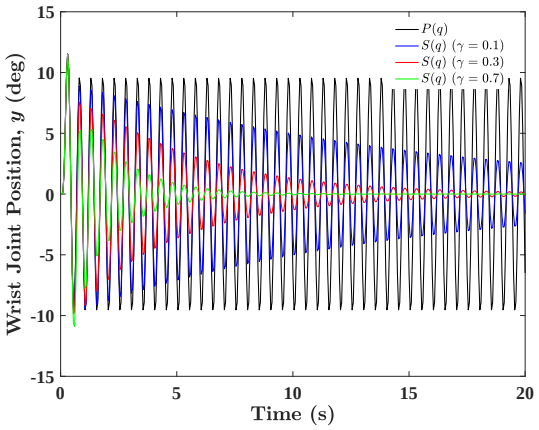

(c)

Figure 3.11: The effects of varying control parameter γ of GB-RC on a) frequency responses, b) convergence and c) time responses of $S(q)$ driven by $\tilde{d}$.

3.3.4 Limitations of RC Algorithms

Comparison of both algorithms shows that FMI-RC can suppress tremor more effectively than GB-RC. However the subject's voluntary action cannot be preserved with both algorithms, and higher tremor suppression inevitably causes more interference in the case of GB-RC due to the waterbed effect. Thus, the RC framework leads to impairment in wrist movement. Moreover, Steinbuch (2002) states that RC requires the knowledge of the period of the disturbance signal to an accuracy of $\pm 0.1\%$. This means RC is unable to suppress tremor completely if tremor frequency is out of this accuracy range. Another drawback is the requirement of the knowledge of the underlying limb dynamics to satisfy the monotonic convergence in either (3.12) or (3.13), as proposed in Section 3.3. Thus it

is critical to obtain a model that can adequately capture the limb dynamics since a more reliable model can increase the performance of RC for tremor suppression. In addition, if the limb dynamics has time-varying characteristics, then it may be difficult to satisfy the monotonic convergence (3.12) or (3.13).

3.4 Summary

To evaluate the feasibility of RC approach for tremor suppression compared with the conventional filtering technique, a number of simulations were performed in which it is assumed that tremor appears a sinusoidal signal and voluntary muscle activation is absent. Time response plots show that RC yields zero steady state error, unlike the conventional filtering technique. In terms of transient response, the minimum amount of tremor suppression produced by RC is 75% while the maximum amount of tremor suppression produced by the filtering technique is 64%. These results confirm that RC is capable of producing complete tremor suppression. Thus RC has far greater potential than conventional filtering techniques to annihilate tremor.

Although the comparison in this chapter was undertaken using the most reliable model available in the literature, there is a distinct lack of identification techniques available for the tremulous limb. In Chapter 4, a model and accompanying identification procedure will therefore be presented to yield a mechanism for practical deployment. This model form is carefully selected to be of a structure that can later be linearised, and hence enable a linear control action to be applied to suppress tremor. Moreover, the simulation results also show that the frequency response of the closed-loop system employing RC approach is different from the response of wrist dynamics for the frequencies less than 1 Hz. This confirms that RC has a significant effect on voluntary action. In Chapter 5, this will be discussed in more detail and then a mechanism will be proposed to address this limitation.

Chapter 4

Modelling and Identification of Wrist Dynamics

The previous chapter has confirmed the potential of developing an RC framework for tremor suppression. In particular, it showed in simulation that RC offered significant advantage compared to conventional filter based compensation. To do this, it employed a leading experimentally validated linear model which enabled a fair comparison between the filtering technique and the RC framework carried out in simulation. The next step is to apply RC experimentally, however the same model cannot be employed since it is not tailored to the individual characteristics of each patient. In addition, the simple form of model may not be sufficiently accurate in representing the critical properties which are crucial for joint movement, while avoiding unnecessary nonlinearities. Therefore in this chapter, a full review of available models will be conducted and a suitable identification method will then be proposed. The key contributions of the model developed in this chapter are as follows:

- To embed accuracy, the model structure incorporates nonlinear recruitment characteristics, together with a co-activation function created to minimise the effects of the dead-zone in the muscle torque.
- The structure can be linearised in a transparent manner to enable subsequent linear tremor suppression control design (undertaken in Chapter 5).
- The identification procedure is suitable for both patients and clinicians. Firstly, it is not time-consuming and can be carried out in less than 1 min. Secondly, it does not require user input and hence can be automated. Thirdly, it can use signals that are comfortable (have no sudden changes, such as present in random signals) and have been employed in previous clinical trials. Finally, it is able to explicitly identify the tremulous action (unlike Prochazka et al. (1992b)).

4.1 Wrist Dynamics Modelling

A variety of biomechanical models exist that connect FES to resulting movement, with applications in rehabilitation, neuroprostheses and assistive technology fields (Bo et al., 2011a; Freeman et al., 2009; Nekoukar and Erfanian, 2011; Popovic et al., 1999; Zhang et al., 2011). These models include properties of the musculoskeletal system, such as physiological, mechanical and electrical components (Zhang et al., 2011). Within tremor suppression, the model must also include a characterisation of both the tremulous motion and voluntary action in order to define the associated control problem (Prochazka et al., 1992a; Zhang and Ang, 2006; Bo and Poignet, 2010; Zhang et al., 2011; Gallego et al., 2013). The first step is to review existing approaches to ascertain their strengths and limitations. In (Prochazka et al., 1992a), FES was applied to the muscles of 6 unimpaired subjects at frequencies ranging from 1 to 12 Hz to produce extension and flexion. The amplitude and phase of the movement response were calculated for each subject. These were then averaged across subjects at each frequency and a linear transfer function was fitted to the resulting frequency response data to identify the system model. Prochazka et al. (1992a) stated that the model was able to adequately predict gain margins, resonant frequencies and tremor attenuation. However, the averaging process caused the model to poorly fit the response of individual subjects, especially at frequencies between 2 and 5 Hz since there was no procedure to identify individual models for each patient. Instead, the same linear model identified in (Prochazka et al., 1992a) was employed, which accounted for the degraded performance. The fitting calculation also required a large number of trial-and-error iterations.

In (Bo and Poignet, 2010), the wrist was approximated by a second order linear system including inertia, passive damping, passive stiffness, and gravity. The Hill-type muscle model was used to model the muscle contraction dynamics. An Extended Kalman Filter (EKF) was used to estimate the parameters of inertia, passive damping, passive stiffness and the maximum moment due to the gravity of the joint. Then a pseudorandom stimulation sequence was applied and the Gauss-Newton method was employed to identify the active parameters from the recorded joint motion. However, a linear model was used to capture the essential nonlinear responses of the relevant muscles to the stimulation input, thereby reducing the reliability of the model in clinical application. The accuracy of these methods was highly dependent on the initial values provided for each parameter set which were chosen arbitrarily. The procedure also involved FES signals that may have been uncomfortable, leading to involuntary muscle activation.

In (Zhang and Ang, 2006; Zhang et al., 2011), the wrist was modelled as a second order system with muscles taking the form of a Hill type model with the force-length (FL) property, the force-velocity (FV) property and the nonlinear muscle activation dynamics under isometric conditions. The parameters appearing in the model were

taken from published literature and no procedure was presented to enable experimental identification.

The above studies highlight the absence of a model identification procedure that are suitable for clinical application. In this scenario, controllers are required to perform satisfactorily, despite limited identification time available due to the onset of fatigue, changes in physiological conditions and subject availability constraints. Ideally, this procedure should also be able to be conducted by a clinician without the need for an engineer being present. Existing methods either: i) assume simplistic forms that inaccurately capture the dynamics (e.g. they negate a static dead zone and/or nonlinearity in torque generated), ii) utilise complex structures that give rise to procedures that can neither be applied in the time available, nor are aligned to subjects' needs, or iii) have not been validated in terms of the accuracy with which the model matches separate data sets. A suitable model must address these shortcomings by affecting a compromise between accuracy and ease of identification. This is further complicated since it is also desirable that the identification procedure yields a linear time-invariant (LTI) form to maximise the class of controllers subsequently employed.

As mentioned in Section 3.1.1, the limb movement is associated with voluntary and tremulous muscle activity. Thus another key component of the model is that it should include a description of the tremor and voluntary motion dynamics. To do it, the tremor frequency must be identified, and together with the frequency of voluntary action, can then be included in the controller design.

In the next section an approach is developed that combines a nonlinear model structure with an identification procedure that meets the demands of the clinical domain and is suitable for use with neurologically impaired subjects.

4.2 Problem Set-up

Previous research on FES based tremor suppression has almost exclusively focused on the wrist because of three reasons: Firstly, wrist motion can be confined to a single plane of motion (extension and flexion). Secondly, the intention tremor occurs more frequently in distal joints of upper limbs such as wrists and fingers. Lastly, the wrist plays an important role in daily life activities (Grimaldi and Manto, 2008; Deuschl et al., 2009). Thus the proposed model comprises horizontal plane-flexion and extension wrist dynamics in response to FES applied to the Flexor Carpi Radialis (FCR) and Extensor Carpi Radialis (ECR) muscles, as well as an oscillatory movement due to tremor. Single joint motion can be accurately modelled through combination of rigid body dynamics (RBD) (characterising mass, inertia, damping and stiffness properties of limb segments) and a Hill-type model representing the response of muscle to the applied stimulation. Note that it is possible to include the neuromuscular reflex in the form of an additional

dynamic function placed before the muscle model. However, it is neglected here since FES produces negligible effect on the reflex loop when applied transcutaneously, and hence on a macroscopic scale (Thompson et al., 2006; Zhang and Ang, 2012).

In most applications, joint ranges and velocities are small so that the isometric behavior of muscle dominates (Le et al., 2012) and additionally, muscle stretching and shortening have minor effect on the generated force because of the low amplitude and frequency of tremulous motion, and thus FL and FV components of the Hill-type model can be neglected. The activation dynamics component is almost uniformly represented by a Hammerstein structure. Recent works have shown that Hill-Huxley models (Bobet and Stein, 1998; Ding et al., 2002; Bobet et al., 2005) may be at least as accurate as a Hammerstein structure in representing the activation dynamics (Frey Law and Shields, 2007). The drawback that their complexity undermines application to control has been countered by the proposal of a Wiener-Hammerstein structure (Bai et al., 2009), but as yet Hill-Huxley models have not been shown to extend to non-isometric conditions, and have not been used in controller derivation. In this paper a Hammerstein structure is therefore employed due to its popularity in the literature (Le et al., 2010), confirmed accuracy, structural simplicity, and correspondence with biophysics. Within it, the linear activation dynamics (LAD) models the muscle contraction dynamics and are preceded by a static mapping function, the isometric recruitment curve (IRC), which accounts for the static gain relation between the applied FES and the steady-state output torque when the muscle is held at a fixed length (Durfee and Maclean, 1989; Hunt et al., 1998).

In addition to the muscle dynamics, the joint dynamics of a human limb are commonly modelled by RBD in which the damping and elastic functions are linear (Iaquinto and Wayne, 2010; Takehara et al., 2012; Curtin and Lowery, 2014). This assumption has been used in previous research and is supported by experimental results over a wide range of movement.

This section will proceed with developing a general model of a tremulous wrist flexion/extension and defining an identification problem to estimate the parameters of the components in the model. Next, a muscle co-activation function will be proposed since it will later be implemented into the control structure to improve the performance of the control approach and it will also enable FES inputs applied to flexors and extensor muscles to be represented by a single FES input. Then some assumptions will be described that enable the identification problem to be solved readily.

4.2.1 Model Structure with the Application of Tremor

The above discussion motivates the overall model shown in Figure 4.1 which corresponds to the following definitions:

Definition 4.1. Let the FCR muscle stimulated by electrical impulse $u_{fcr}(k)$ be modelled by a Hammerstein structure comprising a static mapping $h_{IRC,fcr}(u_{fcr})$ followed by a linear activation dynamics $H_{LAD,fcr}(q)$. Let tremor present as a N_p-periodic signal $\tilde{d}_{fcr}(k)$ which adds to the steady-state torque $\tau_{ss,fcr}(k)$ such that the overall moment $\tau_{fcr}(k) = H_{LAD,fcr}(q)(\tau_{ss,fcr}(k) + \tilde{d}_{fcr}(k))$ produced by FCR muscles. Similarly, the overall moment $\tau_{ecr}(k) = H_{LAD}(q)(\tau_{ss,ecr}(k) + \tilde{d}_{ecr}(k))$ is produced by the ECR muscle. Finally, let each moment feed into the linear wrist rigid body dynamics, $H(q)$, to produce joint angle $y(k) = H(q)(\tau_{fcr}(k) - \tau_{ecr}(k))$.

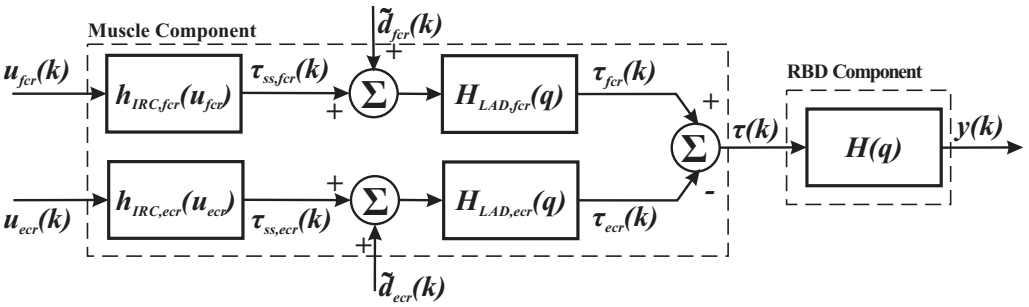

Figure 4.1: General wrist model excited by FES and tremor signal.

As mentioned in Section 2.1.1, the intention tremor is caused by delayed activation of the antagonist muscle, followed by delayed activation of the second agonist muscle. These consecutive activations produce the isometric torques $\tilde{d}_{fcr}(k)$ and $\tilde{d}_{ecr}(k)$ from FCR and ECR muscles, respectively. Thus $\tilde{d}_{fcr}(k)$ and $\tilde{d}_{ecr}(k)$ are imposed by adding to the relevant steady-state torques produced by stimulation. If the delay between the activation of FCR and ECR muscles is $N_p/2$, then a N_p-periodic tremulous motion is monitored in the wrist. With this assumed model, the identification problem can now be defined as follows:

Definition 4.2. Consider the stimulated wrist system defined by Definition 4.1, and let its constituent components be explicitly parametrised by θ. Given a set of sampled input data $\{u_{fcr}(k), u_{ecr}(k)\}_{k=1,\ldots,N}$ and output data$\{y(k)\}_{k=1,\cdots,N}$, the identification problem is stated as finding optimal parameter estimate

$$\hat{\theta} \coloneqq \arg\min_{\theta} \|\varepsilon\|_2 \tag{4.1}$$

with the modelling error characterised by

$$\|\varepsilon\|_2 = \sqrt{\sum_{k=1}^{N} \left(y(k) - \hat{y}(k|k-1)\right)^2} \tag{4.2}$$

where $\hat{y}(k|k-1)$ is the one-step-ahead predicted output associated with the assumed model description

$$\begin{aligned}\hat{y} = H(q,\theta)\Big\{H_{LAD,fcr}(q,\theta)\Big[\tilde{d}_{fcr}(\theta) \ + h_{IRC}(u_{fcr},\theta)\Big] \\ + H_{LAD,ecr}(q,\theta)\ \Big[\tilde{d}_{ecr}(\theta) + h_{IRC}(u_{ecr},\theta)\Big]\Big\} + \nu\end{aligned} \tag{4.3}$$

with a zero mean disturbance ν. Note that the one-step-ahead predicted output $\hat{y}(k|k-1)$ satisfies

$$\min_{\hat{y}(k)} E(y(k) - \hat{y}(k)) \ \Rightarrow \ \hat{y}(k) = \hat{y}(k|k-1). \tag{4.4}$$

The wrist model of Definition 4.1 describes the responses of the wrist joint to the artificial electrical stimulation, u_{fcr} and u_{ecr}, and the tremulous muscle activation, $\tilde{d}_{fcr}$ and $\tilde{d}_{ecr}$. However the joint stability may be worsened by artificial stimulation. To stabilise wrist joint during voluntary movement, flexors (FCR muscles) and extensors (ECR muscles) possess an inherent feature, named muscle co-activation (Sheean, 2002). Thus, a model of the muscle co-activation needs to be added to the controller of FES to guarantee the joint stability. To do this, the muscle co-activation will be modelled in the next subsection and then this model will be employed by the proposed control scheme in Chapter 5.

4.2.2 Muscle Co-activation

Muscle co-activation is defined as the simultaneous activation of antagonist and agonist muscles during voluntary task performance. This modulates mechanical impedance to maintain joint stability (Hogan, 1984; Simmons and Richardson, 1988). Thus FCR and ECR muscles should be stimulated by FES in such a way as to guarantee postural stability. To mimic natural muscle co-activation, the proposed control scheme of Figure 3.1 needs to include an additional component, which is here modelled by a function relating the FES signals to a single control input, defined by $(u_{fcr}(k), u_{ecr}(k))^\top = h_c(u(k))$ where

$$\begin{aligned} u_{fcr} &= \begin{cases} u + u_{c,fcr} & u(k) \in [0, u_{max} - u_{c,fcr}] \\ u_{c,fcr} & u(k) \in [u_{c,ecr} - u_{max}, 0] \end{cases} \\ u_{ecr} &= \begin{cases} u_{c,ecr} & u(k) \in [0, u_{max} - u_{c,fcr}] \\ u_{c,ecr} - u & u(k) \in [u_{c,ecr} - u_{max}, 0] \end{cases} \end{aligned} \tag{4.5}$$

with co-activation levels $u_{c,fcr}$,$u_{c,ecr} \in \mathbb{R}_+$ and maximum stimulation $u_{max} \in \mathbb{R}_+$. FES signals of (4.5) are shown in Figure 4.2. The following proposition addresses selection of co-activation parameters and will be needed in later control development.

Proposition 4.3. *Let the co-activation levels $u_{c,fcr}$ and $u_{c,ecr}$ be chosen to satisfy $h_{IRC,fcr}(u_{c,fcr}) = h_{IRC,ecr}(u_{c,ecr})$. Then the function*

$$h_{IRC}(u) := h_{IRC,fcr}(u_{fcr}) - h_{IRC,ecr}(u_{ecr}) \tag{4.6}$$

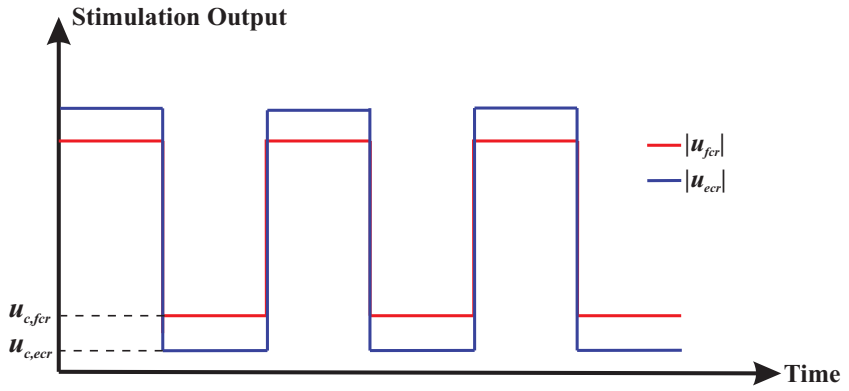

Figure 4.2: Co-activated FES inputs to flexors and extensors over time.

is continuous and monotonic increasing over the domain $u(k) \in [u_{c,ecr} - u_{max}, u_{max} - u_{c,fcr}]$*, with* $h_{IRC}(0) = 0$.

Proof. Inserting (4.5) into (4.6) gives

$$u \mapsto \tau_{ss}, \qquad \tau_{ss} = \tau_{ss,fcr} + \tau_{ss,ecr}$$
$$h_{IRC}(u) = \begin{cases} h_{IRC,fcr}(u + u_{c,fcr}) - h_{IRC,ecr}(u_{c,ecr}) & u \geq 0 \cdot \\ -h_{IRC,ecr}(-u + u_{c,ecr}) + h_{IRC,fcr}(u_{c,fcr}) & u \leq 0 \end{cases} \tag{4.7}$$

From Definition 4.1, $h_{IRC,fcr}(\cdot)$ and $h_{IRC,ecr}(\cdot)$ are continuous and monotonically increasing over their domain $[0, u_{max}]$ and $[-u_{max}, 0]$, respectively. Hence it follows that the domain of $h_{IRC}(u)$ is $[-u_{max}, u_{max}]$. Moreover, since $h_{IRC,fcr}(u_{c,fcr}) = h_{IRC,ecr}(u_{c,ecr})$, $h_{IRC}(u)$ is continuous, monotonic and satisfies $h_{IRC}(0) = 0$. □

Therefore, the co-activation mapping (4.5) has the effect of removing the dead zone inherent in each IRC, with an example shown in Figure 4.3 where a dashed and solid lines are used to denote $u_c \neq 0$ and $u_c = 0$, respectively. The response of (4.7) to the FES inputs in Figure 4.2 is shown in Figure 4.4.

Moreover, the mapping (4.5) transforms the two-input one-output wrist model of Definition 4.1 into a single-input single-output (SISO) model by combining the two input signals $u_{fcr}(k)$ and $u_{ecr}(k)$ into a single input signal $u(k)$. Thus the wrist model illustrated in Figure 4.1 can be simplified by the following assumptions to enable computationally tractable solutions to the identification problem of Definition 4.2.

4.2.3 Model Assumptions

- *Representation of Tremor:* A periodic signal may be represented as a sum of sine and cosine waves at different harmonic frequencies, or integer multiples of the

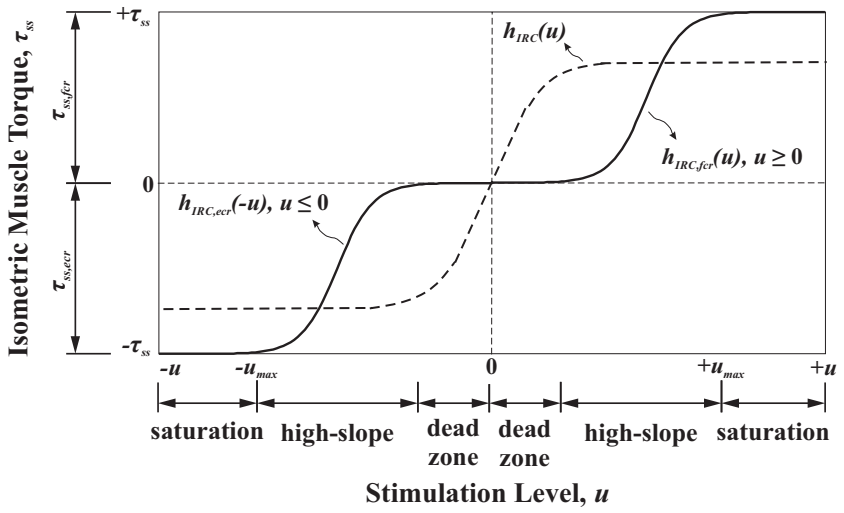

Figure 4.3: The effect of muscle co-activation on IRC function. Solid line represents h_{IRC} without co-activation and dashed line represents h_{IRC} with co-activation.

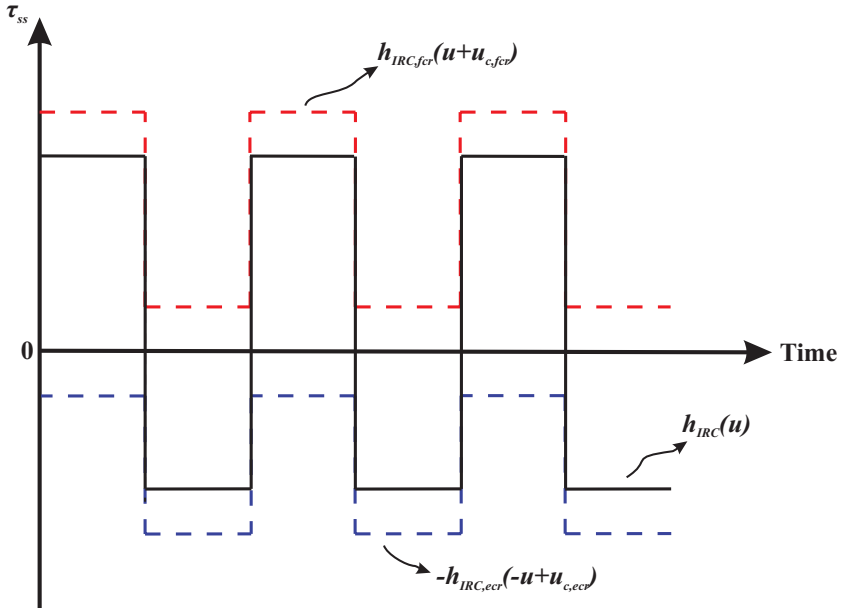

Figure 4.4: Response of $h_{IRC}(u)$ given by (4.7) to the inputs of (4.5) depicted in Figure 4.2.

fundamental frequency (Riviere et al., 1997). Since $\tilde{d}_{fcr}(k)$ and $\tilde{d}_{ecr}(k)$ are N_p-periodic, and can be assumed to contain a maximum N_f harmonic, they can be written as

$$\tilde{d}_{fcr}(k) = A_0^{fcr} + \sum_{i=1}^{N_f} \left\{ A_i^{fcr} \cos\left(\frac{2\pi ik}{N_p}\right) + B_i^{fcr} \sin\left(\frac{2\pi ik}{N_p}\right) \right\}, \tag{4.8}$$

$$\tilde{d}_{ecr}(k) = A_0^{ecr} + \sum_{i=1}^{N_f} \left\{ A_i^{ecr} \cos\left(\frac{2\pi ik}{N_p}\right) + B_i^{ecr} \sin\left(\frac{2\pi ik}{N_p}\right) \right\} \tag{4.9}$$

and hence their sum is given by the N_p-periodic signal

$$\tilde{d}(k) = A_0 + \sum_{i=1}^{N_f} \left\{ A_i \cos\left(\frac{2\pi ik}{N_p}\right) + B_i \sin\left(\frac{2\pi ik}{N_p}\right) \right\} \tag{4.10}$$

with real values $A_i = A_i^{fcr} + A_i^{ecr}$ and $B_i = B_i^{fcr} + B_i^{ecr}$ for $i = 1, \ldots, N_f$. With these definitions, the original model structure of Figure 4.1 is equivalent to Figure 4.5(a).

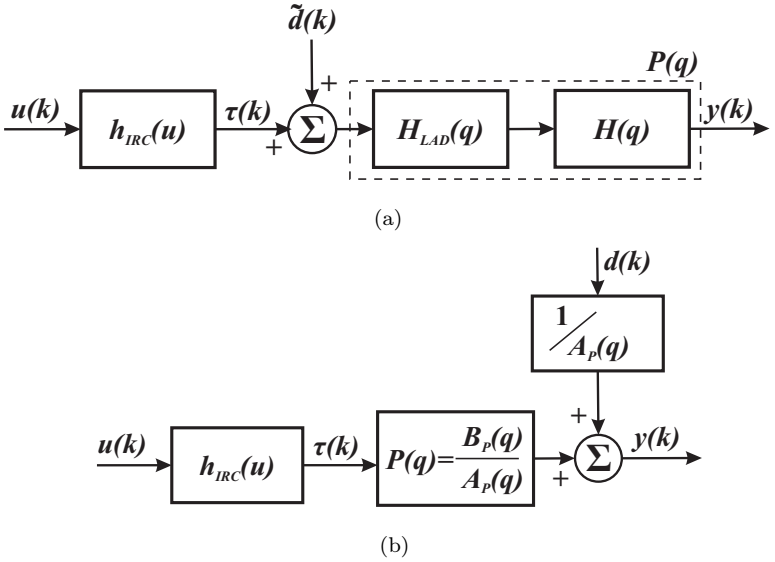

Figure 4.5: Simplified wrist model: (a) Simplified model with co-activation, and (b) Simplified model with equivalent tremor signal representation.

Let the transfer function $P(q) \coloneqq B_P(q)/A_P(q)$. Since $B_P(q)$ is a finite impulse response (FIR) which is inherently stable and $\tilde{d}(k)$ is an N_p-periodic signal, $\lim_{i\to\infty} B_P(q)\tilde{d}(k + iN_P)$ has the form

$$A_0 A_0^P + \sum_{i=1}^{N_f} A_i A_i^P \cos\left(\frac{2\pi ik}{N_p}\right) + B_i B_i^P \sin\left(\frac{2\pi ik}{N_p}\right) \tag{4.11}$$

where A_i^P and B_i^P are real functions of $B_P(q)$. A N_p-periodic signal can then be placed as shown in Figure 4.5(b), which is identical to Figure 4.5(a) given that the tremor signal is steady-state.

Remark 4.4. If only the fundamental frequency component is present in $\tilde{d}(k)$ and non-zero A_0 offset is present, then $N_f = 1$ giving

$$d(k) = A_0 A_0^P + A_1 A_1^P \cos\left(\frac{2\pi k}{N_p}\right) + B_1 B_1^P \sin\left(\frac{2\pi k}{N_p}\right).$$

- *Similarity of LAD of muscles:* It is also assumed that similar muscle groups have similar LAD, so that $H_{LAD,fcr}(q) \cong H_{LAD,ecr}(q)$. This assumption is supported by the similar biophysical properties of the wrist flexors and extensors, and experimental evidence showing that their dynamic responses closely match. Colacino et al. (2012) has modelled LAD of the wrist flexors and extensors as a second-order system consisting of a mass connected in series to a spring and a damper element and reported that these elements of the wrist flexors were very close to those of the wrist extensors. $H_{LAD}(q)$ is further combined with $H(q)$ to form $P(q)$.

Next, the components $h_{IRC}(u)$, $P(q)$ and $d(k)$ appearing in the model of Figure 4.5(b) will be parametrised. Then, the parameters of the components within this simplified model will be defined to form the parameter vector θ given in Definition 4.2. Lastly, an algorithm will be proposed to estimate θ.

4.3 System Identification Algorithm

The components appearing in the model of Figure 4.5(b) are explicitly expressed as linear functions of their parameters. The form of external disturbance ν is then stated, allowing the identification problem of Definition 4.2 to be solved.

4.3.1 Mathematical Representation of System Identification Problem

The linear dynamics of the wrist model take the polynomial form

$$P(q) = \frac{B_P(q)}{A_P(q)} = \frac{b_0 q^{-m_P} + b_1 q^{-(m_P+1)} + \ldots + b_{n_P} q^{-(m_P+n_P)}}{1 + a_1 q^{-1} + \ldots + a_{l_P} q^{-l_P}} \tag{4.12}$$

in which parameters n_P, l_P and m_P denote the number of zeros, poles and the time delay order, respectively. The coefficients of this expression can be written in a vector form

$$\theta_{l_P} = \begin{bmatrix} \theta_{a_P} & \vdots & \theta_{b_P} \end{bmatrix}^\top = \left[a_1 \ \ldots \ a_{l_P} \vdots b_0 \ b_1 \ \ldots \ b_{n_P} \right]^\top.$$

Since $h_{IRC,fcr}(u)$ and $h_{IRC,ecr}(u)$ can be represented as polynomial functions (Le et al., 2010), the continuous compound function $h_{IRC}(u)$ can be represented by the form

$$h_{IRC}(u) = \mu_0 + \mu_1 u + \ldots + \mu_{m-1} u^{m-1} + \mu_m u^m. \tag{4.13}$$

This gives rise to nonlinear parameter vector $\theta_n = [\mu_0 \ \mu_1 \ \dots \ \mu_m]^\top$. Lastly, since $d(k)$ comprises N_f frequency components, (4.11) can be then written in the matrix form:

$$d(k) = \underbrace{\left[1 \cos\left(\frac{2\pi k}{N_p}\right) \sin\left(\frac{2\pi k}{N_p}\right) \cdots \cos\left(\frac{2\pi N_f k}{N_p}\right) \sin\left(\frac{2\pi N_f k}{N_p}\right)\right]}_{X} \underbrace{\left[\lambda_0 \ \lambda_1^A \ \lambda_1^B \ \cdots \ \lambda_{N_f}^A \ \lambda_{N_f}^B\right]^\top}_{\theta_d}$$
$$:= d(\theta_d) \tag{4.14}$$

where λ_0,λ_1^A,λ_1^B,...,$\lambda_{N_f}^A$,$\lambda_{N_f}^B$ are scalar amplitudes. This yields parameter vector $\theta_d = [\lambda_0 \ \lambda_1^A \ \lambda_1^B \ \cdots \ \lambda_{N_f}^A \ \lambda_{N_f}^B]^\top$.

The parameters corresponding to linear model components can be grouped into the linear parameter vector $\theta_l = \left[\theta_{l_p} \ \theta_d\right]^\top$, so that the composite parameter vector is given by $\theta = [\theta_n \ \theta_l]^\top$. It is now necessary to provide a precise form of the external disturbance signal, ν, appearing in (4.3). This is selected as $\nu(k) = A_P(q)^{-1}w(k)$, where w is zero mean white noise, leading to the overall autoregressive exogenous (ARX) model structure shown in Figure 4.6.

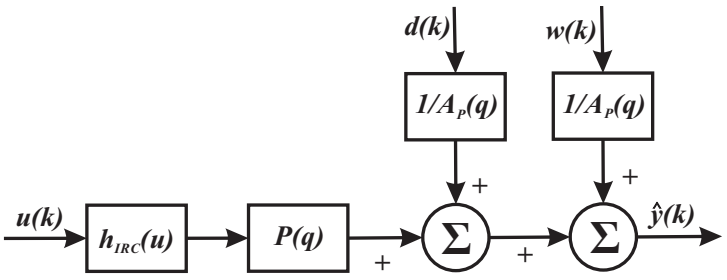

Figure 4.6: ARX type model structure of the wrist model.

Substituting the foregoing expressions into the expression for the output $\hat{y}(k)$ given by (4.3) the model description can be written as

$$\hat{y}(k) = \frac{B_P(q)}{A_P(q)} h_{IRC}(u(k), \hat{\theta}_n) + \frac{1}{A_P(q)} d(k) + \frac{1}{A_P(q)} w(k). \tag{4.15}$$

Using (4.15) and following (Ljung, 1999), the corresponding one-step-ahead minimising solution to the minimisation (4.4) is then given by

$$\hat{y}(k|k-1) = B_P(q) h_{IRC}(u(k), \hat{\theta}_n) + [1 - A_P(q)]y(k) + d(k).$$

Hence the prediction error $\varepsilon(k)$ appearing in the modelling error norm (4.2) is

$$\varepsilon(k) = y(k) - \hat{y}(k|k-1) = A_P(q)y(k) - B_P(q)h_{IRC}(u(k), \hat{\theta}_n) - d(k). \tag{4.16}$$

Next note that the biophysical properties of muscle mean that the function (4.13) is monotonically increasing. Thus θ_n should be estimated such that $h_{IRC}(u)$ is a strictly increasing continuous function on $[-u_{max}, u_{max}]$ with $h_{IRC}(u)$ differentiable at each point

$u_0 \in (u_{-max}, u_{max})$. This corresponds to the condition

$$\left.\frac{dh_{IRC}}{du}\right|_{u=u_0} = \mu_1 + \ldots + \mu_{m-1}(m-1)u^{m-2} + \mu_m m u^{m-1} \geq 0. \tag{4.17}$$

Substituting (4.16) into (4.1), the original identification problem (4.1) now becomes

$$\hat{\theta} = \arg\min_{\theta} \left\| A_P(q)y - B_P(q)h_{IRC}(u, \hat{\theta}_n) - d(\hat{\theta}_d) \right\|_2 \tag{4.18}$$

subject to the monotonicity constraint of (4.17). Now, the identification problem (4.18) can be solved by the following iterative method.

4.3.2 Nonlinear Parameter Identification

The problem (4.18) cannot be solved using standard methods due to its nonlinear form and hence, an iterative scheme is now proposed.This involves firstly identifying nonlinear parameter θ_n using fixed θ_l, and subsequently identifying linear parameter θ_l with fixed θ_n. The former optimisation is given by

$$\hat{\theta}_n = \arg\min_{\theta_n} \left\| A_P(q)y - B_P(q)\, h_{IRC}(u, \hat{\theta}_n) - d(\hat{\theta}_d) \right\|_2 \quad \text{subject to} \quad A\theta_n \geq 0 \tag{4.19}$$

where the constraint enforces monotonic condition (4.17). Now, $A_P(q)y$ of (4.19) can be expressed as

$$y(k) + \hat{a}_1 y(k-1) + \cdots + \hat{a}_{l_P} y(k-l_P)\ ;\ k = l_P + 1, \ldots, N \tag{4.20}$$

or equivalently in matrix form

$$Y_n\left(y, \hat{\theta}_{a_P}\right) = \begin{bmatrix} y(l_P+1) + \hat{a}_1 y(l_P) + \cdots + \hat{a}_{l_P} y(1) \\ y(l_P+2) + \hat{a}_1 y(l_P+1) + \cdots + \hat{a}_{l_P} y(2) \\ \vdots \\ y(N) + \hat{a}_1 y(N-1) + \cdots + \hat{a}_{l_P} y(N-l_P) \end{bmatrix}. \tag{4.21}$$

From (4.13), it follows that $h_{IRC}(u, \theta_n)$ is linear in θ_n, and hence

$$\begin{aligned}\left(\hat{B}_P(q)\, h_{IRC}(u, \hat{\theta}_n)\right)(k) = \mu_0 \underbrace{\left(\hat{b}_0 + \cdots + \hat{b}_{n_P}\right)}_{h_{IRC_0}(u(k), \hat{\theta}_{b_P})} + \mu_1 \underbrace{\left(\hat{b}_0 u(k-m_P) + \cdots + \hat{b}_{n_P} u(k-m_P-n_P)\right)}_{h_{IRC_1}(u(k), \hat{\theta}_{b_P})} \\ + \cdots + \mu_m \underbrace{\left(\hat{b}_0 u(k-m_P)^m + \cdots + \hat{b}_{n_P} u(k-m_P-n_P)^m\right)}_{h_{IRC_m}(u(k), \hat{\theta}_{b_P})}\end{aligned} \tag{4.22}$$

and can be written in matrix form

$$\Phi_n\left(u,\hat{\theta}_{b_P}\right)\hat{\theta}_n = \begin{bmatrix} h_{IRC_0}(u(l_P+1),\hat{\theta}_{b_P}) & \cdots & h_{IRC_m}(u(l_P+1),\hat{\theta}_{b_P}) \\ h_{IRC_0}(u(l_P+2),\hat{\theta}_{b_P}) & \cdots & h_{IRC_m}(u(l_P+2),\hat{\theta}_{b_P}) \\ \vdots & & \vdots \\ h_{IRC_0}(u(N),\hat{\theta}_{b_P}) & \cdots & h_{IRC_m}(u(N),\hat{\theta}_{b_P}) \end{bmatrix} \begin{bmatrix} \mu_0 \\ \mu_1 \\ \vdots \\ \mu_m \end{bmatrix}. \tag{4.23}$$

Using (4.14), $d(\hat{\theta}_d)$ of (4.19) can be written as

$$\begin{aligned} D(\hat{\theta}_d) &= \begin{bmatrix} \hat{\lambda}_0+\hat{\lambda}_1^A\cos\frac{2\pi(l_P+1)}{N_p}+\hat{\lambda}_1^B\sin\frac{2\pi(l_P+1)}{N_p}+\cdots+\hat{\lambda}_{N_f}^A\cos\frac{2\pi N_f(l_P+1)}{N_p}+\hat{\lambda}_{N_f}^B\sin\frac{2\pi N_f(l_P+1)}{N_p} \\ \hat{\lambda}_0+\hat{\lambda}_1^A\cos\frac{2\pi(l_P+2)}{N_p}+\hat{\lambda}_1^B\sin\frac{2\pi(l_P+2)}{N_p}+\cdots+\hat{\lambda}_{N_f}^A\cos\frac{2\pi N_f(l_P+2)}{N_p}+\hat{\lambda}_{N_f}^B\sin\frac{2\pi N_f(l_P+2)}{N_p} \\ \vdots \\ \hat{\lambda}_0+\hat{\lambda}_1^A\cos\frac{2\pi N}{N_p}+\hat{\lambda}_1^B\sin\frac{2\pi N}{N_p}+\cdots+\hat{\lambda}_{N_f}^A\cos\frac{2\pi N_f N}{N_p}+\hat{\lambda}_{N_f}^B\sin\frac{2\pi N_f N}{N_p} \end{bmatrix} \\ &= \underbrace{\begin{bmatrix} 1 & \cos\frac{2\pi(l_P+1)}{N_p} & \sin\frac{2\pi(l_P+1)}{N_p} & \cdots & \cos\frac{2\pi N_f(l_P+1)}{N_p} & \sin\frac{2\pi N_f(l_P+1)}{N_p} \\ 1 & \cos\frac{2\pi(l_P+2)}{N_p} & \sin\frac{2\pi(l_P+2)}{N_p} & \cdots & \cos\frac{2\pi N_f(l_P+2)}{N_p} & \sin\frac{2\pi N_f(l_P+2)}{N_p} \\ \vdots & \vdots & \vdots & & \vdots & \vdots \\ 1 & \cos\frac{2\pi N}{N_p} & \sin\frac{2\pi N}{N_p} & \cdots & \cos\frac{2\pi N_f N}{N_p} & \sin\frac{2\pi N_f N}{N_p} \end{bmatrix}}_{X} \underbrace{\begin{bmatrix} \hat{\lambda}_0 \\ \hat{\lambda}_1^A \\ \hat{\lambda}_1^B \\ \vdots \\ \hat{\lambda}_{N_f}^A \\ \hat{\lambda}_{N_f}^B \end{bmatrix}}_{\hat{\theta}_d}. \end{aligned} \tag{4.24}$$

Substituting (4.21), (4.23) and (4.24) into (4.19), the constrained linear least-squares problem of (4.19) hence becomes

$$\hat{\theta}_n = \arg\min_{\theta_n} \left\| Y_n\left(y,\hat{\theta}_{a_P}\right) - \Phi_n\left(u,\hat{\theta}_{b_P}\right)\hat{\theta}_n - D(\hat{\theta}_d)\right\|_2 \quad \text{subject to} \quad A\theta_n \geq 0 \tag{4.25}$$

where

$$A = \begin{bmatrix} 0 & 1 & \cdots & (m-1)u(l_P+1)^{m-2} & mu(l_P+1)^{m-1} \\ 0 & 1 & \cdots & (m-1)u(l_P+2)^{m-2} & mu(l_P+2)^{m-1} \\ \vdots & \vdots & & \vdots & \vdots \\ 0 & 1 & \cdots & (m-1)u(N)^{m-2} & mu(N)^{m-1} \end{bmatrix}.$$

This type of constrained nonlinear problem can be readily solved using an *interior-point method* to yield $\hat{\theta}_n$.

4.3.3 Linear Parameter Identification

Given an estimate $\hat{\theta}_n$ of nonlinear parameter vector θ_n, cost function (4.18) can be minimized with respect to the linear parameter vector. This linear least squares minimisation

problem is given by

$$\hat{\theta}_l = \arg\min_{\theta_l} \left\| A_P(q)y - B_P(q)\, h_{IRC}(u, \hat{\theta}_n) - d(\hat{\theta}_d) \right\|_2$$

where

$$\begin{aligned} B_P(q)\, h_{IRC}(u,\, \hat{\theta}_n) =& b_0 \underbrace{\left[\hat{\mu}_m u(k-m_P)^m + \hat{\mu}_{m-1} u(k-m_P)^{m-1} + \ldots + \hat{\mu}_1 u(k-m_P) + \hat{\mu}_0\right]}_{h_{IRC}\left(u(k-m_P),\hat{\theta}_n\right)} + \cdots \\ & + b_{n_P} \underbrace{\left[\hat{\mu}_m u(k-m_P-n_P)^m + \ldots + \hat{\mu}_1 u\,(k-m_P-n_P) + \hat{\mu}_0\right]}_{h_{IRC}\left(u(k-m_P-n_P),\hat{\theta}_n\right)} \end{aligned}$$

or equivalently in matrix form

$$\hat{\theta}_l = \arg\min_{\theta_l} \left\| Y_l - \Phi_l\left(u, y, \hat{\theta}_n\right)\theta_{l_P} - X\hat{\theta}_d \right\|_2 \tag{4.26}$$

where

$$Y_l = \left[y\,(l_P+1) \;\; y\,(l_P+2) \;\; \ldots \;\; y\,(N)\right]^\top,$$

$$X = \begin{bmatrix} 1 & \cos\frac{2\pi(l_P+1)}{N_p} & \sin\frac{2\pi(l_P+1)}{N_p} & \cdots & \cos\frac{2\pi N_f(l_P+1)}{N_p} & \sin\frac{2\pi N_f(l_P+1)}{N_p} \\ 1 & \cos\frac{2\pi(l_P+2)}{N_p} & \sin\frac{2\pi(l_P+2)}{N_p} & \cdots & \cos\frac{2\pi N_f(l_P+2)}{N_p} & \sin\frac{2\pi N_f(l_P+2)}{N_p} \\ \vdots & \vdots & \vdots & & \vdots & \vdots \\ 1 & \cos\frac{2\pi N}{N_p} & \sin\frac{2\pi N}{N_p} & \cdots & \cos\frac{2\pi N_f N}{N_p} & \sin\frac{2\pi N_f N}{N_p} \end{bmatrix}, \tag{4.27}$$

$$\Phi_l\left(u, y, \hat{\theta}_n\right) =$$

$$\begin{bmatrix} -y(l_P) & \cdots & -y(1) & h_{IRC}(u(l_P+1-m_P),\hat{\theta}_n) & \cdots & h_{IRC}(u(l_P+1-m_P-n_P),\hat{\theta}_n) \\ -y(l_P+1) & \cdots & -y(2) & h_{IRC}(u(l_P+2-m_P),\hat{\theta}_n) & \cdots & h_{IRC}(u(l_P+2-m_P-n_P),\hat{\theta}_n) \\ \vdots & & \vdots & \vdots & & \vdots \\ -y(N-1) & \cdots & -y(N-l_P) & h_{IRC}(u(N-m_P),\hat{\theta}_n) & \cdots & h_{IRC}(u(N-m_P-n_P),\hat{\theta}_n) \end{bmatrix} \tag{4.28}$$

Concatenating (4.28) and (4.27) horizontally yields

$$\Phi_{ld}\left(u, y, \hat{\theta}_n, X\right) = \left[\; \Phi_l\left(u, y, \hat{\theta}_n\right) \quad X \;\right].$$

Hence (4.26) can be rewritten in the form

$$\hat{\theta}_l = \arg\min_{\theta_l} \left\| Y_l - \Phi_{ld}\left(u, y, \hat{\theta}_n, X\right)\theta_l \right\|_2. \tag{4.29}$$

The solution of (4.29) is

$$\hat{\theta}_l = \left(\Phi_{ld}\left(u, y, \hat{\theta}_n, X\right)^\top \Phi_{ld}\left(u, y, \hat{\theta}_n, X\right)\right)^{-1} \Phi_{ld}\left(u, y, \hat{\theta}_n, X\right)^\top Y_l.$$

4.3.4 Algorithmic Summary

Minimization over the θ_n and θ_l parameters can be executed iteratively assuming the initial component values $\hat{\theta}_l^0$ and $\hat{\theta}_n^0$, an input/output data set $\{u(k),\, y(k)\}_{k=1,2,\ldots,N}$ and a convergence tolerance ϵ. This yields Algorithm 1.

Algorithm 1: Iterative algorithm for identifying the parameter vector θ

$j = 0$
repeat
$j = j + 1$
$\hat{\theta}_n^j \coloneqq \arg\min_{\theta_n} \left\| A_P(q)y - B_P(q)\, h_{IRC}(u, \hat{\theta}_n^j) - d(\hat{\theta}_d^j) \right\|_2$ subject to (4.19)
$\hat{\theta}_l^j = \left(\Phi_{ld}(u, y, \hat{\theta}_n^j, X)^\top \Phi_{ld}(u, y, \hat{\theta}_n^j, X)\right)^{-1} \Phi_{ld}(u, y, \hat{\theta}_n^j, X) Y_l$
until $\left| \begin{bmatrix} \hat{\theta}_n^j & \hat{\theta}_l^j \end{bmatrix}^\top - \begin{bmatrix} \hat{\theta}_n^{j-1} & \hat{\theta}_l^{j-1} \end{bmatrix}^\top \right| < \epsilon$
Output: $\hat{\theta} = \begin{bmatrix} \hat{\theta}_n^j & \hat{\theta}_l^j \end{bmatrix}^\top$

4.4 Simulation Study

Before applying Algorithm 1 experimentally within Chapter 6, simulations are now performed using a known wrist model in order to evaluate the performance of Algorithm 1 for estimating parameter vector θ. This pre-existing model has been obtained using an identification method involved isometric tests using a force sensor followed by nonisometric tests using encoder measurement (Verstappen et al., 2012; Copur et al., 2014). The large number of tests made the procedure unsuitable for clinical application, but yielded an accurate model. This model comprised a 4^{th} order polynomial function $h_{IRC}(u)$ and 4^{th} order transfer function of $P(q)$. The most accurate model has been chosen amongst the identified models whose the nonlinear part were modelled by

$$h_{IRC}(u) = 1 + 4.5573u - 2.0307u^2 + 1.2345u^3 + 0.6710u^4 \tag{4.30}$$

and the linear part was modelled by

$$P(q) = \frac{0.0157q^{-1} - 0.0781q^{-2} + 0.1205q^{-3} - 0.0729q^{-4}}{1 - 1.4156q^{-1} + 0.2196q^{-2} + 0.2234q^{-3} - 0.0017q^{-4}}. \tag{4.31}$$

Algorithm 1 was applied to estimate the parameters of (4.30) and (4.31) using purely input and output data. Then the estimated parameters $\hat{\theta}$ has been compared with the real parameters given by

$$\theta_l = [-1.4156\ 0.2196\ 0.2234\ -0.0017\ 0.0157\ -0.0781\ 0.1205\ -0.0729]^\top$$

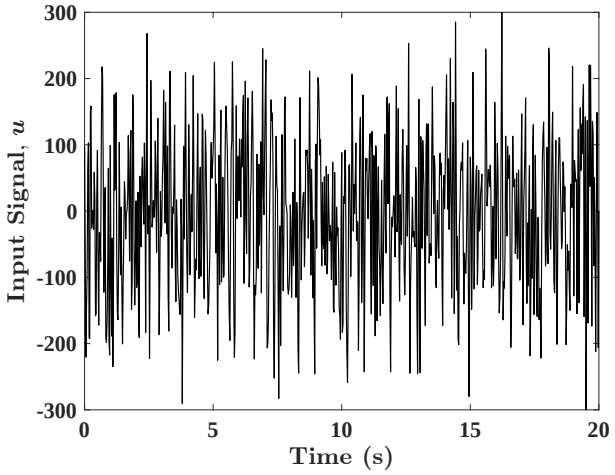

Figure 4.7: Plot of the Gaussian white noise signal.

and

$$\theta_n = [1 \ 4.5573 \ -2.0307 \ 1.2345 \ 0.6710]^\top.$$

As mentioned previously, Algorithm 1 requires selecting initial values of $\hat{\theta}$. The initial nonlinear component value $\hat{\theta}_n^0$ has been selected as the mean value of the parameter estimates $\hat{\theta}_n$ of 4^{th} order polynomial functions which have been previously identified by Copur et al. (2014). The initial linear component value $\hat{\theta}_l^0$ has been defined in an analogous manner to that of $\hat{\theta}_n^0$. The resulting initial component values were $\hat{\theta}_n^0 = [0.5687 \ -0.9168 \ 0.6027 \ -1.3913 \ -0.2634]^\top$ and $\hat{\theta}_l^0 = [-1.7207 \ 0.5626 \ 0.3639 \ -0.1868 \ -0.0303 \ 0.0312 \ -0.0563 \ 0.0092]^\top$. Then the model comprising of (4.30) and (4.31) has been excited by a Gaussian white noise signal u as shown in Figure 4.7 to acquire an output signal y that included sufficient dynamical information to characterise the wrist model. Following this, the iterative computation has been performed until the error ϵ in Algorithm 1 is less than 10^{-4}.

The algorithm solved the identification problem in less than 4 seconds and produced an estimate of the parameter vector at the end of 13 iterations. Figure 4.8 compares the acquired output y with the predicted output $\hat{y}$. Figure 4.9 compares the results of the isometric muscle torque τ_{ss} obtained from (4.30) and that produced by the modelled $h_{IRC}(u)$ function, with parameters identified by Algorithm 1. Figure 4.10 shows the convergence of $\hat{\theta}_n$ and $\hat{\theta}_l$ as a function of the iteration number. From Figure 4.10, it can be seen that all parameters converge to fixed values at the conclusion of the iterations.

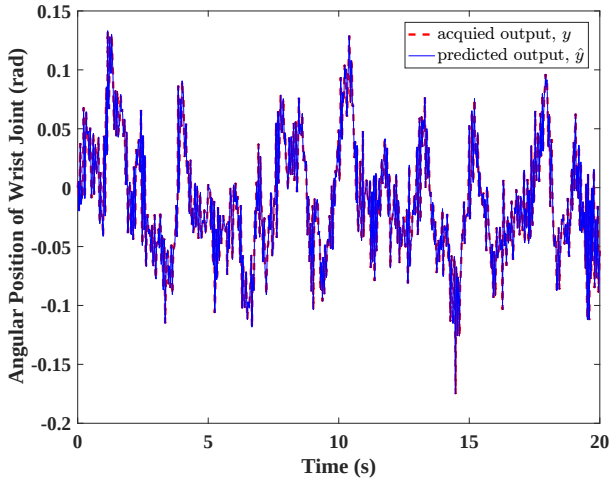

Figure 4.8: Comparison of the acquired output y and the predicted output $\hat{y}$ obtained from the solution of the Algorithm 1.

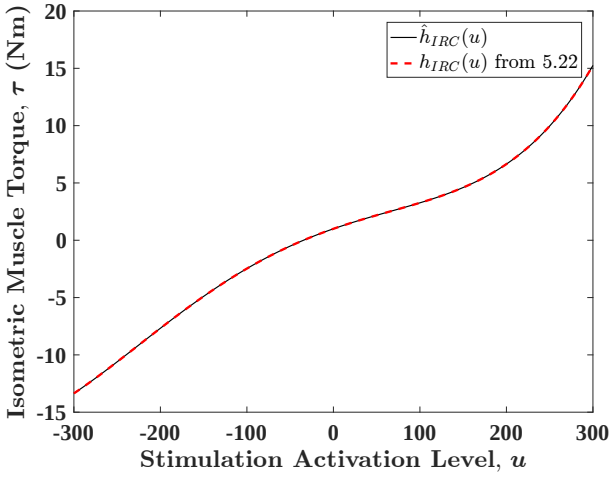

Figure 4.9: The comparison of h_{IRC} in 4.30 (dashed line) with h_{IRC} identified by Algorithm 1 (solid line).

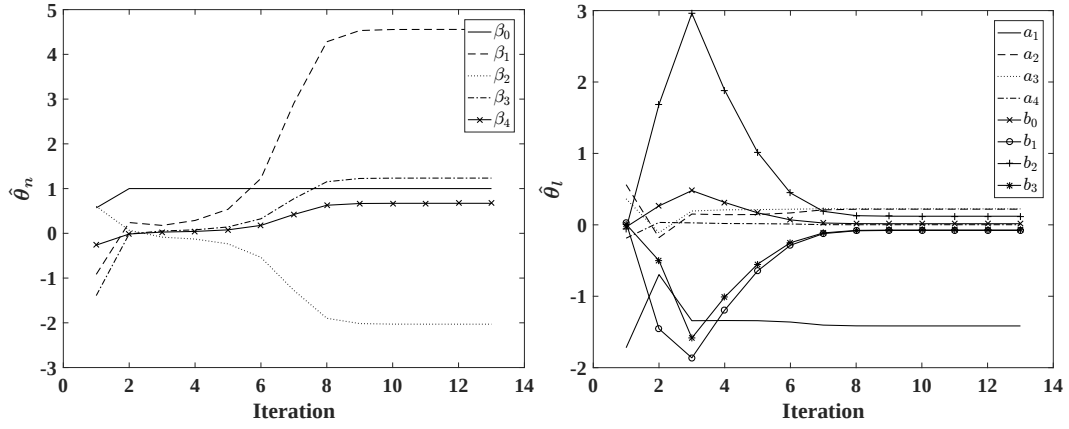

(a) (b)

Figure 4.10: Converges of a) $\hat{\theta}_n$ and b) $\hat{\theta}_l$ at each iteration.

Table 4.1 and Table 4.2 show the final values obtained by application of Algorithm 1 and compares them with the known parameters of the model in (4.30) and (4.31). It is clear that Algorithm 1 succeeded in solving the linear and nonlinear problems.

Table 4.1: The final values of the solution of the linear problem.

	a_1	a_2	a_3	a_4	b_0	b_1	b_2	b_3
θ_l	-1.4156	0.2196	0.2234	0.0017	0.0157	-0.0781	0.1205	-0.0729
$\hat{\theta}_l$	-1.4156	0.2196	0.2234	0.0017	0.0157	-0.0781	0.1205	-0.0729

Table 4.2: The final values of the solution of the nonlinear problem.

	β_0	β_1	β_2	β_3	β_4
θ_n	1.0000	4.5573	-2.0307	1.2345	0.6710
$\hat{\theta}_n$	1.0000	4.5573	-2.0307	1.2345	0.6710

To examine the sensitivity of the identification procedure to the initial component values $\hat{\theta}_l^0$ and $\hat{\theta}_n^0$, the proposed algorithm is executed again using a number of initial values. Figure 4.11 shows that the parameters can converge to their true values in 12 iterations, like in the previous simulation, when the initial values are selected to be $\hat{\theta}_n^0 = [\ 0.5 \quad \mathbf{0}_{1\times 4}\ ]^\top$ and $\hat{\theta}_l^0 = \mathbf{0}_{8\times 1}$ where $\mathbf{0}_{i\times j}$ denotes a zero matrix of a dimension $i \times j$. Thus the algorithm is insensitive to a change in the initial values.

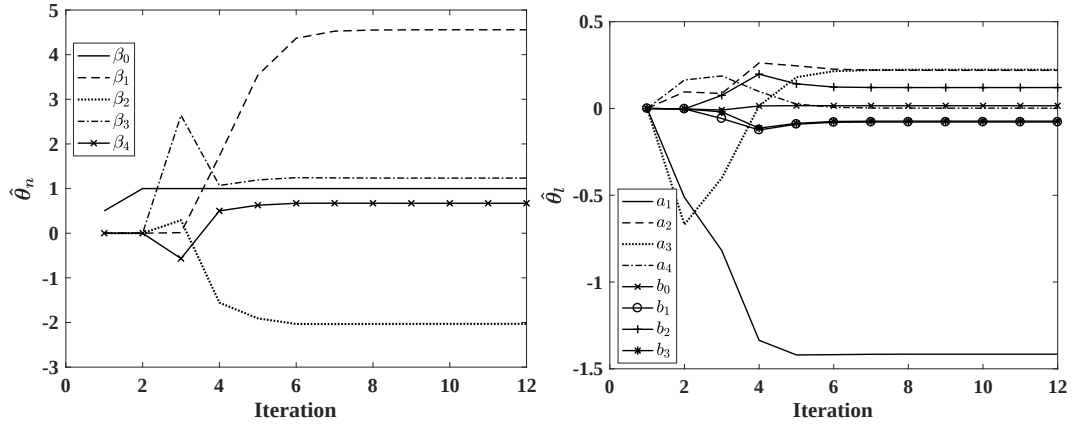

(a) (b)

Figure 4.11: Converges of a) $\hat{\theta}_n$ and b) $\hat{\theta}_l$ at each iteration with different initial values.

4.5 Summary

This chapter has introduced a model structure and identification procedure that are appropriate for clinical application with patients. A nonlinear model structure has been proposed to model wrist joint dynamics for the purpose of tremor suppression. Simulation results showed that the parameters approach their true values. In modelling, the following assumptions have been made:

- FL and FV components of muscle dynamics can be neglected since joint ranges and velocities are small in most applications. Thus the muscle dynamics can be represented by a Hammerstein structure.
- Joint dynamics $H(q)$ can be represented by a linear, time invariant system.
- Tremor can be represented by a sum of finite number of harmonics and similar muscle groups have similar linear dynamics.

The key advantages of the proposed model structure with the identification procedure are as follows:

- The model captures critical nonlinear recruitment characteristics to overcome the accuracy limitations of the previous approaches, while simultaneously embedding muscle co-activation to reduce deadzone.
- With the aforementioned assumptions, the model in Definition 4.1 can be transformed to a SISO form which simplifies the identification problem in Definition 4.2.
- The overall structure can be linearised in a transparent manner in order to extend the range of admissible control schemes for subsequent tremor suppression. Since h_{IRC} is invertible on its domain due to its monotonicity, linearising action is applied by adding the inverse of h_{IRC} into the control structure and its inverse cancels the nonlinearity of the simplified model shown in Figure 4.5(a). Then the system can be represented in the linear form of Figure 3.1 and therefore the RC scheme of Section 3.3 can be directly applied.
- The proposed identification procedure is of short duration and can be automated. Additionally, it is appropriate for use by both patients and clinicians since it does not require fine-tuning, which can only be achieved by a technician, to identify a reliable model for the design of an effective RC, thereby addressing major shortcomings encountered in previous studies.

However, the identification algorithm and the model structure have some limitations which are as follows:

- Higher number of harmonics in (4.10) enables $\tilde{d}(k)$ to correspond more closely to the actual input that produces tremulous motion. Likewise, a more accurate model can be identified using a model $P(q)$ with higher order. However these selections also lead to more parameters to be estimated. Thus the solution of the identification problem becomes more difficult or an accurate parameter estimation cannot be achieved.

- Note that the SISO system is obtained based on the assumption that the FCR and ECR muscles have similar linear activation dynamics. This may not be reasonable for all patients. If this is the case, then the accuracy of the model becomes poorer. However this limitation can be addressed by solving an identification problem of a multi-input single-output system including two different Hammerstein structures arranged in parallel and then connected in cascade with the joint dynamics, as shown in Figure 4.1. Established identification methods for MISO Hammerstein systems (Kortmann and Unbehauen, 1987; Boutayeb and Darouach, 1995) can be adopted to solve such an identification problem.

Despite of the possible limitations, experimental results in Chapter 6 will confirm that the proposed identification procedure is successful to identify a model with a good performance in both validation and cross-validation. Having developed the system procedure in this section to identify a reliable model, a linear tremor suppression control design will be proposed in the next chapter where RC algorithms will be examined in detail and a mechanism will be proposed to preserve the voluntary actions.

Chapter 5

Repetitive Control Framework for Tremor Suppression

This chapter will combine the RC scheme proposed in Section 3.3 and the wrist model developed in Chapter 4 in order to produce a closed-loop control scheme which is suitable for clinical application. In doing so, the framework exploits the linearising control action studied in Chapter 4 which will lead to a transparent design procedure. To do this, a fuller description of the internal model principle is first provided, and is used to derive more explicit convergence criteria, with focus on the RC algorithms proposed previously. Then a mechanism is introduced to preserve the voluntary action of the user in the presence of the FES control scheme. This addresses the issue highlighted in Chapter 3 which indicates that a conflict exists between FES and voluntary intention. The outcome of this conflict is higher voluntary interference as a result of a demand of higher tremor suppression.

5.1 Internal Model Principle

Having shown in simulation the advantage of the RC framework over the filtering techniques described and implemented in Chapter 3, this section explains in detail why IMP based RC schemes enable tremor to be suppressed completely. As mentioned in Section 3.3, the IMP was developed by Francis and Wonham (1975), and states that to reject a disturbance $\tilde{d}$ completely or track a reference y_{ref} perfectly, a signal generator, which is capable of producing disturbance $\tilde{d}$ or reference y_{ref}, must be implemented in the controller $C(q)$ (Steinbuch, 2002; Van den Eerenbeemt, 2003). Section 3.3 proposed an internal model, $IM(q)$, taking the form of $(q^{N_p} - 1)^{-1}$, which represents a memory loop consisting of a positive feedback loop with a time-delay element in the forward path. This form of $IM(q)$ clearly can generate any N_p-periodic signal through a suitable choice of initial conditions, and hence $IM(q)$ is capable of learning the N_p-periodic signal $\tilde{d}$ that

is desired to be cancelled. The IMP then simply requires that the closed-loop system is stabilised. To examine further how this form led to complete tremor suppression in the simulations of Section 3.3, consider the closed-loop system shown in Figure 5.1, which is identical to Figure 3.9.

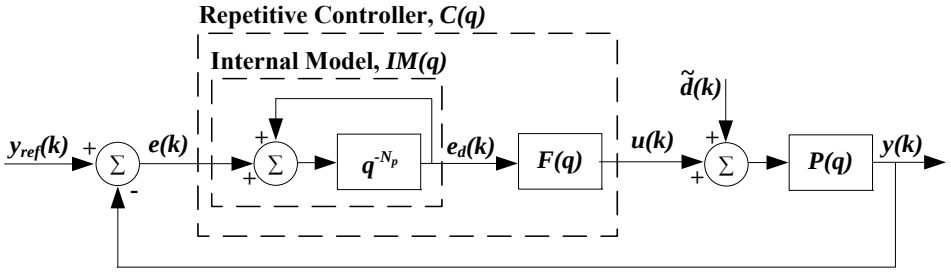

Figure 5.1: Standard repetitive control scheme.

Assuming that y_{ref} and $\tilde{d}$ have periods of N_p samples, the internal model in this system is clearly $(q^{N_p}-1)^{-1}$ which can be rearranged as

$$IM(q) = q^{-N_p}\left(1-q^{-N_p}\right)^{-1}. \tag{5.1}$$

Without loss of generality, let the sampling period be $T_s = 1$. Then substituting $q = e^{j\omega}$ into (5.1) yields

$$IM(e^{j\omega}) = e^{-j\omega N_p}\left(1-e^{-j\omega N_p}\right)^{-1} \tag{5.2}$$

Now consider the response at the frequency of the periodic disturbance, and its multiples, given by $\omega = k(2\pi/N_p)$, $k \in \mathbb{N}^+$. Rearranging (5.2) yields

$$IM(e^{j\omega}) = \frac{e^{-jk2\pi}}{1-e^{-jk2\pi}} = \frac{1}{e^{jk2\pi}-1} \quad ; \quad k = 1, 2, \ldots \tag{5.3}$$

and the magnitude response of (5.3) clearly goes to infinity at the fundamental frequency and harmonics of the disturbance/reference signal since

$$e^{jk2\pi} - 1 = \cos(k2\pi) + j\sin(k2\pi) - 1 = 0 \quad ; \quad k = 1, 2, \ldots \tag{5.4}$$

This is illustrated in Figure 5.2. The relationship linking the disturbance input, $\tilde{d}$ and the output, y, depicted in Figure 5.1, is

$$y(k) = P(q)\left(1 + C(q)P(q)\right)^{-1}\tilde{d}(k) = P(q)\left(1 + IM(q)F(q)P(q)\right)^{-1}\tilde{d}(k) \tag{5.5}$$

in which $F(q)$ is chosen to satisfy the convergence criteria given in Chapter 3 by either

$$\left\|1 - P(q)F(q)\right\|_\infty < 1 \tag{5.6}$$

or

$$\sup_{\omega\in[0,2\pi]} \left|1 - P(e^{j\omega})F(e^{j\omega})\right| < 1, \tag{5.7}$$

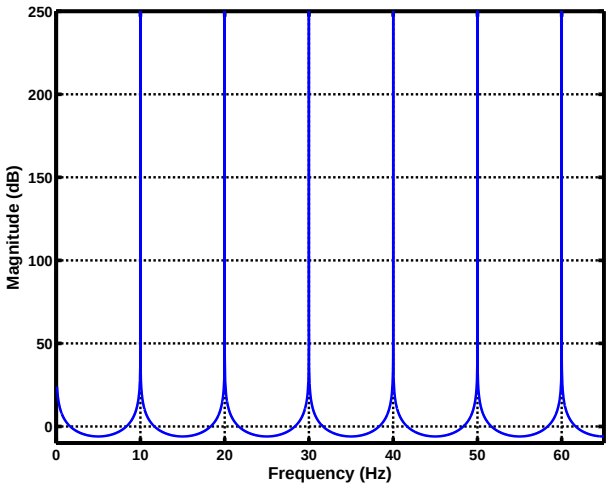

Figure 5.2: Magnitude of the frequency response of $IM(z)$ for a periodic signal at 10 Hz with $T_s = 0.001s$ (here $N_pT_s = 0.1$, $\omega = 20\pi k$).

assuming that $1 - P(q)F(q)$ is internally stable. Substituting $q = e^{j\omega}$ and internal model (5.3) into (5.5), and then rearranging the resulting equation leads to

$$\frac{y}{\tilde{d}} = \frac{P\left(e^{j\omega}\right)\left(e^{jk2\pi} - 1\right)}{e^{jk2\pi} - 1 + F\left(e^{j\omega}\right)P\left(e^{j\omega T}\right)} \quad ; \quad k = 1, 2, \ldots \tag{5.8}$$

over the choice of frequencies $\omega = k(2\pi/N_p)$, $k \in \mathbb{N}^+$. Applying (5.4) to (5.8) confirms complete suppression of N_p-periodic disturbance signals at the fundamental frequency and its harmonics. Additionally, the output, y and the reference signal, y_{ref} are related by

$$y(k) = IM(q)F(q)P(q)\left(1 + IM(q)F(q)P(q)\right)^{-1} y_{ref}(k) \tag{5.9}$$

in which $F(q)$ is chosen to satisfy the stability condition of either (5.6) or (5.7). Similarly, substituting $q = e^{j\omega}$ and internal model (5.3) into (5.5), and then rearranging the resulting equation leads to

$$\frac{y}{y_{ref}} = \frac{F\left(e^{j\omega}\right)P\left(e^{j\omega}\right)}{e^{jk2\pi} - 1 + F\left(e^{j\omega}\right)P\left(e^{j\omega T}\right)} \quad ; \quad k = 1, 2, \ldots \tag{5.10}$$

over the choice of frequencies $\omega = k(2\pi/N_p)$, $k \in \mathbb{N}^+$. Applying (5.4) to (5.10) confirms perfect tracking of N_p-periodic reference signals at the fundamental frequency and its harmonics. Thus a RC scheme is theoretically able to eliminate the disturbance signals completely and to track the reference signals perfectly, which operate at these frequencies. However, the convergence condition of either (5.6) or (5.7) must be satisfied to produce perfect tracking and/or complete suppression. As mentioned in Section 3.3, both conditions are certainly satisfied if $F(q)$ is selected to be the right inverse of the modelled plant $P(q)$. However, this is mostly impossible due to the instability arising from either the zeros outside unit circle of $P(q)$ or the difference between the modelled and true plants. Therefore $F(q)$ should be designed to satisfy either (5.6) and (5.7).

To achieve it, Section 3.3 introduced two popular methods, namely frequency modified inverse RC (FMI-RC) and gradient based RC (GB-RC).

Now, the following section will first explain why the recursive form of $F(q)$, which is used by both algorithms, is needed. Next, it will present a modified FMI-RC algorithm that can address some issues related to a small change in tremor frequency or the sensitivity of RC scheme to high frequency noise. Lastly, it will introduce a method for the GB-RC algorithm to guarantee that the length of the impulse response of $P(q)$ is less than N_p since $F(q)$ is designed based on this assumption in Section 3.3.

5.2 Compensator Design for RC

The general RC law introduced in Chapter 3 was given by

$$u(k) = F(q)\left(q^{N_p} - 1\right)^{-1} e(k) \tag{5.11}$$

with $F(q)$ taking the form

$$F(q) = \kappa_1 q^{\beta-1} + \kappa_2 q^{\beta-2} + \cdots + \kappa_\beta q^0 + \cdots + \kappa_{\alpha-1} q^{-(\alpha-\beta-1)} + \kappa_\alpha q^{-(\alpha-\beta)} \tag{5.12}$$

and satisfying the convergence criteria of either of (5.6) or (5.7). Longman (2000) states that the simplest form of RC law can be formulated as

$$u(k) = u(k - N_p) + \xi e(k - N_p + 1) \tag{5.13}$$

where $e = y_{ref} - y$ and ξ is a scalar learning gain, usually assumed to be in the range of $0 < \xi \leq 1$. From (5.13), the relationship from e to u can be written as

$$u(k) = \xi q\left(q^{N_p} - 1\right)^{-1} e(k) \tag{5.14}$$

which is a special case of (5.11) since here $F(q) = \xi q$. Longman (2000) also states that this simple RC scheme can be made less sensitive to noise by setting a lower learning gain. This typically yields a lower steady state error although the response takes longer to reach steady state. In this case, the convergence criteria given by (5.6) and (5.7) becomes

$$\|1 - \xi q P(q)\|_\infty < 1 \tag{5.15}$$

or

$$\sup_{\omega \in [0, 2\pi]} \left|1 - \xi e^{j\omega} P(e^{j\omega})\right| < 1. \tag{5.16}$$

However (5.15) and (5.16) cannot be satisfied with an arbitrary plant $P(q)$ since to satisfy either (5.6) or (5.7) ideally requires $F(q)$ to be designed as $P(q)^{-1}$ and the inverse of an arbitrary plant $P(q)$ cannot be represented as $F(q) = \xi q$. In addition, if a more aggressive

approach is required, then $F(q)$ should also be ideally designed as $P(q)^{-1}$ to achieve the most rapid response. However, as mentioned in Section 3.3, either inaccuracies in the model or zeros of the model outside the unit circle makes this design method infeasible in practice. It is therefore suggested that the $F(q)$ form (5.12) be designed in accordance with the more general requirement of satisfying either (5.6) or (5.7). To design $F(q)$, Section 3.3 briefly introduced two methods, namely frequency modified inverse RC (FMI-RC) and gradient based RC (GB-RC), with accompanying motivation for each method. Now, FMI-RC and GB-RC methods will be examined in more detail within the following subsections. In particular, their formulation will be expanded to unlock more design flexibility for practical applications.

5.2.1 A modified FMI-RC Algorithm

In section 3.3, it is stated that parameters $\phi = [\kappa_1 \ \kappa_2 \ \cdots \ \kappa_\alpha]^\top$ appearing in $F(q)$ definition (5.12) can be selected appropriately by minimising the cost function

$$J=\sum_{i=0}^{L}[1-P(e^{j\omega_i})F(e^{j\omega_i})][1-P(e^{j\omega_i})F(e^{j\omega_i})]^* \tag{5.17}$$

to form $F(q)$ as an approximation of $P^{-1}(q)$. This selection enables (5.7) to be satisfied.

Panomruttanarug and Longman (2004) states that a frequency weighting can be added to (5.17) to guarantee that (5.7) is satisfied. This weighting is used to stabilise the system by preventing the Nyquist plot of $P(e^{jw_i})F(e^{jw_i})$ from going outside the unit circle near the origin, going into the left hand plane, and coming back in. Otherwise, there is no way to stabilise the system once the Nyquist plot is outside the unit circle (Panomruttanarug and Longman, 2004). In addition, this frequency weighting can be also used to achieve robustness for small changes in the disturbance period according to (Steinbuch et al., 2007). In this case, (5.17) has to be replaced with the more general form

$$J=\sum_{i=0}^{L}[1-P(e^{j\omega_i})F(e^{j\omega_i})]W_i[1-P(e^{j\omega_i})F(e^{j\omega_i})]^* \tag{5.18}$$

where $\omega_i = 2\pi f_i T_s$ in which T_s is the sampling period and $\{f_i\}_{i=0,\ldots,L}$ is an appropriate set of frequencies selected from 0 to $f_N = 1/2T_s$. Recall that α and β determine the order of $F(q)$ via its definition (5.12). Similarly, condition (5.7) can be addressed by selecting $F(q)$ as an approximation of $P^{-1}(q)$ through suitable choice of parameters $\kappa_i, i = 1, \ldots, \alpha$ of $F(q)$ given by (5.12). This is achieved by minimising the cost function

(5.18). The solution, ϕ^*, to (5.18) is given by $\phi^* = \Gamma^{-1}\Phi$ where

$$\Gamma = \sum_{i=0}^{L} W_i M^2(\omega_j) \begin{bmatrix} 1 & \cos(\omega_i) & \cdots & \cos((\alpha-1)\omega_i) \\ \cos(\omega_i) & 1 & \cdots & \cos((\alpha-2)\omega_i) \\ \vdots & \vdots & \ddots & \vdots \\ \cos((\alpha-1)\omega_i) & \cos((\alpha-2)\omega_i) & \vdots & 1 \end{bmatrix},$$
$$\Phi = \sum_{i=0}^{L} W_i M(\omega_j) \begin{bmatrix} \cos((\beta-1)\omega_i + \varphi(\omega_i)) \\ \\ \vdots \\ \cos((\beta-\alpha)\omega_i + \varphi(\omega_i)) \end{bmatrix} \tag{5.19}$$

in which $M(\omega)$ and $\varphi(\omega)$ are the magnitude and phase of $P(q)$, respectively, and ,W_i is a weighting factor applied to the i-th frequency. It is further shown in (Panomruttanarug and Longman, 2004) that computation of ϕ^* over a suitably wide range of α and β values can be utilised to ensure (5.7) is satisfied. This effectively enables the designer to transparently manipulate selection of $F(q)$ in the frequency domain in order to compute an approximation of the inverse of $P(q)$ which satisfies (5.7).

In order to reduce the value of ϕ, the cost function (5.18) can be further transformed into the following modified cost function

$$J = \sum_{i=0}^{L} [1 - P(e^{j\omega_i})F(e^{j\omega_i})] W_j [1 - P(e^{j\omega_i})F(e^{j\omega_i})]^* + V(\kappa_1^2 + \kappa_2^2 + \cdots + \kappa_\alpha^2) \tag{5.20}$$

where V is positive scalar gain that prevents the value of ϕ from increasing too much. In this case, the solution, ϕ^*, to (5.20) is given by $\phi^* = \Gamma_2^{-1}\Phi$ where $\Gamma_2 = \Gamma + VI$. Here, Γ is given by (5.20) and I is an identity matrix. Panomruttanarug and Longman (2004) found that $\left|1 - P(e^{j\omega})F(e^{j\omega})\right|$ approaches 1 at high frequencies with decreasing the value of ϕ. Thus RC become less sensitive to high frequency noise. Instead, the sensitivity to high frequency uncertainties can also be eliminated by implementing a zero-phase low pass filter into RC scheme.

5.2.2 GB-RC Algorithm

The gradient based RC update is described in (Hatonen et al., 2006b,a) which establishes its attractive robustness and convergence properties. This algorithm describes the general RC law given by (5.11) as

$$u(k) = \gamma P^*(q) \left(q^{N_p} - 1\right)^{-1} e(k) \tag{5.21}$$

with $F(q) = \gamma P^*(q)$. Here, $P^*(q)$ is defined as

$$P^*(q) \coloneqq \sum_{i=1}^{N_p} h_{N_p-i} q^{N_p-i} \tag{5.22}$$

in which h_i are the Markov parameters of $P(q)$ with $h_i = 0 \; \forall i > N_p$. This finite impulse response (FIR) of $P(q)$ is needed to guarantee that the RC law (5.21) is causal. By choosing $\alpha = \beta = N_p$ in (5.12), $F(q)$ becomes

$$F(q) = \gamma P^*(q) = \gamma P(q^{-1}) = \gamma \sum_{i=0}^{N_p} h_{N_p-i} q^{N_p-i} \tag{5.23}$$

from which the parameter of (5.12) is found as

$$\kappa_i = \gamma h_{N_p-i}, \quad i = 1, \ldots, N_p. \tag{5.24}$$

Substituting (5.23) into the left-hand side of the convergence criteria (5.7) yields

$$\sup_{\omega\in[0,2\pi]} \left|1 - P(e^{j\omega})F(e^{j\omega})\right| = \sup_{\omega\in[0,2\pi]} \left|1 - \gamma P(e^{j\omega})P^*(e^{j\omega})\right| = \sup_{\omega\in[0,2\pi]} \left|1 - \gamma \left|P(e^{j\omega})\right|^2 \right| < 1. \tag{5.25}$$

From (5.25), it follows that

$$-1 < 1 - \gamma \left|P(e^{j\omega})\right|^2 < 1 \; \forall \omega \in [0, 2\pi] \tag{5.26}$$

and rearranging (5.26) yields

$$0 < \gamma < \frac{2}{\left|P(e^{j\omega})\right|^2} \; \forall \omega \in [0, 2\pi] \, .$$

Recalling (5.25), γ must be selected as

$$0 < \gamma < \frac{2}{\sup\limits_{\omega\in[0,2\pi]} \left|P(e^{j\omega})\right|^2}. \tag{5.27}$$

to satisfy (5.7). Note that evaluating (5.23) approximates a plant inverse at low frequencies, but the learning rate reduces for higher frequencies. This embeds robustness to plant uncertainty into the RC structure, which is also discussed in (Hatonen et al., 2006a).

Remark 5.1. The assumption that $h_i = 0$, $\forall i > N_p$ can be addressed through the introduction of appropriate feedback action, e.g. deadbeat control, pole-placement (see Appendix B). The plant $P(q)$ is then replaced by the resulting closed-loop structure.

The following section will combine the model of wrist dynamics proposed in Chapter 4 and the RC scheme designed by the algorithms proposed in the previous section to

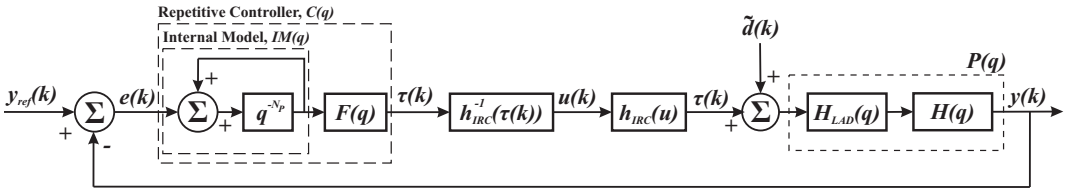

Figure 5.3: Closed-loop control system structure including the simple RC scheme in Figure 5.1 and the simplified wrist model.

generate a FES based closed loop system which can employ a linear RC action to suppress tremor.

5.3 Closed-loop Stimulation System

Having shown the advantage of the RC framework over the conventional filtering techniques in Chapter 3, now RC algorithms proposed in Section 5.2.1 and Section 5.2.2 will be designed based on the simplified wrist model shown in Figure 5.3. This replaces the linear tremulous wrist model of (3.8) employed by the leading filter based studies (Prochazka et al., 1992a,b). Hence the purely linear closed-loop system shown in Figure 3.1 is replaced with the closed-loop system illustrated in Figure 5.3. This will enable the RC framework to be implementable in clinical applications. The necessary control strategy therefore combines linearising action and the RC algorithm to result in the following form.

Theorem 5.2. *Let the repetitive control action*

$$u(k) = h_{IRC}^{-1}\left(F(q)\left(q^{N_p}-1\right)^{-1}e(k)\right) \tag{5.28}$$

with $F(q)$ taking the form of (5.12) *where $\beta \leq N_p + 1$, applied to the system of Definition 4.1 with components satisfying the monotonicity criteria in Proposition 4.3. Recall from Section 5.1 that N_p-periodic disturbance $\tilde{d}$ is then completely rejected if either* (5.6) *or* (5.7) *is satisfied, assuming that $1 - P(q)F(q)$ is internally stable.*

Proof. The polynomial model (4.13) of $h_{IRC}(u)$ with satisfying the derivative condition (4.17) guarantees that $h_{IRC}(u)$ is monotonically increasing and hence has an inverse $h_{IRC}^{-1}(\tau)$ defined over $[-\tau_{max}, \tau_{max}]$. Having applied this function, the standard linear repetitive control action with form

$$\tau(k+N_p) = \tau(k) + F(q)e(k) \tag{5.29}$$

can be applied and generates the control action (5.28). This has a sufficient condition for complete disturbance rejection given by either (5.6) or (5.7). □

Theorem 5.2 introduces the linearising action $h_{IRC}^{-1}(\tau)$ which eliminates the nonlinear dynamics $h_{IRC}(u)$ embedded in the wrist model shown in Figure 5.3. This enables a linear RC to be designed using the algorithms proposed in Section 5.2.

5.4 Interference of RC with Voluntary Motion

The simulation results of Section 3.3 showed that the RC action can interfere with the patients' ability to extend or flex their wrist voluntarily, and thereby impair their performance of functional activities. Thus this section will introduce a mechanism employing a general class of RC update together with a zero-phase high-pass (ZPHP) filter to eliminate distortion of voluntary intention at low frequencies and prevent FES from producing large high frequency stimulation transients. This will mean that the controller does not interfere with voluntary motion or cause discomfort.

This section will firstly explore the question of why the proposed RC scheme has an undesirable effect on voluntary motion, and secondly will explain whether the mechanism mentioned above can abolish this effect while suppressing tremor. Lastly, it discusses how to apply this ZPHP filter based method to the RC design algorithms proposed in Section 5.2. Recall the following assumptions from Chapter 3, which will be necessary to examine the key questions above:

- Voluntary wrist movement occurs at frequencies less than 1 Hz, as shown in (Stiles and Hahs, 1991).
- Involuntary movement associated with intention tremor occurs at a single frequency between 2 Hz and 5 Hz, as shown in (Koch et al., 2007; Deuschl et al., 1998).
- Voluntary action manifests as an additive signal, v, appearing in the summation blocks within Figure 5.1 that precede H_{LAD}. This is consistent with the underlying mechanism assumed to produce the tremor signal $\tilde{d}$.

5.4.1 Distortion of Voluntary Intention

Suppose the control action is applied to suppress tremor while voluntary action v is also exerted by the patient. Then the distortion in the intended movement is

$$\Delta y_v \coloneqq \|y_v - y\|_2 \tag{5.30}$$

where $y_v = P(q)v$ and $y = S(q)v$ with

$$S(q) = P(q)\big(1 + P(q)F(q)(q^{N_p} - 1)^{-1}\big)^{-1}. \tag{5.31}$$

Recall the conditions from Section 3.1.2, given by

$$|S(j\omega)| = |P(j\omega)|\,, \text{ and } \angle S(j\omega) = \angle P(j\omega) \tag{5.32}$$

in order to preserve the voluntary action below 1 Hz. It follows that to minimise the distortion (5.30), a necessary and sufficient condition is that the closed-loop system must satisfy (5.32) for frequencies less than 1 Hz.

Theorem 5.3. *It is impossible for any $F(q)$ satisfying either convergence condition* (5.6) *or* (5.7) *to satisfy either of the conditions given in* (5.32)*. It follows that there always exists a voluntary control action v such that $\Delta y_v \neq 0$, i.e. voluntary action is distorted.*

Proof. Equation (5.31) can be rewritten as

$$S(q) = P(q)\frac{q^{N_p} - 1}{q^{N_p} - (1 - P(q)F(q))}. \tag{5.33}$$

It is then obvious that $\left|S(e^{i\omega})\right|$ approaches 0 as $\omega \to 0$ for all $F(q)$ satisfying either (5.6) or (5.7), and hence never satisfies (5.32) since $\lim_{\omega\to 0}\left|P(e^{i\omega})\right| \neq 0$. □

Theorem 5.3 is explained by the following example:

Example 5.1. *Let $\left[0, \omega_c\right]$ be the frequency range of voluntary action. For the ideal case, $F(q) = P(q)^{-1}$, then (5.31) becomes*

$$S(q) \coloneqq P(q)\left(1 + (q^{N_p} - 1)^{-1}\right)^{-1}. \tag{5.34}$$

Without loss of generality, let the sampling period be $T_s = 1$. Substituting $q = e^{j\omega}$ into (5.34)*, the frequency components are*

$$\left|S(e^{j\omega})\right| = \left|P(e^{j\omega})\left(1 + (e^{j\omega N_p} - 1)^{-1}\right)^{-1}\right|, \tag{5.35a}$$

$$\angle S(e^{j\omega}) = \angle P(e^{j\omega})\left(1 + (e^{j\omega N_p} - 1)^{-1}\right)^{-1}. \tag{5.35b}$$

It follows that (5.35a) *can be rewritten as*

$$20\log_{10}\left|S(e^{j\omega})\right| = 20\log_{10}\left|P(e^{j\omega})\right| + 20\log_{10}\left|\left(1 + (e^{j\omega N_p} - 1)^{-1}\right)^{-1}\right|. \tag{5.36}$$

The second term in the right hand side of (5.36) *results in*

$$\left|\left(1 + (e^{j\omega N_p} - 1)^{-1}\right)^{-1}\right| = \left|1 - e^{-j\omega N_p}\right| = 2 - 2\cos\left(\omega N_p\right) \tag{5.37}$$

which yields

$$\left|1 - e^{-j\omega N_p}\right| = 1 \;;\; \omega = \frac{(4k+1)\pi}{3N_p}\;,\; k = 0, 1, \ldots \tag{5.38}$$

and so (5.36) *becomes*

$$\left|S(e^{j\omega})\right| = \left|P(e^{j\omega})\right| \; ; \; \omega = \frac{(4k+1)\pi}{3N_p} \; , \; k = 0, 1, \ldots \tag{5.39}$$

Let (5.35b) *be rewritten as*

$$\angle S(q) = \angle P(q) + \angle \left(1 + (q^{N_p} - 1)^{-1}\right)^{-1} . \tag{5.40}$$

Similarly, the second term in the left hand side of (5.40) *results in*

$$\angle 1 - e^{-j\omega N_p} = \tan^{-1}\left[\frac{\sin\left(\omega N_p\right)}{\cos\left(\omega N_p\right) - 1}\right] - \tan^{-1}\left[\frac{\sin\left(\omega N_p\right)}{\cos\left(\omega N_p\right)}\right] = 0 \; ; \omega = \frac{(2k+1)\pi}{N_p}, k = 0, 1, \ldots \tag{5.41}$$

and so (5.35b) *becomes*

$$\angle S(q) = \angle P(q) \; ; \; \omega = \frac{(2k+1)\pi}{N_p}, \; k = 0, 1, \ldots \tag{5.42}$$

From (5.39) *and* (5.42)*, the conditions of* (5.32) *are clearly not satisfied.*

5.4.2 Distortion Elimination

This subsection proposes a method to address the interference of the controller with the voluntary movement that is established in Theorem 5.3. This is achieved by adding a ZPHP filter, $F_H(q)$, in series with the repetitive control

$$C(q) = F(q)\left(q^{N_p} - 1\right)^{-1} \tag{5.43}$$

as shown in Figure 5.4.

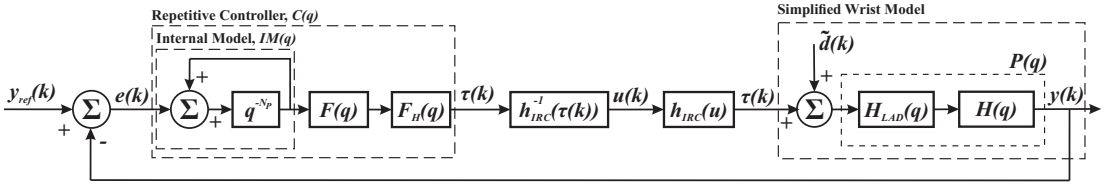

Figure 5.4: RC scheme with ZPHP filter $F_H(q)$.

The aim is to shape the frequency response of the closed-loop system at low frequencies in order to satisfy (5.32), while preserving tremor suppression at higher frequencies.

Theorem 5.4. *Suppose the control action of Theorem 5.2 is implemented with* $F(q)$ *satisfying either* (5.6) *or* (5.7)*. Then suppose an ideal, non-causal ZPHP filter,* $F_H(q)$*,*

with cut-off frequency ω_c and characteristic

$$|F_H(\omega)| = \begin{cases} 0, & \omega \in [0, \omega_c] \\ 1, & \omega \in (\omega_c, 2\pi] \end{cases}, \qquad \angle F_H(\omega) = 0 \quad \forall \omega \in (\omega_c, 2\pi] \tag{5.44}$$

is added immediately following $F(q)$, as shown in Figure 5.4. Then (5.32) *is satisfied for $\omega \in [0, \omega_c]$, thereby eliminating voluntary distortion. In addition, $\omega \in (\omega_c, 2\pi]$ frequency components of y asymptotically converge to zero, thereby eliminating tremor.*

Proof. Adding $F_H(q)$ means (5.33) is replaced by

$$S(q) \coloneqq P(q)V(q) \tag{5.45}$$

where

$$V(q) = (1 + P(q)C(q)F_H(q))^{-1} = \left(1 + P(q)F(q)\left(q^{N_p} - 1\right)^{-1} F_H(q)\right)^{-1}. \tag{5.46}$$

Due to the frequency response characteristic (5.44), the frequency response of $V(q)$ is

$$\begin{aligned} \left|V(e^{j\omega})\right| &= \left| \frac{q^{N_P} - 1}{q^{N_P} - (1 - P(q)F(q)F_H(q))} \right|_{q=e^{j\omega}} = 1, \\ \angle V(e^{j\omega}) &= \angle \left(\frac{q^{N_P} - 1}{q^{N_P} - (1 - P(q)F(q)F_H(q))} \right) \Bigg|_{q=e^{j\omega}} = 0, \end{aligned} \quad , \forall \omega \in [0, \omega_c]$$

so that the magnitude and phase responses of (5.45) equate to $|P(q)|$ and $\angle P(q)$ for $\forall \omega \in [0, \omega_c]$, respectively. It follows that an ideal ZPHP filter satisfies (5.32) for $\omega = [0, \omega_c]$. Replacing $F(q)$ by $F(q)F_H(q)$ in (5.7) results in

$$\left|1 - F(e^{j\omega})F_H(e^{j\omega})P(e^{j\omega})\right| \leq \left|1 - F(e^{j\omega})P(e^{j\omega})\right| < 1 \, , \, \forall \omega \in (\omega_c, 2\pi]$$

since $\angle F_H(e^{j\omega}) = 0$ and $\left|F_H(e^{j\omega})\right| = 1$, $\forall \omega \in (\omega_c, 2\pi]$. Hence the RC convergence criterion for the augmented system is satisfied over the involuntary frequency range. □

Theorem 5.4 is explained by the following example which examines whether the voluntary interference of the RC scheme in Example 5.1 can be eliminated:

Example 5.2. *Recalling the selection of $F(q) = P(q)^{-1}$ from Example 5.1 and substituting it into* (5.46) *results in*

$$V(q) = \frac{q^{N_P} - 1}{q^{N_P} - 1 + F_H(q)} \tag{5.47}$$

Without loss of generality, let the sampling period again be $T_s = 1$. *Substituting* $q = e^{j\omega}$ *into* (5.47), *the magnitude response of* (5.47) *then becomes*

$$\left|V(e^{j\omega})\right| = \left|\frac{e^{j\omega N_P} - 1}{e^{j\omega N_P} - 1 + F_H(e^{j\omega N_P})}\right|. \tag{5.48}$$

With $D(\omega) \coloneqq |F_H(\omega)|$, *rearranging* (5.48) *yields*

$$\left|V(e^{j\omega})\right| = \left|\frac{\cos(\omega N_p) - 1 + i\sin(\omega N_p)}{\cos(\omega N_p) - 1 + i\sin(\omega N_p) + D(\omega)}\right|, \tag{5.49}$$

which can be expressed by the following function

$$\frac{2 - 2\cos(\omega N_p)}{2 - 2\cos(\omega N_p) + 2\big(\cos(\omega N_p) - 1\big)D(\omega) + D(\omega)^2}. \tag{5.50}$$

In addition, the phase response of $V(q)$ *is found as*

$$\angle V(e^{j\omega}) = \tan^{-1}\left[\frac{\sin(\omega N_p)}{\cos(\omega N_p) - 1}\right] - \tan^{-1}\left[\frac{\sin(\omega N_p)}{\cos(\omega N_p) - 1 + D(\omega)}\right]. \tag{5.51}$$

Using (5.44), *the image of* (5.50) *and* (5.51) *are respectively calculated as*

$$\left|V(e^{j\omega})\right| = \begin{cases} 1 & \text{for } \omega \in [0, \omega_c] \\ 2 - 2\cos\big(\omega N_p\big) & \text{for } \omega \in (\omega_c, 2\pi] \end{cases} \tag{5.52}$$

and

$$\angle V(e^{j\omega}) = \begin{cases} 0 & \text{for } \omega \in [0, \omega_c] \\ \tan^{-1}\left[\frac{\sin\left(\omega N_p\right)}{\cos\left(\omega N_p\right) - 1}\right] - \tan^{-1}\left[\frac{\sin\left(\omega N_p\right)}{\cos\left(\omega N_p\right)}\right] & \text{for } \omega \in (\omega_c, 2\pi] \end{cases}. \tag{5.53}$$

From (5.45), *the frequency response components are*

$$20\log_{10}\left|S(e^{j\omega})\right| = 20\log_{10}\left|P(e^{j\omega})\right| + 20\log_{10}\left|V(e^{j\omega})\right|, \tag{5.54a}$$

$$\angle S(e^{j\omega}) = \angle P(e^{j\omega}) + \angle V(e^{j\omega}). \tag{5.54b}$$

Substituting (5.52) *and* (5.53) *into* (5.54), *the frequency response of* $S(q)$ *results in*

$$\left|S(e^{j\omega})\right| = \begin{cases} \left|P(e^{j\omega})\right| & \text{for } \omega \in [0, \omega_c] \\ 2 - 2\cos\big(\omega N_p\big) & \text{for } \omega \in (\omega_c, 2\pi] \end{cases} \tag{5.55}$$

and

$$\angle S(e^{j\omega}) = \begin{cases} \angle P(e^{j\omega}) & \text{for } \omega \in [0, \omega_c] \\ \tan^{-1}\left[\frac{\sin\left(\omega N_p\right)}{\cos\left(\omega N_p\right) - 1}\right] - \tan^{-1}\left[\frac{\sin\left(\omega N_p\right)}{\cos\left(\omega N_p\right)}\right] & \text{for } \omega \in (\omega_c, 2\pi] \end{cases}. \tag{5.56}$$

Finally, it is clear from (5.55) *and* (5.56) *that a ZPHP filter enables* (5.32) *to be satisfied for* $\omega = [0, \omega_c]$.

Remark 5.5. Since an ideal ZPHP filter requires an infinite amount of data to obtain the desired characteristic (5.44) it must be realised instead by the finite length approximation

$$F_H(q) = f_0 q^{-N_H} + f_1 q^{-N_H+1} + \cdots + f_{N_H} + f_{N_H+1} q + \cdots + f_{2N_H} q^{N_H}$$

with a cut-off frequency ω_c, in which $2N_H + 1$ is the filter length, which must be chosen to satisfy $N_H \leq N_p - \beta + 1$.

The next subsection illustrates how to apply Theorem 5.4 using the specific RC designs of Section 3.3.

5.4.3 Application of Theorem 5.4 to RC Design

Theorem 5.3 confirms that RC has an inevitable interference with voluntary actions. To eliminate the voluntary distortion due to this interference of RC, a mechanism, in which RC employs a ZPHP filter, is proposed in Section 5.4.2 and Theorem 5.4 confirms that this mechanism can shape the frequency response of the closed-loop system at low frequencies in order to preserve voluntary actions. However adding a ZPHP filter to RC requires a balance between designing a ZPHP filter characteristics close to ideal characteristics (5.44) and satisfying the monotonic convergence criteria (5.6) or (5.7). This trade-off can be explained using Remark 5.5.

Remark 5.5 indicates that filter parameter N_H must be suitably large to realise characteristics (5.44) within Theorem 5.4. However this restricts the parameter β needed to satisfy either (5.6) or (5.7) within the same theorem. This section provides guidelines for satisfying Theorem 5.4 for the case of the two RC approaches considered previously, enabling the designer to balance the competing objectives.

5.4.3.1 FMI-RC Case

For the FMI-RC Algorithm in Section 5.2.1, β is prescribed by the designer. However as β is reduced, it becomes increasing difficult to produce a suitable inverse which satisfies (5.6) and (5.7).

To investigate whether the proposed Theorem 5.4 is capable of eliminating the voluntary distortion found in Section 3.3.3, the same wrist model used in the simulations of Chapter 3 is also employed in the following simulations. In addition, N_P was selected to be 10 in previous simulations. Thus the same value of N_p is also used here. With this selection, the criteria in Remark 5.5 becomes $N_H \leq 11 - \beta$.

Figure 5.5 and Figure 5.6 illustrate the balance between satisfying monotonic convergence (5.7) and filter characteristics (5.44) that exists in the implementation of a FMI-RC scheme employing a ZPHP filter. Figure 5.5 shows the low frequency responses of $S(q)$ given by (5.45), which have been designed with the FMI-RC method for varying β of $F(q)$ and N_H of the ZPHP filter. From Figure 5.5, it is apparent that a higher N_H length makes the ZPHP characteristics approach the ideal characteristics (5.44), thereby enabling the convergence criteria (5.32) to be satisfied more fully. However Figure 5.6 shows that a higher N_H length leads to a lower β value and this makes it more difficult for $F(q)$ to satisfy the monotonic convergence of either (5.6) or (5.7). These results confirm the trade-off in Theorem 5.4 for the FMI-RC case mentioned above.

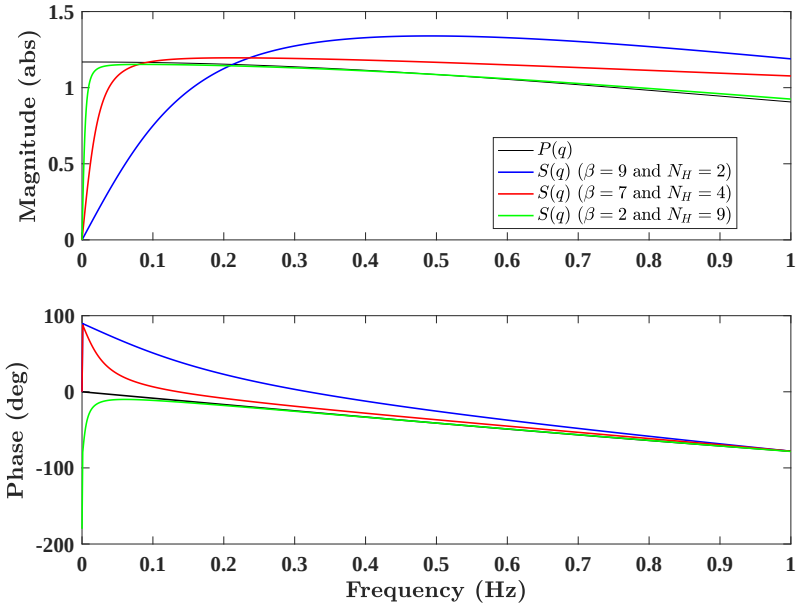

Figure 5.5: Low frequency responses of $S(q)$ employing FMI-RC with varying β of $F(q)$ and N_H of ZPHP filter.

5.4.3.2 GB-RC Case

For the GB-RC Algorithm in Section 5.2.2, β is dictated by the impulse response length of $P(q)$. Decreasing β causes the assumption in GB-RC Algorithm to be replaced by $h_i = 0\ \forall i > \beta$ and results in increasing difficulty in fulfilling the assumption. However by applying Remark 5.1, this effect can be reduced by the introduction of an appropriate feedback action. To illustrate this, simulations are now performed. Figure 5.7 shows that the model proposed previously has an impulse response which reaches zero after 13 steps. This does not satisfy the assumption in Remark 5.1 that $h_i = 0$, $\forall i > N_p$ since $N_P = 10$ and $h_i = 0$, $\forall i > 13$ (after 0.60 s). To achieve an impulse response length less than N_p, the feedback system proposed in Appendix B can be used. Figure 5.7 shows the feedback system is able to reduce the impulse response length to 10. This satisfies the assumption and yields $\beta = 10$ (0.5 s) due to the $F(q)$ form (5.23) in which $\alpha = \beta = N_p$.

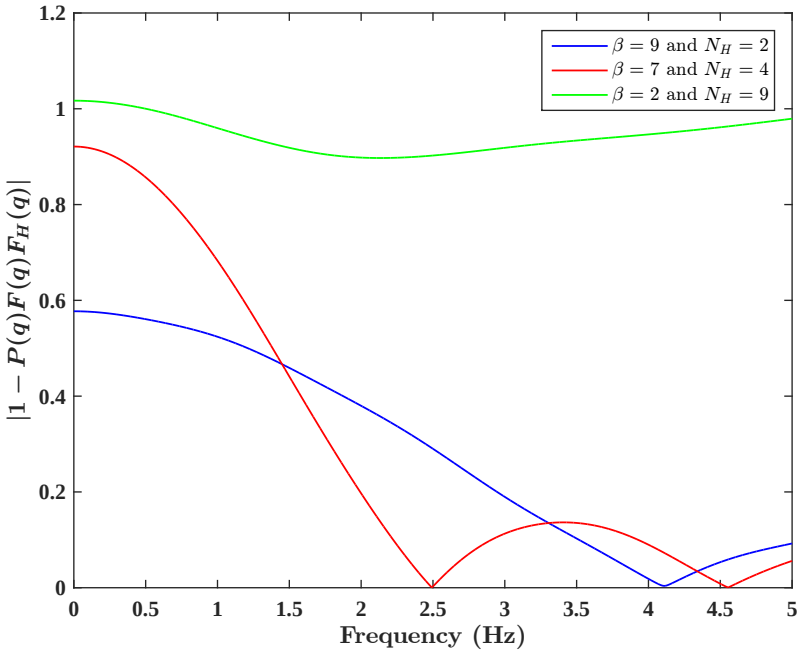

Figure 5.6: Convergence of $S(q)$ employing FMI-RC with varying β of $F(q)$ and N_H of ZPHP filter.

This selection enables only one ZPHP filter, which has the form of $f_0 q^{-1} + f_1 + f_2 q$, to

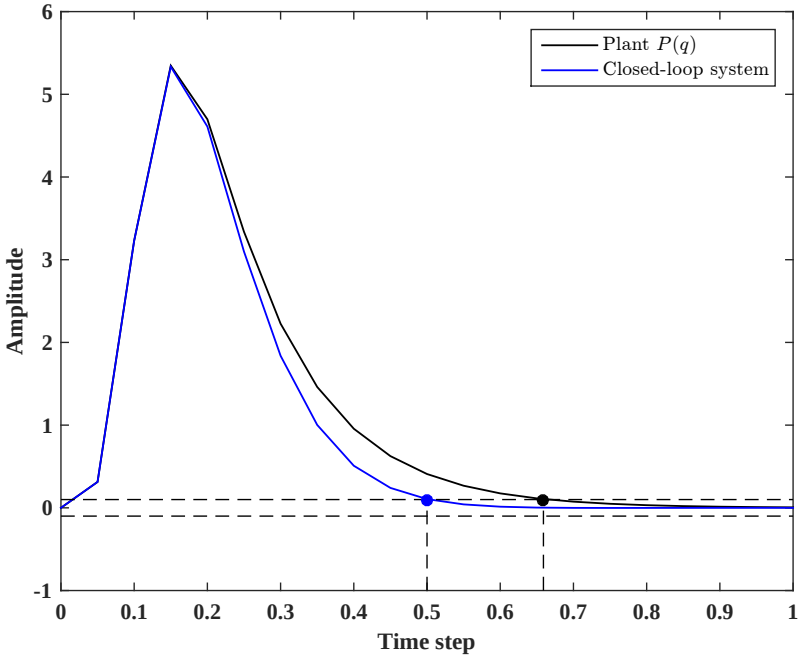

Figure 5.7: Full length impulse response and reduced impulse response of plant $P(q)$.

be designed since the condition in Remark 5.5 becomes $N_H = 1$. From Figure 5.5, it is apparent that this ZPHP filter is unable to satisfy the desired frequency characteristics (5.44), thereby being incapable of satisfying (5.32). Thus a ZPHP filter with a higher N_H length is needed. To design this, the state feedback system must produce a further

reduction in the impulse response. Figure 5.8 shows the state feedback system is able to reduce the impulse response length to 8 (0.40 s) and the condition in Remark 5.5 becomes $N_H \leq 3$. Like the results presented previously, Figure 5.9 shows that increasing the N_H length of the ZPHP filter enables (5.32) to be satisfied. However this results in increasing the difficulty in satisfying (5.7), as shown in Figure 5.10.

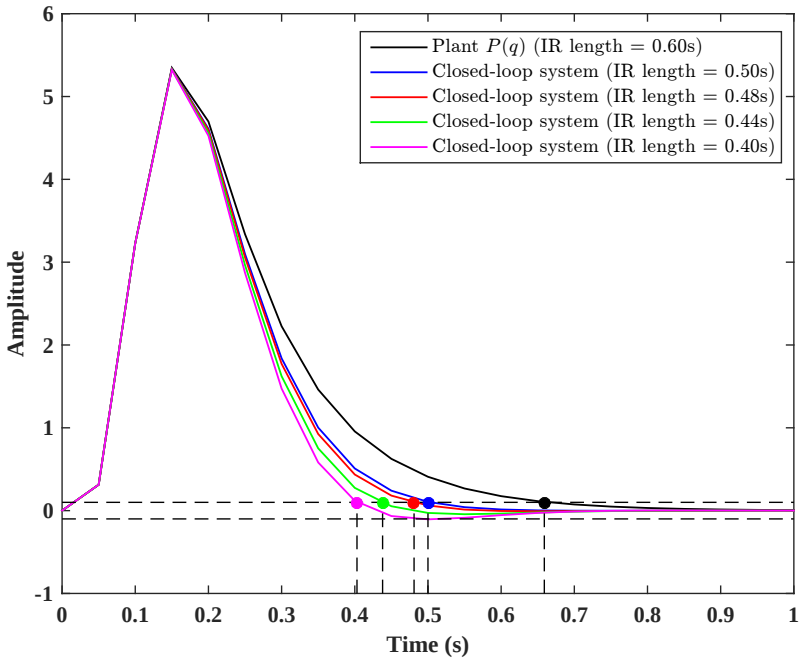

Figure 5.8: Reduced impulse responses of different state feedback systems.

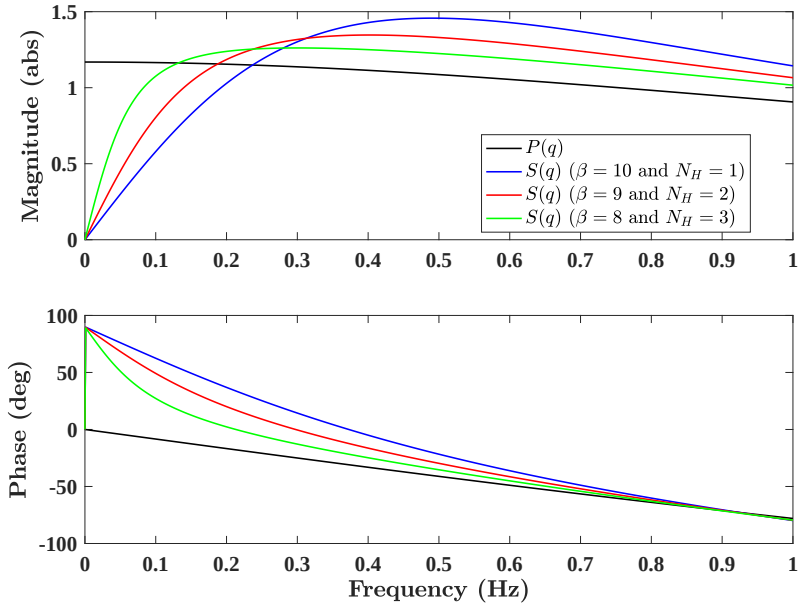

Figure 5.9: Low frequency responses of $S(q)$ employing GB-RC with varying β of $F(q)$ and N_H of ZPHP filter.

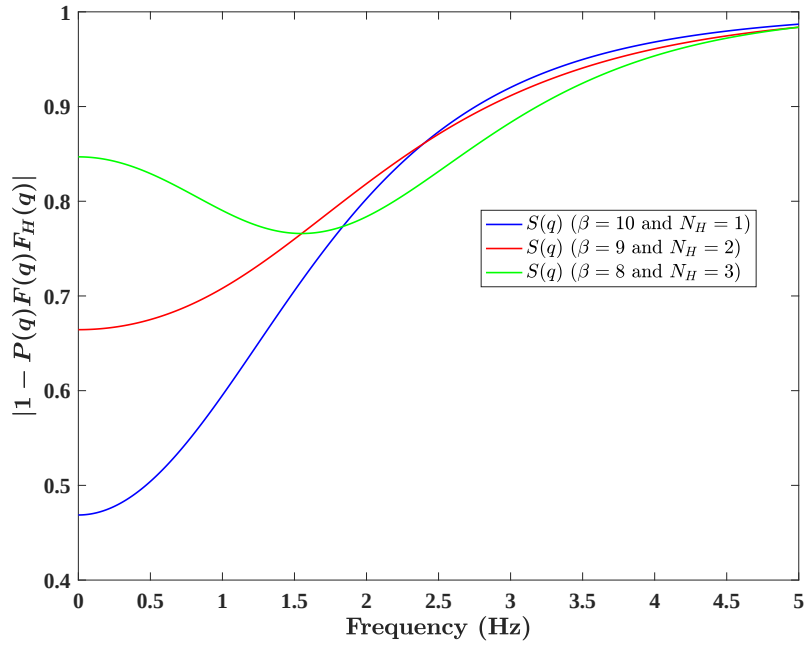

Figure 5.10: Convergence of $S(q)$ employing GB-RC with varying β of $F(q)$ and N_H of ZPHP filter.

5.5 Summary

This chapter proposes a linearising action to enable the RC scheme in Section 3.3 to be applied to the system model developed in Chapter 4. In the light of the simulation results in Section 3.3, it is then proved that RC schemes have inevitable interference with voluntary action. Thus a ZPHP filter is introduced and added to RC in series to preserve voluntary action. However adding a ZPHP filter makes difficult to satisfy the monotonic convergence criteria (5.7) since the filter length N_H of ZPHP filter limits the parameter β in $F(q)$ due to the inequality of $N_H \leq N_p - \beta + 1$ required to preserve the causality. Higher N_H enables a ZPHP filter to be designed closer to the ideal filter, but enables smaller value of β to be selected, leading to satisfying the monotonic convergence criteria becoming more difficult. Since $N_p = 1/f_p T_s$, higher T_s leads to higher N_p. Considering computational effort and hardware limitations, higher T_s can thus be used to select the values of N_H and β within a wider range. These developments result in a closed-loop stimulation system as shown in Figure 5.11

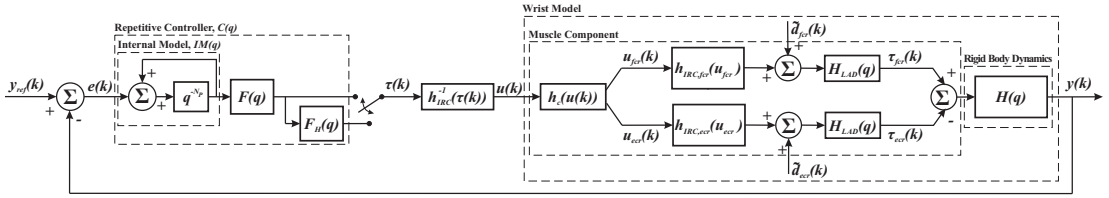

Figure 5.11: Closed-loop control system structure in which wrist model of Definition 4.1 excited by electrical stimulation and tremor.

In the next chapter, this closed-loop system will be tested using a validated experimental set-up and then the results will be benchmarked against the conventional filtering technique to validate experimentally the potential of the RC approach for tremor suppression, which has been established in Chapter 3.

Chapter 6

Experimental Evaluation

In this chapter an experimental test platform will first be described which incorporates the sensors, actuators and control hardware necessary to undertake rigorous evaluation. This platform embeds an innovative artificial tremor injection mechanism whose development is outlined. Then a systematic experimental procedure will be developed to assess the feasibility of FES based tremor suppression using RC. This experimental study consists of two separate phases. In the first phase the accuracy of the identification procedures of Chapter 4 will be evaluated and it will be examined whether the order of the linear component $P(q)$ of wrist model can be fixed in advance for all participants to reduce the computational time of the identification procedure for further experiments. To do it, the response of the wrist joint to a suitable FES input is collected for each participant. Using the input/output data set of each participant, a linear component is identified for a number of different orders within a range. Additionally, the parameters of the components for the selected order are averaged over all participants and used as an initial component values for further tests. In second phase, the nonlinear component, and the linear component whose order is defined in first phase will be identified using the procedures of Chapter 4 for each participant to design the control approaches presented in Chapter 5. Then, these approaches will be tested, and the experimental results produced from these tests will be compared to the conventional filtering technique detailed in Section 3.2.

6.1 Experimental Test Facility

This section describes the development of the platform used to assess both the identification procedure developed in Chapter 4, and control approaches developed in Chapter 5.

6.1.1 Wrist Rig

An instrumental wrist rig was selected that has been specifically designed and validated to detect changes in upper limb function, described in Turk et al. (2008). The rig is designed to present tracking tasks to patients and assess their performance in completing them. To do this, it includes 80 LED lights spaced at 2° increments measuring an arc of wrist joint movement from 80° flexion to 80° extension. To prevent any confounding movement of the arm, this rig supports the participant's arm using two Velcro straps wrapped around the top and bottom of the elbow, and a foam splint placed on a location near the wrist joint, as shown in Figure 6.1. All angular motions of the wrist

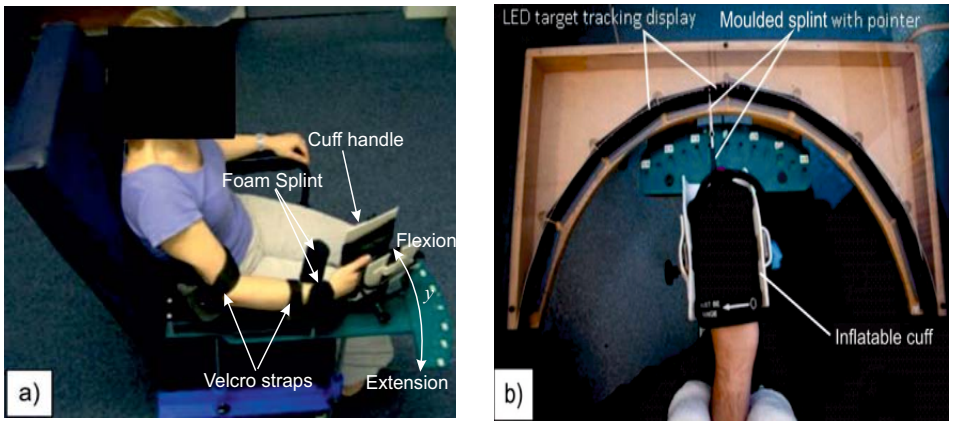

Figure 6.1: Experimental set-up (permission obtained to reproduce (Turk et al., 2008)) showing a) how the participant's arm is supported by the wrist rig, and b) an overhead view of the wrist.

joint are thus limited to the flexion/extension plane. The rotation of the wrist, y, is measured by a potentiometer aligned with the wrist joint axis and perpendicular to the flexion/extension plane, as shown in Figure 6.2. The potentiometer data is acquired by a real-time hardware comprising a dSpace 1103 board which interfaces directly with Matlab/Simulink to enable rapid controller development and implementation of the proposed control scheme which generates FES signals u_{fcr} and u_{ecr}. Since a stimulation pulse frequency of 40 Hz generally leads to a smooth and comfortable tetanic contraction, these comprise 40 Hz biphasic and asymmetrical PWM sequences with a maximum pulse width of $u_{max} = 300\mu s$ which are fed to the FES device. The maximum pulse width is set to be $u_{max} = 300\mu s$ since it provides a comfortable contraction (Lyons et al., 2004). The amplitude of the PWM waveform can be increased using the potentiometer for each channel on the stimulator. The amplification level is set for each participant prior to treatment by maximising the pulse-width to $300\mu s$ and incrementing the voltage to a level that the participant finds comfortable. Setting the amplitude to the highest value possible enables the relevant muscle to produce a torque sufficient for identification and tremor suppression. This setting remains unchanged during all experiments with the same participant. Since PWM sequences are controlled by waveforms with a fixed pulse frequency of 40 Hz and a fixed amplitude, the only controlled variable is the pulsewidth.

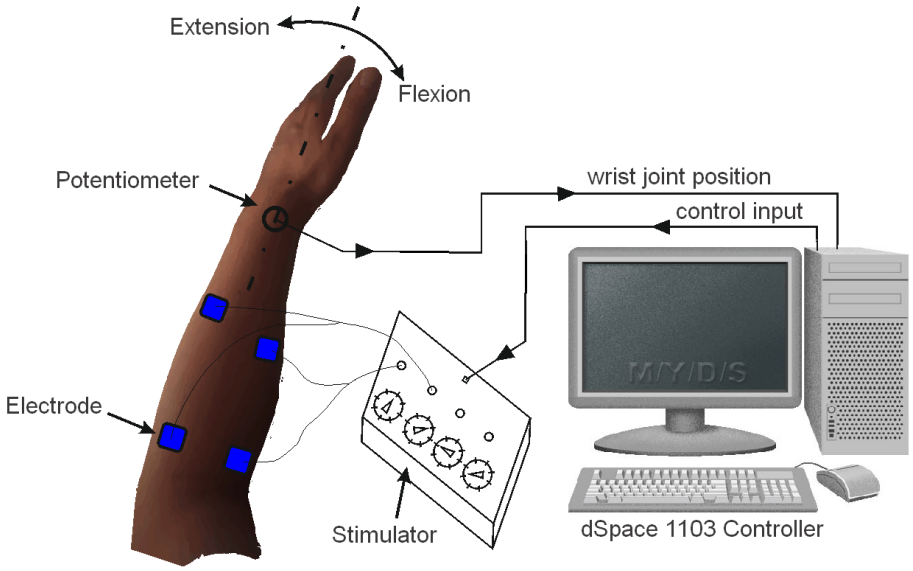

Figure 6.2: Schematic diagram of test set-up.

6.1.2 Induced Tremor

As the feasibility tests are conducted with unimpaired participants, it is necessary to induce tremor artificially at realistic frequencies between 2 and 5 Hz. Since intention tremor is based on the delayed activation of an agonist/antagonist muscle pair, as mentioned in Section 2.1.1, tremor can be artificially induced by stimulating a suitable muscle pair. This method has achieved by (Bo and Poignet, 2010) in which FCR and Palmaris Longus (PL) muscles were stimulated by FES. Therefore, the first attempt undertaken was to induce tremor using FES applied to the Flexor Carpi Ulnaris (FCU) and Extensor Digitorum (ED) muscles at the same time as FES was applied to FCR and ECR muscles to suppress tremor. However this attempt was not successful because some participants reported feeling uncomfortable during tests and wanted to withdraw from the study.

An alternative way is to produce a periodic oscillation mechanically. This is done by modifying the wrist rig to include a mechanical system driven by a geared DC motor. This system consists of three units, a brushed DC motor (Beijing V.T.V) equipped with a gearbox of 5:1 gear ratio and 1.28 Nm at 360 rpm, a 24 V battery to drive the motor and a motor controller (Maxon Motor ESCON). The motor torque is transmitted through a shaft to the link connected with the molded splint on which participants places their wrist and hand, as shown in Figure 6.3. Thus the wrist and hand oscillates at the desired frequency when the motor applied torque and this oscillation is independent of joint angle.

Within brushed DC electric motors, torque is directly related to the current that flows through the windings in the rotor, and this relation can be used to control the motor torque. To produce the desired torque, a closed-loop current control system is implemented, as shown in Figure 6.4. The motor controller ensures the torque is independent of

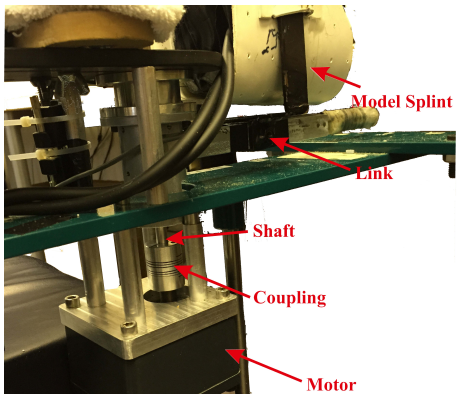

Figure 6.3: DC motor atachment to the wrist rig.

speed in order to match the model assumption of Definition 4.1 that tremulous motion manifests as the involuntary muscle torque d. Thus the motor controller selected is set to operate in torque mode. The current is instantaneously measured using a current sensor embedded in the motor controller to calculate the error between the demand and actual current. The demand current is generated in Simulink to be a sinusoidal signal of a predefined tremor frequency and supplied to the motor controller by the dSpace 1103 board. To minimise the error, the motor controller employs a PI controller operating in real-time. A PC-based configuration utility developed by Maxon Motor is used to tune the gains of the PI controller at the initial stage of testing.

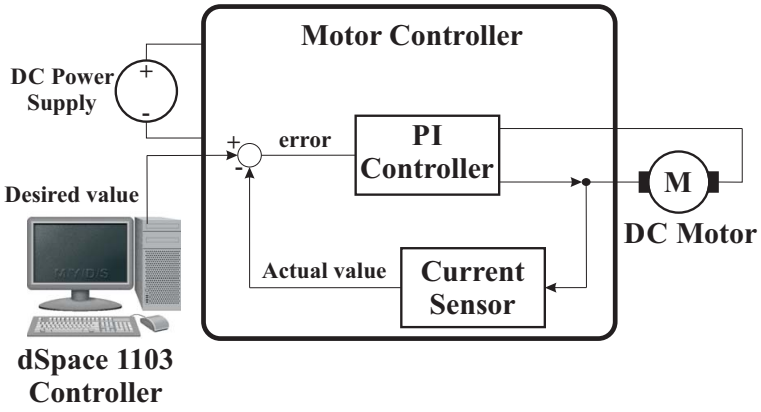

Figure 6.4: The test facility layout for torque control.

Figure 6.5: Torque sensor mounted to the output shaft of the geared motor.

Since the current-torque curve is unavailable for this specific motor, the peak amplitude of the supplied demand that produces the desired periodic torque is found experimentally. To measure the torque at the output shaft of the geared motor, a 6 degree-of-freedom force-torque sensor (JR3 model 67M25A3) depicted in Figure 6.5 is mounted on the motor shaft. Then a set of current signals with varied peak amplitudes is supplied by the dSpace 1103 card to the closed-loop current system, and the torque response of the motor is monitored using the sensor output. Finally, the peak amplitude of the output response to each input is calculated and a lookup table is generated in Simulink that maps the desired torque to the relevant current needed to be supplied.

To confirm that the desired torque was reliably generated at the desired frequency, two tests were conducted using current demands of 2 and 3 Hz frequencies, which are within the frequency range of intention tremor. Then a Fourier transform was applied to both measured torque signals to determine the frequency content of the signals and examine whether the base frequency is the desired frequency at which the torque oscillates. Figure 6.6 shows that the closed-loop system is capable of producing a sinusoidal signal at a single frequency which satisfactorily matches the specified tremor signal. To achieve the specified amplitude is not critical since it is only required that the frequency of the induced tremor signal matches the underlying assumption.

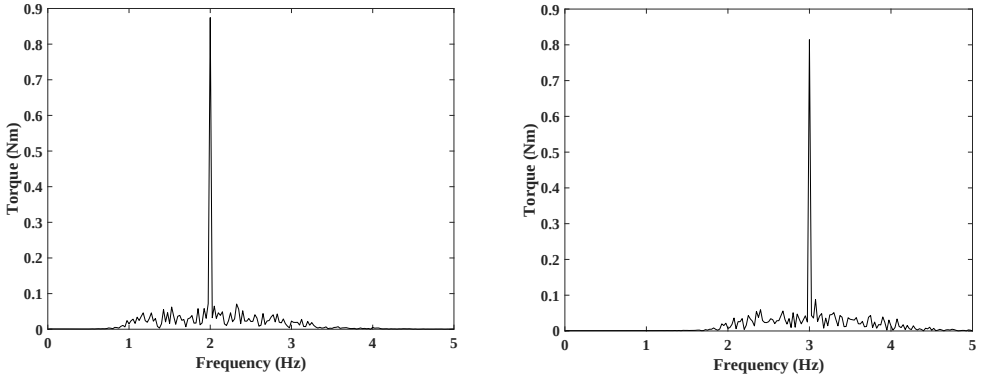

(a) (b)

Figure 6.6: The amplitude of the Fourier transform of the measured torque signal at a frequency of a) 2 Hz b) 3 Hz.

6.2 Preparations Prior to Testing

Ethical approval was obtained from the University of Southampton (ERGO Ref: 16530). Four unimpaired people were recruited to participate in this experimental study, who satisfied the following criteria: (i) no motor dysfunction or diagnosed systemic conditions; (ii) no pacemakers/attached electronic equipment; (iii) no cognitive/visual impairments; (iv) no diagnosed skin disorder; (v) able to provide informed consent. All participants also gave written informed consent (see Appendix C).

Advice from a therapist was provided to ensure procedure was suitable for patients (even though no patients were tested at this time). Potential participants were invited to take part and given a participation information sheet (see Appendix D). Participants placed their right arm into the wrist rig's adjustable padded armrest. The length of the armrest was adjusted to allow the wrist joint to be lined up directly over the potentiometer so the wrist joint angle was accurately measured. Using standard guidelines (Freriks et al., 1999), two sets of PALS Plus adhesive 5×5 cm surface electrodes were placed on the forearm to stimulate the FCR and ECR muscles as shown in Figure 6.7. These were connected to the corresponding outputs of the Odstock® stimulator via a 3.5 mm jack connector. The amplitude level of each channel was individually set to a maximum value which did not cause discomfort to participants while the nominal pulse width (300μs) was applied.

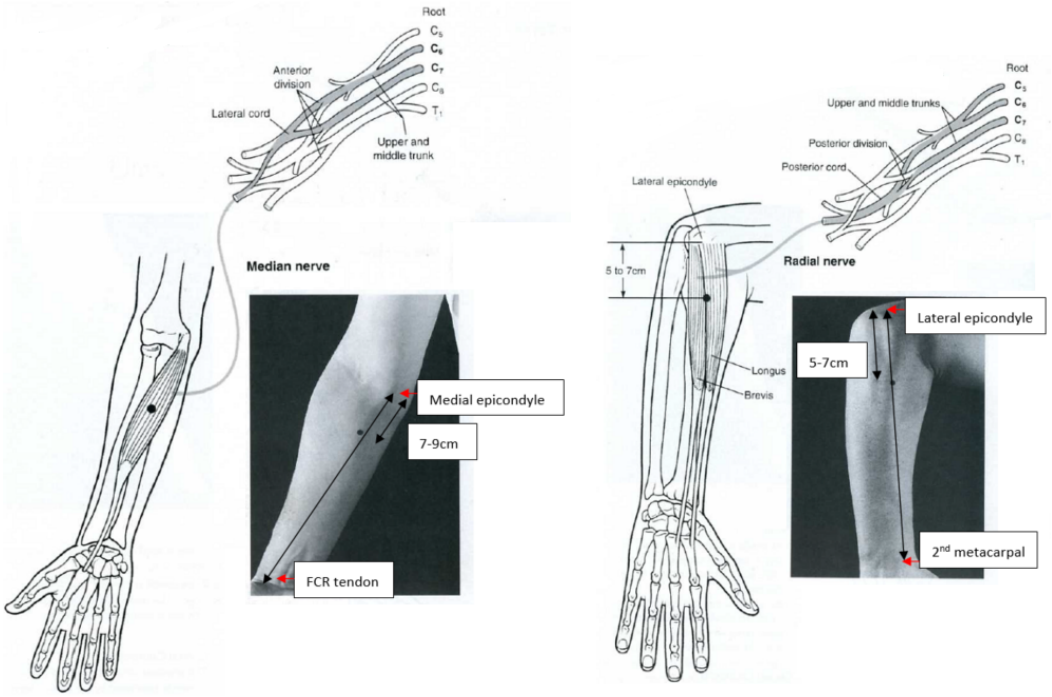

Figure 6.7: Locations of electrodes on FCR and ECR muscles. a) activation of the FCR muscle is on the volar surface of the forearm, 7-9 cm distal to the medial epicondyle along a line directed towards the muscle tendon at the wrist, and b) activation of ECR is in the upper forearm, 5-7 cm distal to the lateral epicondyle along a line connecting the epicondyle and the 2^{nd} metacarpal bone.

6.3 Modelling and Identification Evaluation

This section describes the test procedure employed to evaluate the system identification procedure described in Chapter 4. Experimental results are then presented and discussed.

6.3.1 Test Procedure

For each of the four male participants, data collection comprised two experiments separated by a rest period of 10 minutes. FES recruits fast-twitch muscle fibres before slow-twitch fibres which increases the rate of fatigue (Lynch and Popovic, 2008), therefore a rest of 10 minutes took place after each test, a time frame recommended for patients with disability (McGruder et al., 2003) in order to prevent muscle fatigue. Each experiment consisted of a prediction trial and a validation trial, each lasting for approximately 3 minutes, which together are termed a "data set". Another rest period was taken for at least 10 minutes between each trial in order to reduce effects of muscle fatigue. Additionally, the electrode pads were not moved between experiments and no change was made in FES amplitude settings.

The aim of the trial was not only to evaluate the accuracy of the model shown in Figure 4.6, but also to establish whether parameters m_P, n_P and l_P of $P(q)$ can be fixed in advance. Recall the linear transfer function component of the model is given by $P(q) = B_P(q)/A_P(q)$ with the polynomial form

$$\begin{aligned} B_P(q) =& b_0 q^{-m_P} + b_1 q^{-(m_P+1)} + \ldots + b_{n_P} q^{-(m_P+n_P)} \\ A_P(q) =& 1 + a_1 q^{-1} + \ldots + a_{l_P} q^{-l_P} \end{aligned} .$$

This was necessary to enable efficient clinical application in the future. The input/output set associated with each trial was written as follows:

$$Z_i^N = \{u_i(1), y_i(1), u_i(2), y_i(2), \ldots, u_i(N), y_i(N)\} \tag{6.1}$$

where N is the data length and i denotes the trial number, of which a total of 4 were performed for each participant. For each set of data obtained from the experiment, Algorithm 1 proposed in Section 4.3.4 was applied. In order to provide sufficient excitation, the input u was chosen to comprise a set of sinewaves that spanned the frequency range from 0.2 to 4 Hz as shown in Figure 6.8. This captured a substantial component of the range of voluntary motion (0-1 Hz), and the typical tremor range (2-5 Hz). Higher frequencies were not used due to their inherent attenuation by the arm dynamics. Eight frequencies over this range were applied separately, since the form of the signal has been found to be well-tolerated by patients. Note that this signal form has been shown to be sufficiently exciting over the system bandwidth, while white band-limited noise caused discomfort or involuntary muscle response in patients (Le et al., 2010). Alternatives include random step levels or pseudo-random multi-level sequences. Figure 6.9 shows a measured response of the wrist joint y to the input u, in which positive position values represent the wrist movements in flexion and negative values are related to the motions in extension.

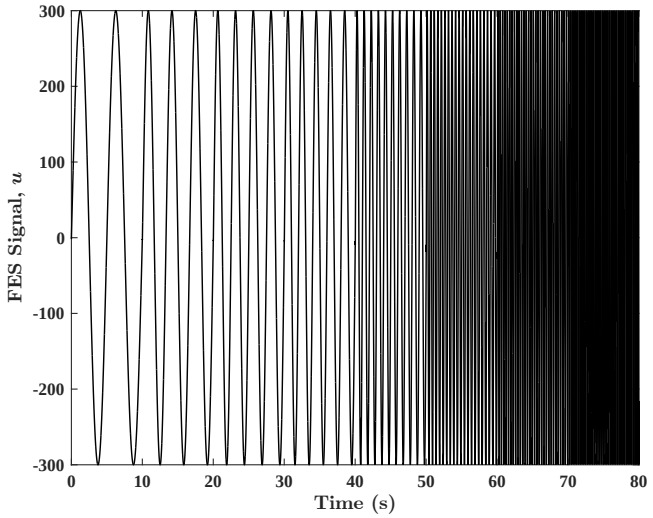

Figure 6.8: Input signal used for the estimation of relationship between wrist joint angle and torque.

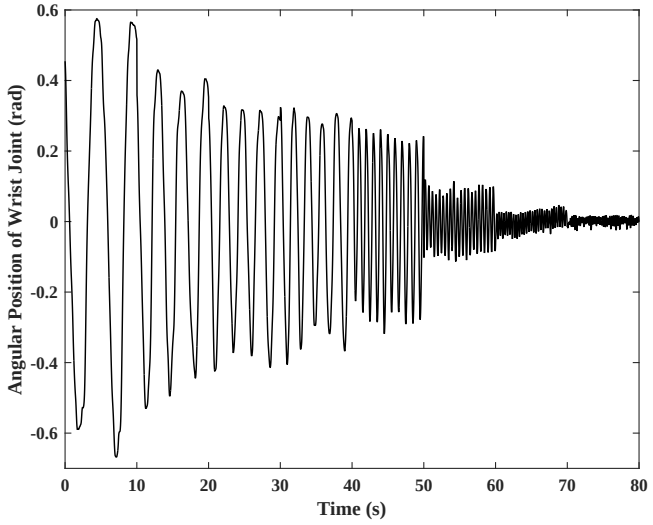

Figure 6.9: Measured wrist joint response y to the input u.

6.3.2 Data Analysis

In this evaluation, the 1^{st} and 3^{rd} sets of input/output data are used to identify a model associated with predicted output $\hat{y}$, and the other sets are used for validating the model on a new input/output set. The fitness of cross-validation is expressed in terms of Best Fit value, defined as the percentage

$$\text{Best Fit}_{CV} = 100\left(1 - \frac{\|y_{i+1} - \hat{y}_{s_i}\|}{\|y_{i+1} - \overline{y}_{i+1}\|}\right)\%, \tag{6.2}$$

where $\hat{y}_{s_i}$ denotes the simulated output obtained from the model identified on trial i, and y_{i+1} is the experimental output on validation trial $i+1$. The mean value of y is denoted by $\bar{y}$. To calculate the fitness of validation, the term y_{i+1} is replaced with y_i in

(6.2), resulting in

$$\text{Best Fit}_V = 100\left(1 - \frac{\|y_i - \hat{y}_{s_i}\|}{\|y_i - \overline{y}_i\|}\right)\%. \tag{6.3}$$

Parameters m_P, n_P and l_P are varied within a set of range. Then for each delay order m_P, the fitness values calculated from all data sets of each participant are averaged in order to examine the effects of any changes in n_P or l_P on the model accuracy.

6.3.3 Identification Evaluation Results

The variation in the average fitness values calculated for Participant 4 is shown in Figure 6.10 where n_P and l_P are each varied from 1 to 100 for different values of m_P and the colorbar indicates the percent fitness values. It is apparent from Figure 6.10 that any increase in m_P does not affect the averaged fitness values significantly when n_P is specified higher than 3 and l_p is kept constant. If n_p is lower than 3 and l_P is kept constant, then the averaged fitness values fluctuate for all values of m_P. In addition, m_P can be chosen equal to 1 because increasing m_P does not cause any significant change in the Best Fit value.

In Participant 2, Figure 6.11(a) reveals that higher values of l_P and n_P provide higher fitness values of between 60% and 65% when $m_P = 1$. This region is indicated by a red color in Figure 6.11(a). If m_P is selected to be 2, then the fitness values in that region reduce to between 55% and 65% but high fitness value can be obtained for n_P values greater than 4.. This is shown in Figure 6.11(b). Finally, the results obtained when $m_P = 3$ are shown in Figure 6.11(c). From all these cases, there is evidence that a mathematical model of Participant 2's wrist joint can be identified with $m_P = 1$ because increasing m_P does not cause any significant increase in the fitting accuracy.

Figure 6.12 shows how the averaged fitness values calculated from the experimental data sets of Participant 1 change when m_P is varied from 1 to 3. Based on the results illustrated in Figure 6.12, it can be seen that decreasing m_P results in decreasing the modelling fitness values when l_P is increased for either $n_p = 1$ or $n_P = 2$. For all m_p values, increasing n_P gives an increase in the averaged fitness values. Therefore m_P can also be selected to be 1 for Participant 1 if n_P is selected to be higher than 2.

The same averaging analysis is also made with the acquired data sets of Participant 3. The results are similar to the results obtained form Participant 4 and are illustrated in Figure 6.13. In the light of the results obtained by these analyses, $m_P = 1$ can be selected a priori to identify a model for an arbitrary participant's data set. The next step is to investigate how to select l_P and n_P in advance to enable an ARX model to be identified for an arbitrary participant's wrist joint. The fitness values remain approximately unchanged when l_P and n_P are chosen to be higher than 3 as shown in Figure 6.14(a). On the other hand, considering that 10^4 different models have been

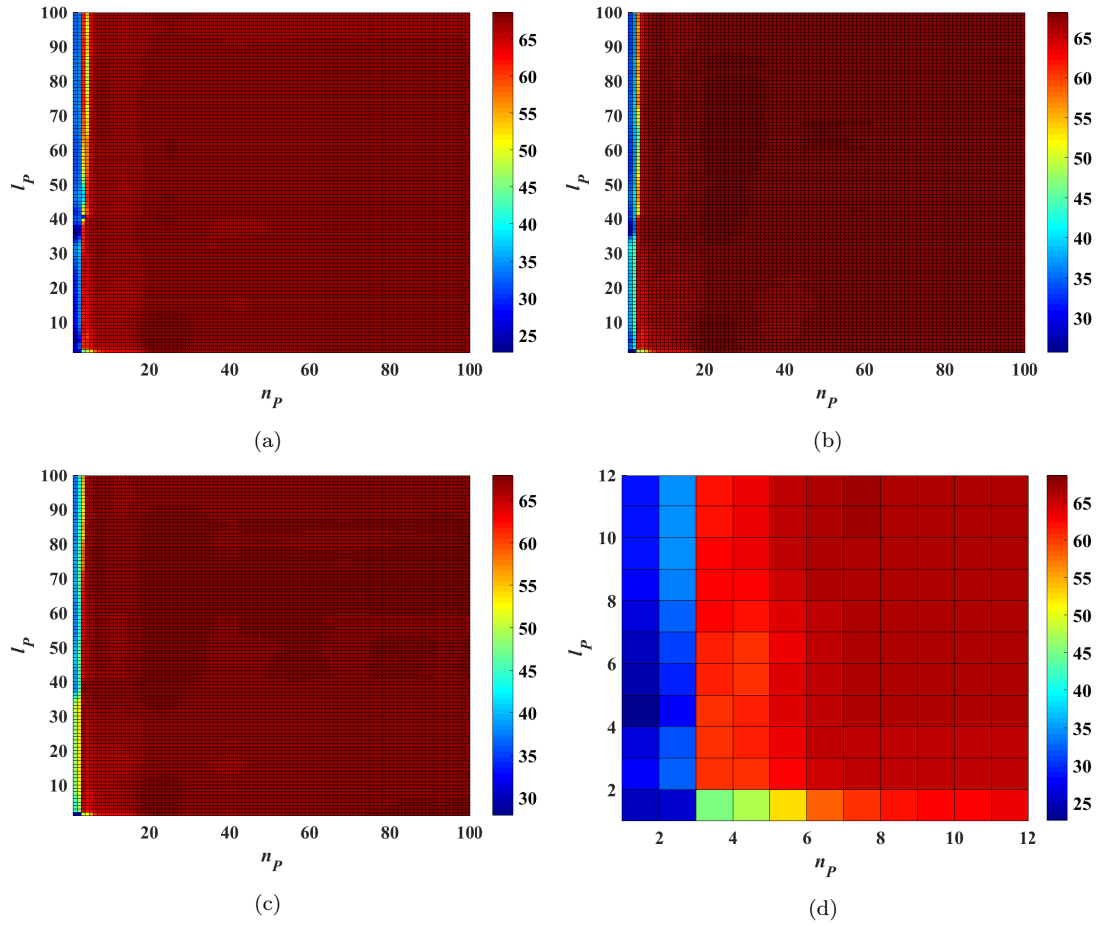

Figure 6.10: Variation in Best Fit values of ARX models identified using 2^{nd} data set of Participant 4 when l_P and n_P are varied from 1 to 100 for a) $m_P = 1$, b) $m_P = 2$, c) $m_P = 3$, and d) from 1 to 12 for $m_P = 1$. These values are obtained from cross-validation tests.

obtained by varying l_P and n_P from 1 to 100 as shown in Figure 6.10 and Figure 6.11 for each participant, the selection of l_P and n_P may produce models with completely different dynamical responses to the same input. This makes choosing a single model difficult. Moreover, to select l_P and n_P in a way which generates the highest fitness values is also not an effective way to produce the best mathematical model for subsequent design, because, for example, a model with high order zeros may have more zeros outside the unit circle, thereby increasing the difficulty of designing $F(q)$ to satisfy the stability condition ((5.6) or (5.7) given in Chapter 5). Thus, these mathematical models must be compared to investigate their differences in terms of dynamical responses in the time and frequency domain. As a first step to simplifying this comparison, it is now examined whether the wide range of values can be narrowed. To do this, all fitness values of each participant that are obtained when $m_P = 1$ are first averaged. These averaged fitness values are then plotted in Figure 6.14(a) from which it is clearly apparent that the wide ranges of l_P and n_P may be restricted to a narrow band from 4 to 12 because the averaged fitness values are higher than 50%, as shown in Figure 6.14(b).

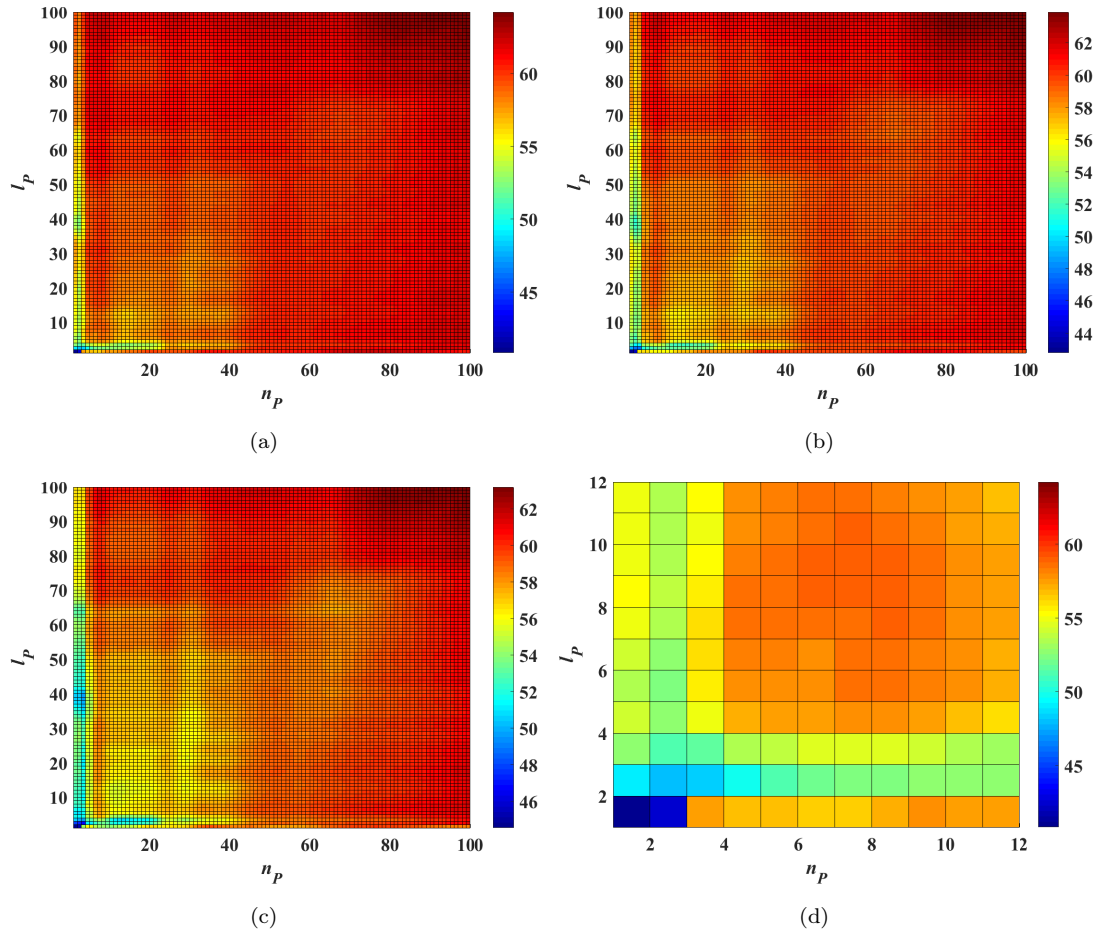

Figure 6.11: Variations in averaged fitness values of ARX models identified using 1^{st} and 2^{nd} data sets of Participant 2 when l_P and n_P are varied from 1 to 100 for a) $m_P = 1$, b) $m_P = 2$, c) $m_P = 3$, and d) from 1 to 12 for $m_P = 1$. These values are obtained from cross-validation tests.

The average fitness values of the validation tests are found to be 82.55% for Participant 1, 74.67% for Participant 2, 72.09% for Participant 3 and 78.73% for Participant 4 when both n_P and l_P are set to 250. The averaged fitness values of the cross-validation tests for the same values of l_P and n_P are calculated as 71.22% for Participant 1, 68.31% for Participant 2, 60.50% for Participant 3 and 70.39% for Participant 4. These results evidently show that higher values give rise to higher accuracy. However higher order requires more computational effort which makes the identification procedure less practical for FES application. Thus limitations in computational resources may necessitate a lower order plant model to be identified. The effect of selecting lower values of l_P and n_P is examined next.

The previous computations are repeated with n_P and l_P kept within a narrow range of between 4 and 12. Table 6.1, Table 6.2, Table 6.3 and Table 6.4 show the Best Fit values in terms of average fitness calculated using the two experimental data sets corresponding

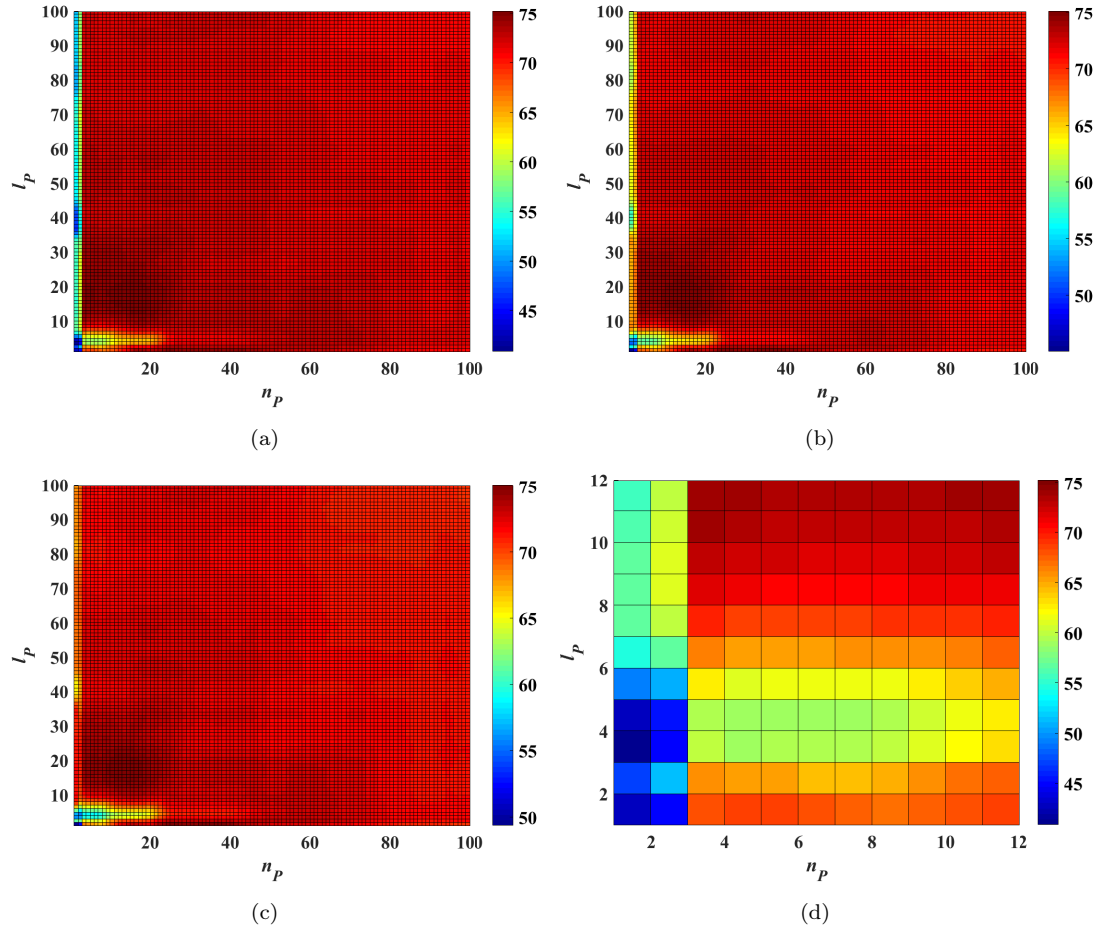

Figure 6.12: Variations in averaged fitness values of ARX models identified using 1^{st} and 2^{nd} data sets of Participant 1 when l_P and n_P are varied from 1 to 100 for a) $m_P = 1$, b) $m_P = 2$, c) $m_P = 3$, and d) from 1 to 12 for $m_P = 1$. These values are obtained from cross-validation tests.

to each participant. Table 6.5 shows the overall average Best Fit values calculated using the values from Table 6.1, Table 6.2, Table 6.3 and Table 6.4.

Validation and cross-validation Best Fit values in all tables are higher than 50%, confirming that a sufficiently accurate lower order model is obtained for each participant. The highest fitness values, those greater than 70%, are obtained for Participant 1. However, the changes in Best Fit values of each participant are not significant when n_P and l_P are varied from 4 to 12. This is deduced from the mean and standard deviation of the Best Fit values in Table 6.1, Table 6.2, Table 6.3 and Table 6.4. The values of the mean (standard deviation) are 66.61 (4.12), 57.95 (0.73), 59.51 (1.26) and 65.57 (1.39) for cross-validation tests and 70.79 (4.12), 62.29 (0.55), 63.14 (3.23) and 66.76 (2.26) for validation tests. There are slight differences between the values in these tables. Examination of the average Best Fit values in Table 6.5 enables suitable parameters to be selected that can subsequently be prescribed in future identification tests. Since these parameters provide confirmed accuracy, it is reasonable to conclude that the procedure can be employed in

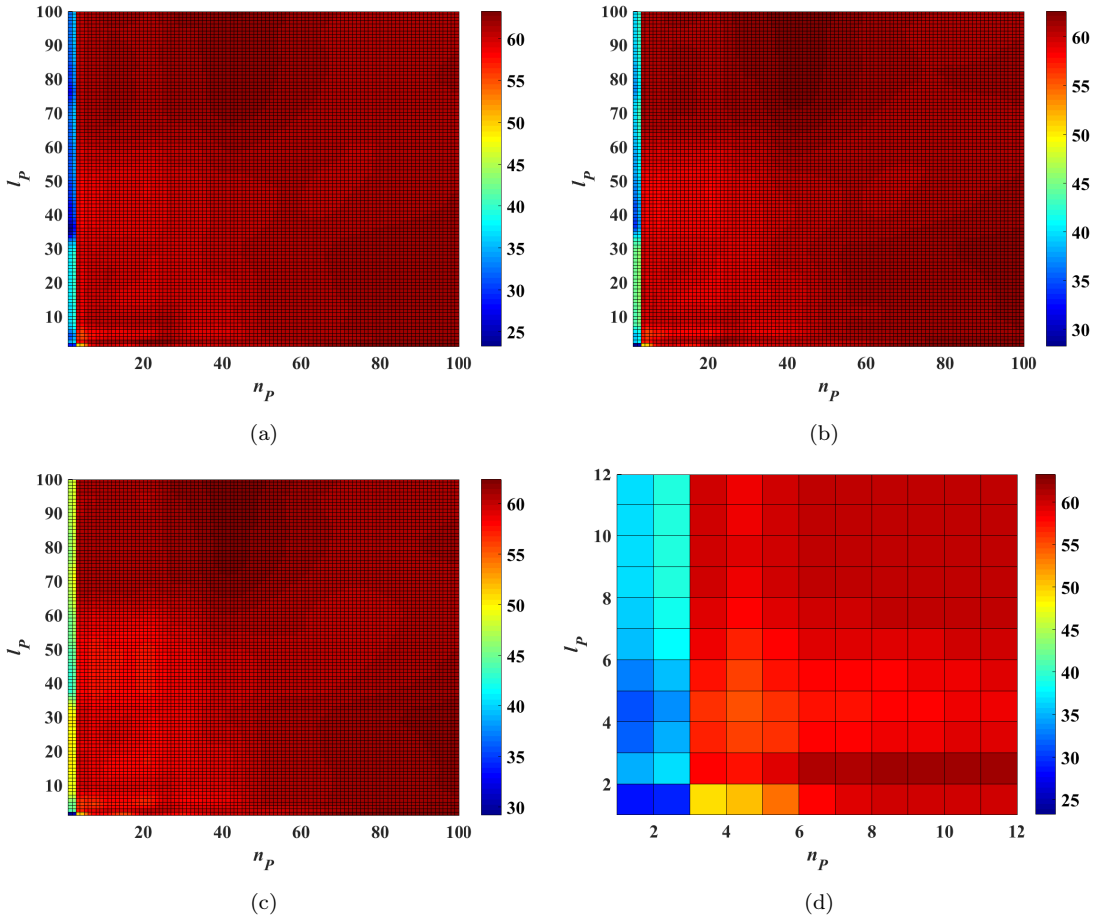

Figure 6.13: Variations in averaged fitness values of ARX models identified using 1^{st} and 2^{nd} data sets of Participant 3 when l_P and n_P are varied from 1 to 100 for a) $m_P = 1$, b) $m_P = 2$, c) $m_P = 3$, and d) from 1 to 12 for $m_P = 1$. These values are obtained from cross-validation tests.

clinical trials without the need to undertake cross-validation tests. When the Best Fit values of the cross-validation trial in Table 6.5 are compared, the most suitable n_P and l_P values are found to be 7 and 12, respectively, since this selection provides the highest Best Fit value which is highlighted in Table 6.5. With this choice, there is the degradation in accuracy of cross-validation, as much as 1.08% for Participant 1, 14.13% for Participant 2, 0.53% for Participant 3 and 5.55% for Participant 4 compared to the highest values of accuracy calculated when $l_P = m_P = 250$. From the results in Table 6.1, Table 6.2, Table 6.3 and Table 6.4, it is also found that the model of the selected order is identified with a fitting accuracy close to the highest Best Fit value of each participant highlighted in each table. Hence it can be asserted that the use of lower values of n_P and l_P does not give rise to a significant decrease in accuracy.

To confirm that the identified models are consistent representations of the underlying dynamics, the frequency responses of some randomly chosen models corresponding to two participants are plotted in Figure 6.15 and Figure 6.16. In these figures, it can clearly be seen that all frequency responses within the frequency range of input signal are similar.

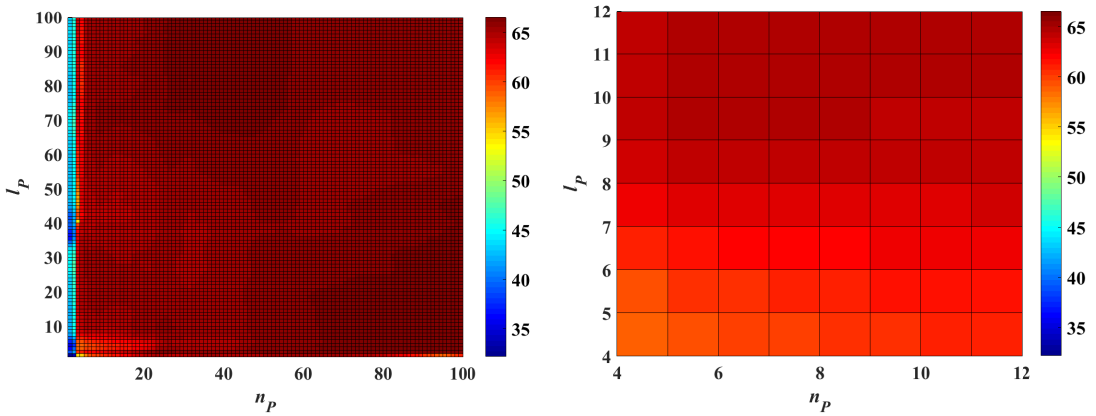

(a) (b)

Figure 6.14: Averaged fitness values obtained from fitness values of all participants.

In Figure 6.17, the comparison between the measured outputs used for validation and cross validation tests and the simulated output obtained from the model identified with $l_P = 12$, $n_P = 7$ and $m_P = 1$ is shown for Participant 1.

Table 6.1: Averaged Best Fit values (%) of Participant 1 when $m_P = 1$.

	l_P	n_P								
		4	**5**	**6**	**7**	**8**	**9**	**10**	**11**	**12**
CV	**4**	57.75	57.48	57.64	57.67	58.00	59.00	60.21	61.21	61.87
V		61.44	61.48	61.95	62.06	62.30	63.18	64.38	65.42	66.11
CV	**5**	60.15	60.43	60.30	60.31	60.39	60.97	61.93	62.83	63.48
V		63.78	64.69	64.55	64.68	64.74	65.21	66.11	67.01	67.65
CV	**6**	63.57	63.47	63.41	63.81	63.86	64.04	64.52	65.12	65.66
V		67.14	67.64	67.93	68.19	68.23	68.37	68.80	69.36	69.84
CV	**7**	66.55	66.17	65.93	65.89	66.62	66.76	66.91	67.19	67.52
V		70.10	70.26	70.33	70.35	70.96	71.09	71.25	71.49	71.74
CV	**8**	68.53	68.01	67.68	67.62	67.69	68.41	68.54	68.64	68.79
V		72.11	72.05	71.97	71.96	71.98	72.66	72.85	72.96	73.05
CV	**9**	69.71	69.15	68.79	68.74	68.85	68.97	69.52	69.60	69.65
V		73.36	73.19	73.03	72.99	73.05	73.13	73.74	73.88	73.92
CV	**10**	70.43	69.87	69.51	69.47	69.62	69.77	69.87	70.21	70.24
V		74.15	73.95	73.74	73.70	73.78	73.91	74.01	74.43	74.50
CV	**11**	70.94	70.41	70.05	70.03	70.19	70.37	70.48	70.52	70.70
V		74.73	74.55	74.33	74.28	74.38	74.54	74.67	74.71	74.96
CV	**12**	**71.33**	70.84	70.48	70.45	70.62	70.81	70.93	70.97	70.98
V		75.14	75.02	74.82	74.77	74.87	75.04	75.19	75.24	75.24

V: Validation, CV: Cross-Validation

Table 6.2: Averaged Best Fit values (%) of Participant 2 when $m_P = 1$.

	l_P	n_P								
		4	**5**	**6**	**7**	**8**	**9**	**10**	**11**	**12**
CV	**4**	57.15	57.42	57.56	57.92	58.03	57.63	56.83	56.12	55.70
V		62.42	61.72	60.95	61.16	61.51	61.49	61.09	60.80	60.87
CV	**5**	57.99	57.90	57.98	58.41	58.59	58.31	57.73	57.24	56.91
V		62.78	61.98	61.30	61.74	62.24	62.38	62.20	62.06	62.11
CV	**6**	58.20	58.12	58.04	58.46	58.60	58.31	57.75	57.28	56.98
V		62.94	62.12	61.33	61.77	62.26	62.41	62.27	62.17	62.21
CV	**7**	58.51	58.56	58.58	58.75	58.82	58.43	57.81	57.31	56.97
V		63.27	62.59	61.93	62.05	62.47	62.50	62.28	62.14	62.15
CV	**8**	58.54	58.75	58.91	**59.09**	58.98	58.53	57.90	57.41	57.05
V		63.37	62.85	62.40	62.59	62.72	62.65	62.36	62.18	62.15
CV	**9**	58.29	58.60	58.86	59.04	58.88	58.42	57.83	57.38	57.05
V		63.25	62.83	62.51	62.74	62.85	62.67	62.36	62.17	62.12
CV	**10**	58.00	58.32	58.62	58.79	58.62	58.14	57.59	57.18	56.89
V		63.12	62.73	62.46	62.69	62.79	62.58	62.25	62.05	62.00
CV	**11**	57.88	58.13	58.42	58.59	58.41	57.90	57.32	56.93	56.67
V		63.11	62.69	62.40	62.64	62.72	62.48	62.11	61.89	61.85
CV	**12**	58.09	58.24	58.49	58.66	58.48	57.94	57.31	56.88	56.63
V		63.29	62.81	62.50	62.75	62.83	62.56	62.16	61.91	61.86

V: Validation, CV: Cross-Validation

Table 6.3: Averaged Best Fit values (%) of Participant 3 when $m_P = 1$.

	l_P	n_P								
		4	**5**	**6**	**7**	**8**	**9**	**10**	**11**	**12**
CV	**4**	54.98	56.38	57.50	57.71	57.80	58.25	58.68	58.82	58.76
V		55.83	56.67	57.67	57.91	58.11	58.60	59.03	59.19	59.22
CV	**5**	55.45	57.21	57.87	58.13	58.17	58.51	58.90	59.02	58.95
V		56.53	57.90	58.26	58.55	58.68	59.03	59.38	59.52	59.52
CV	**6**	56.78	58.21	59.34	59.25	59.27	59.45	59.69	59.77	59.68
V		58.96	59.84	60.60	60.59	60.67	60.83	61.02	61.09	61.09
CV	**7**	58.04	59.19	60.05	60.13	60.24	60.36	60.48	60.50	60.40
V		61.67	62.11	62.49	62.54	62.81	62.91	62.96	62.95	62.93
CV	**8**	58.78	59.78	60.46	60.48	60.49	60.75	60.83	**60.84**	60.77
V		63.80	64.00	64.12	64.07	64.12	64.53	64.55	64.53	64.50
CV	**9**	58.99	59.96	60.55	60.54	60.55	60.68	60.74	60.74	60.71
V		65.11	65.24	65.24	65.14	65.20	65.33	65.58	65.57	65.58
CV	**10**	58.86	59.88	60.47	60.45	60.45	60.56	60.59	60.44	60.41
V		65.78	65.94	65.92	65.81	65.88	66.05	66.09	66.21	66.23
CV	**11**	58.65	59.70	60.32	60.30	60.30	60.40	60.40	60.30	60.06
V		66.05	66.30	66.31	66.20	66.28	66.47	66.54	66.54	66.63
CV	**12**	58.52	59.55	60.19	60.18	60.18	60.27	60.24	60.10	59.94
V		66.14	66.46	66.52	66.41	66.49	66.69	66.78	66.78	66.79

V: Validation, CV: Cross-Validation

Table 6.4: Averaged Best Fit values (%) of Participant 4 when $m_P = 1$.

	l_P	n_P								
		4	**5**	**6**	**7**	**8**	**9**	**10**	**11**	**12**
CV	**4**	60.85	63.81	65.76	66.20	66.20	66.06	65.99	66.02	66.14
V		60.44	63.21	64.94	65.37	65.49	65.50	65.51	65.62	65.89
CV	**5**	60.74	63.91	65.70	66.16	66.18	66.07	65.99	66.03	66.13
V		60.48	63.64	64.96	65.45	65.63	65.68	65.70	65.79	66.04
CV	**6**	60.79	63.61	65.54	65.97	66.02	65.95	65.90	65.94	66.04
V		60.69	63.20	64.81	65.14	65.38	65.49	65.54	65.64	65.85
CV	**7**	61.68	64.18	65.69	66.14	66.09	66.02	65.98	66.03	66.13
V		62.15	64.24	65.21	65.60	65.64	65.75	65.83	65.93	66.10
CV	**8**	62.81	64.76	66.05	66.35	66.30	66.18	66.14	66.19	66.30
V		64.57	65.86	66.50	66.59	66.64	66.62	66.69	66.79	66.95
CV	**9**	63.43	65.25	66.29	66.56	66.48	66.33	66.28	66.33	66.45
V		66.54	67.62	67.85	67.83	67.74	67.68	67.70	67.79	67.93
CV	**10**	63.44	65.38	66.41	**66.62**	66.55	66.40	66.32	66.36	66.47
V		67.49	68.76	68.94	68.79	68.66	68.55	68.51	68.63	68.78
CV	**11**	63.17	65.20	66.33	66.57	66.51	66.37	66.29	66.29	66.36
V		67.92	69.40	69.70	69.57	69.40	69.27	69.24	69.28	69.52
CV	**12**	62.92	64.98	66.18	66.48	66.44	66.33	66.25	66.23	66.27
V		68.06	69.74	70.20	70.14	69.98	69.84	69.81	69.87	70.02

V: Validation, CV: Cross-Validation

Table 6.5: Averaged Best Fit values (%) of all participants when $m_P = 1$.

	l_P	n_P								
		4	**5**	**6**	**7**	**8**	**9**	**10**	**11**	**12**
CV	**4**	57.68	58.77	59.62	59.87	60.01	60.24	60.43	60.54	60.62
V		60.03	60.77	61.38	61.63	61.85	62.19	62.50	62.76	63.03
CV	**5**	58.58	59.86	60.46	60.75	60.83	60.96	61.14	61.28	61.37
V		60.89	62.05	62.26	62.61	62.82	63.07	63.35	63.60	63.83
CV	**6**	59.83	60.85	61.58	61.87	61.94	61.94	61.97	62.03	62.09
V		62.43	63.20	63.67	63.92	64.13	64.27	64.41	64.57	64.75
CV	**7**	61.20	62.03	62.56	62.73	62.94	62.89	62.80	62.76	62.76
V		64.29	64.80	64.99	65.13	65.47	65.56	65.58	65.63	65.73
CV	**8**	62.16	62.83	63.28	63.39	63.37	63.47	63.35	63.27	63.23
V		65.96	66.19	66.25	66.30	66.36	66.62	66.61	66.61	66.66
CV	**9**	62.60	63.24	63.62	63.72	63.69	63.60	63.59	63.51	63.47
V		67.06	67.22	67.16	67.18	67.21	67.20	67.35	67.35	67.39
CV	**10**	62.68	63.36	63.75	63.83	63.81	63.72	63.59	63.55	63.50
V		67.63	67.84	67.76	67.75	67.78	67.77	67.72	67.83	67.88
CV	**11**	62.66	63.36	63.78	63.87	63.85	63.76	63.62	63.51	63.45
V		67.96	68.23	68.19	68.17	68.19	68.19	68.14	68.10	68.24
CV	**12**	62.71	63.40	63.84	**63.95**	63.93	63.84	63.68	63.55	63.46
V		68.16	68.51	68.51	68.52	68.54	68.54	68.48	68.45	68.48

V: Validation, CV: Cross-Validation

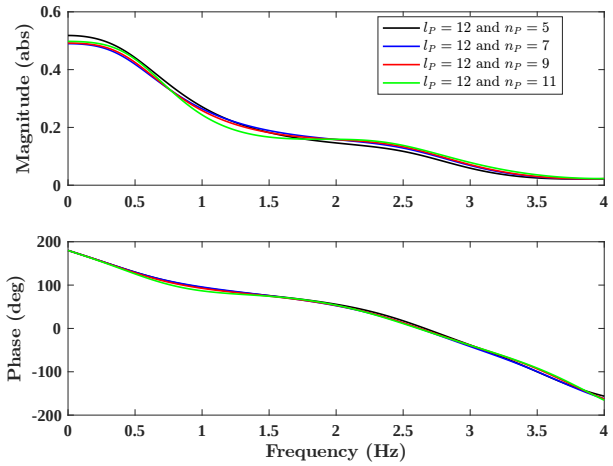

Figure 6.15: Bode plots of models identified using 2^{nd} data set of Participant 2 with different values of n_P when $l_P = 12$ and $m_P = 1$.

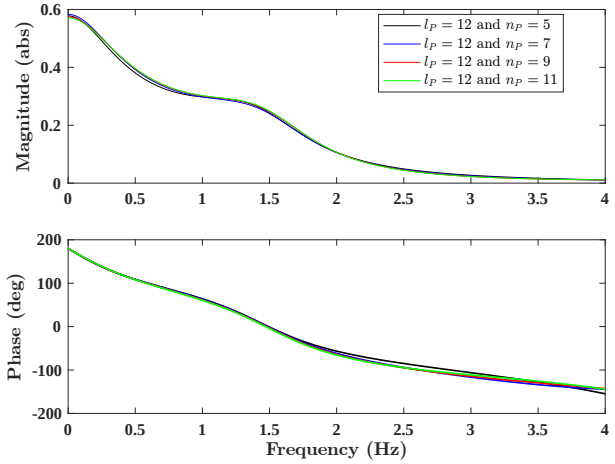

Figure 6.16: Bode plots of models identified using 1^{st} data set of Participant 1 with different values of n_P when $l_P = 12$ and $m_P = 1$.

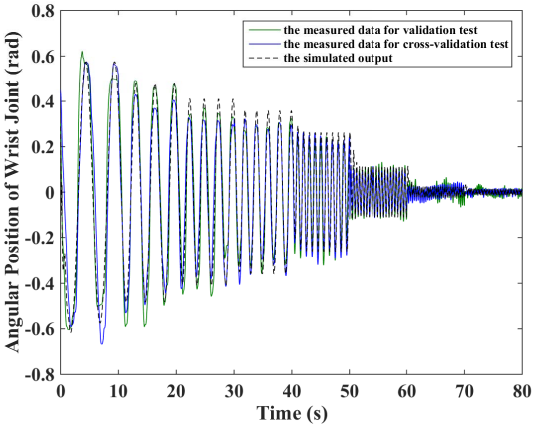

Figure 6.17: The comparisons of validation data, cross-validation data and time response of the model identified using 1^{st} data set of Participant 1 with the values of when $l_P = 12$, $n_P = 7$ and $m_P = 1$.

6.3.4 Summary

This section presented the experimental results corresponding to the system identification procedure proposed in Chapter 4. These results confirm that the procedure can identify the proposed wrist model that can simulate the wrist response to the stimulation input accurately. In addition, these results show also that the parameters l_P, n_P and m_P appearing in polynomials of $P(q)$ can be respectively selected to be 12, 7 and 1 in advance. Although comparison of the results of all participants show that this selection enables a model to be identified with a reliable accuracy for each participant, the model accuracy is limited by the following factors:

- The model does not demonstrate the muscle fatigue in the response to FES inputs which is a limitation to the clinical applications of FES since the nonlinear component of the model structure has been approximated by a polynomial function in Section 4.3. Although this approximation has been previously used and validated experimentally by both Westwick and Kearney (2001) and Le et al. (2010), an alternative approximation has been developed by Riener and Fuhr (1998) which describes the muscle fatigue and chemical reactions. However Lynch and Popovic (2008) state that its complexity makes a model difficult to be identified for a particular subject. Thus the model proposed in Chapter 4 can be re-identified regularly to represent the wrist dynamics accurately which may be changed due to the muscle fatigue.

- It is assumed in Chapter 4 that the muscle lengths of FCR and ECR are held constant because of the low amplitude and frequency of tremulous motion. However, the muscle length is varied if the angular variation of the wrist joint is large enough to be considered. In next section, participants will be asked to follow a tracking path voluntarily, together with the application of FES to suppress tremor. To track this reference trajectory, they will have to move their wrist joint in flexion-extension direction between $-40°$ and $20°$. This voluntarily muscle contraction can lead to a change in muscle length. Thus the model identified under the assumption that muscle length is unchanged may not be able to represent the wrist dynamics accurately during this voluntary motion.

- Another limitation is that the joint dynamics $P(q)$ is represented by a time-invariant system with linear elastic and damping properties. However, Riener and Fuhr (1998) state that the joint dynamics has nonlinear elastic and damping properties in reality.

- As mentioned previously, the assumption that the FCR and ECR muscles have similar linear activation dynamics may not be reasonable for all patients in reality.

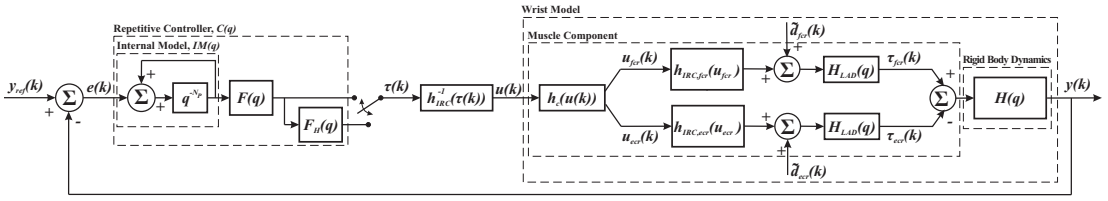

Figure 6.18: Closed-loop control system structure in which wrist model of Definition 4.1 excited by electrical stimulation and tremor.

However the experimental results in next section will show that the proposed procedure enables a reliable model to be identified to design an effective RC for satisfactory tremor suppression.

6.4 Repetitive Control Evaluation

This section describes the experimental procedure employed to validate the control scheme developed in Chapter 5. The proposed closed-loop control system is show in Figure 6.18.

6.4.1 Test Procedure

To fully evaluate the control approaches (with and without the ZPHP filter), the following tests were performed:

T1. Tracking task with neither induced tremor nor FES.

T2. Tracking task with induced tremor but without FES.

T3. Tracking task with induced tremor and FES.

Tracking test *T1* consisted of a step-tracking task, in which participants were instructed to flex or extend their wrist to track the position indicated by the LEDs which were illuminated in a pseudo-random pattern. Each LED was lit for 6 seconds and the test lasted for 40 seconds. Tracking test *T2* examined the effect of induced tremor on the ability of patients to perform the same tracking task. Tracking test *T3* examined the capability of FES to suppress the induced tremor while preserving the ability of participants to perform the voluntary task.

6.4.2 Control Design/Parameter Selection

The sampling frequency was set to 200 Hz ($T_s = 0.005$ s). Since the power spectrum of EMG signals measured from patients with intention tremor typically shows that tremor

has a dominant frequency between 2-5 Hz Lenz et al. (2002), an artificial tremor of frequency $f_p = 2$ Hz ($N_p = 100$) was induced using the mechanical system.

As discussed previously, having obtained the model using the procedure outlined in Section 6.3, the control approach of Theorem 5.4 was applied. To suppress tremor, y_{ref} was chosen to be 0. First, RC was designed without a ZPHP filter $F_H(q)$. In this case, $\beta \leq N_p = 100$ was selected and RC forms were designed to satisfy either stability condition (5.6) or (5.7). Then the ZPHP filter of Theorem 5.4 was designed using the filter length N_H of 50 and the cut-off frequency ω_c of 0.012π (1.2 Hz), following the guidelines of Remark 5.5. RC forms were modified with the more restrictive condition $N_H \leq N_p - \beta + 1 = 51$. Thus Theorem 5.4 for both FMI-RC and GB-RC Algorithms of RC was satisfied. The coefficients of $F_H(q)$ were obtained from the convolution of the impulse response of a 6^{th} order high-pass Butterworth filter with itself. The frequency response of the ZPHP filter is shown in Figure 6.19, which approximates the desired response given by (5.44) within Theorem 5.4.

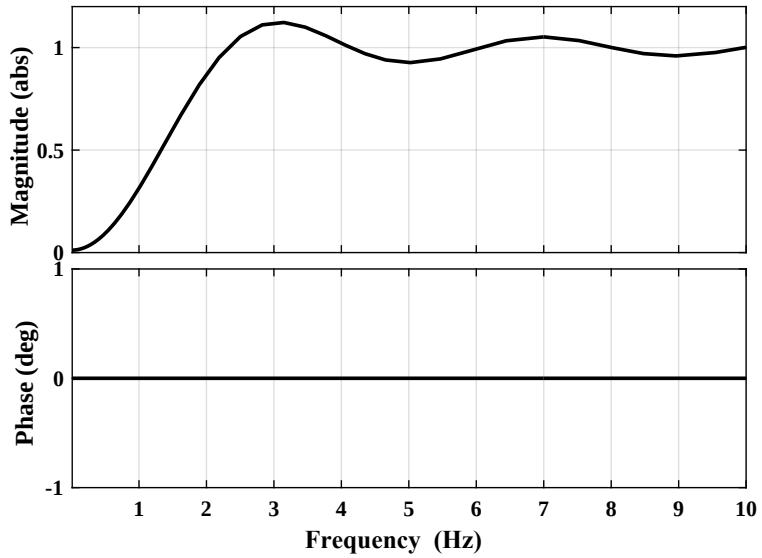

Figure 6.19: Bode plot of the ZPHP filter used experimentally.

To illustrate the design procedure, frequency responses of the relationship between v and y are shown in Figure 6.20 (corresponding to (5.31) and (5.45) respectively). Comparison with $P(q)$ reveals that RC without employing the ZPHP filter has a marked interference with voluntary motion. This interference would cause RC to provide high stiffness in the low frequency region. Therefore, participants may be expected to have difficulty in moving their wrist, thereby impairing wrist function. In contrast, it is apparent from Figure 6.20 that employing the ZPHP filter in RC can satisfy the desired low frequency characteristics (5.32), thereby leading to minimal interference with voluntary motion at frequencies less than 1 Hz.

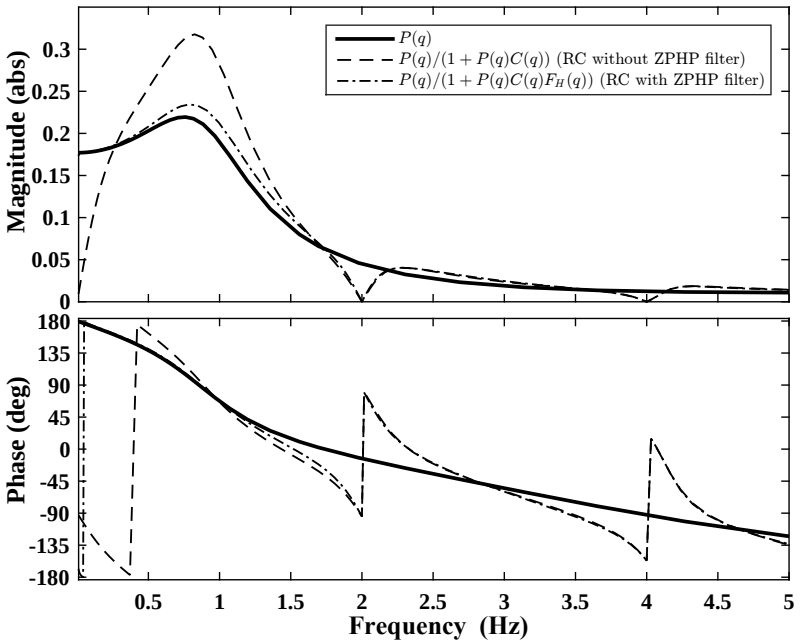

Figure 6.20: Bode plots of $P(q)$ and the closed-loop relationship $S(q)$.

6.4.3 Data Analysis

To quantify both tremor suppression and preservation of voluntary intention during tests *T2* and *T3*, their outputs, y were first subtracted from the free response of test *T1* (termed y_v). The norm of the output over the involuntary frequency range was derived from (3.7), and was used to quantify tremor suppression. This was denoted by

$$\Delta y_t = \|(y_v - y)|_{[\omega_c, 2\pi]}\|_2 = \|y|_{(\omega_c, 2\pi]}\|_2. \tag{6.4}$$

The norm over the voluntary frequency response, defined by (5.30), was used to quantify the preservation of voluntary intention, and was denoted by

$$\Delta y_v = \|(y_v - y)|_{[0, \omega_c]}\|_2. \tag{6.5}$$

The above frequency components of y were obtained via Discrete Fourier Transform (DFT) and subsequent inverse DFT analysis for the corresponding frequency regions. To allow more transparent interpretation, (6.4) and (6.5) were scaled by $1/\sqrt{N}$ to yield RMSE values, where N is the total sample number ($= 40/T_s$).

6.4.4 Effectiveness of RC Algorithms on Tremor Suppression

In this section, the first RC design (without employing the ZPHP filter F_H) is evaluated. This was developed in Section 5.2. A representative result from tracking test *T1* is shown in Figure 6.21 and confirms that voluntary action contains only frequencies contents below 1 Hz, and results in accurate completion when no tremor is present. A representative

result from tracking test *T2* is also shown in Figure 6.21 and confirms that the induced tremor manifests as an oscillation of $f_p = 2$ Hz in conjunction with voluntary action.

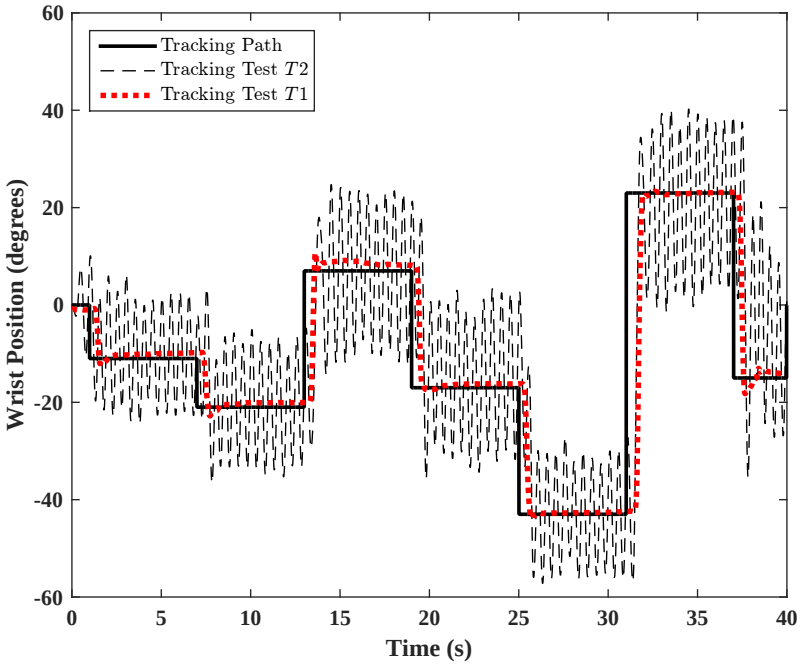

Figure 6.21: Wrist angular positions from tests *T1* and *T2* of Participant 1.

Figure 6.22 shows wrist joint position data acquired from tracking tests *T1*, *T2* and *T3*. To quantify these results, values of the suppression and voluntary interference norm (6.4) and (6.5) respectively are given in Table 6.6. For each participant, tracking test *T3* was repeated several times for different controller parameters to explore the balance between tremor suppression and voluntary interference. Tests were halted if the participant experienced any discomfort. To aid comparison, the results in Table 6.6 without the ZPHP filter are sorted in descending order of Δy_t .

The value of Δy_t from tracking test *T2* indicates large tremulous movements (0.1407 in Participant 1, 0.1790 in Participant 2, 0.1249 in Participant 3 and 0.2246 in Participant 4). Results show that FMI-RC and GB-RC applications result in an average suppression of 89.0% and 82.7%, respectively. To provide comparative results, the proposed control structures are compared with the leading conventional filtering technique which comprises a high-pass filter. This filter was described in detail in Section 3.2. Table 6.6 shows that the average tremor suppression provided by the filter is 59.8% confirming the advantage of RC.

In Participant 2, FMI-RC suppresses involuntary movements by up to 93% (reducing Δy_t from 0.1790 to 0.0119) whilst GB-RC suppresses involuntary movements by up to 92% (reducing Δy_t from 0.1790 to 0.0144). However, the largest suppression in tremor amplitude is less in other participants. In Participant 1, FMI-RC and GB-RC can suppress tremor by up to 91% (reducing Δy_t from 0.1407 to 0.0128) and by up to 87% (reducing Δy_t from 0.1407 to 0.0188), respectively. Tremor suppression provided by FMI-RC in

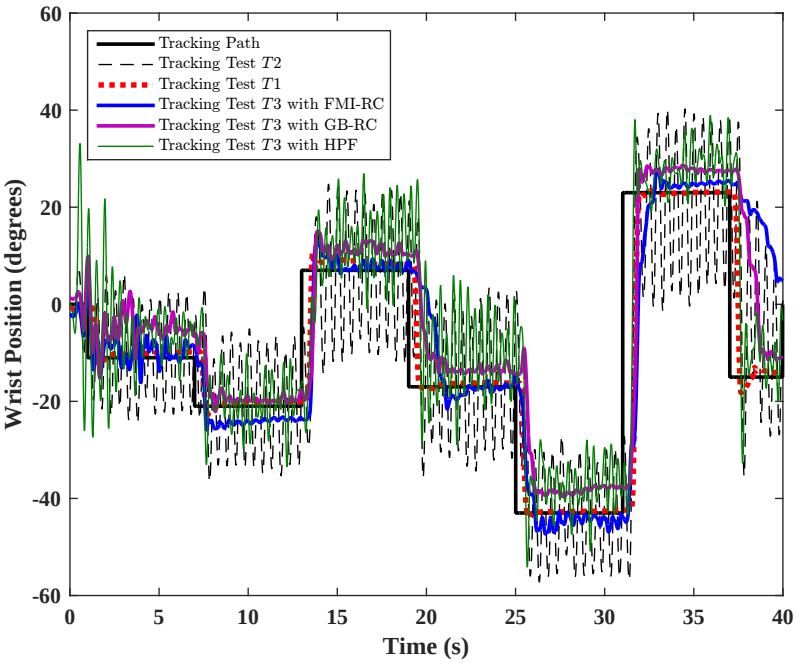

Figure 6.22: Wrist angular positions from all tracking tests of Participant 1 with GB-RC of $\gamma = 60$ and FMI-RC of $\alpha = 65$ and $\beta = 51$.

Participant 4, which is found as 90% (reducing Δy_t from 0.2266 to 0.0545), is very close to that in Participant 1. The lowest suppression in FMI-RC approach is found as 89% in Participant 3 (reducing Δy_t from 0.1249 to 0.0137). In addition, the GB-RC approach can suppress tremor in Participant 3 and Participant 4 by approximately 80%.

Table 6.6 indicates that the HPF exhibits a decrease of 71% (reducing Δy_t from 0.1790 to 0.0524) and 51% (reducing Δy_t from 0.2266 to 0.2018) in tremor amplitude in Participant 2 and Participant 4, respectively. In addition, the poorest performance of the HPF is obtained in Participant 1 with the tremor suppression of 28% (reducing Δy_t from 0.1407 to 0.1016) and the highest is obtained in Participant 3 with 89% (reducing Δy_t from 0.1249 to 0.0143) tremor suppression, which is due to the lowest Δy_t of 0.1249 from tracking test *T2* experienced by Participant 3.

Table 6.6 also shows that Δy_v corresponding to tracking test *T1* is 0.1827 in Participant 1, 0.1624 in Participant 2, 0.1867 in Participant 3 and 0.1827 in Participant 4. Comparison of these results with those relevant to the tracking test *T3* indicates that FMI-RC, GB-RC and HPF increase Δy_v by an average of 29.3%, 35.2% and 33.7%. This means that voluntary distortion is experienced in all control approaches, except the HPF in Participant 3. In this one case Δy_v is actually smaller than the baseline value from tracking test *T1*, which may be due to participants learning how to track better over time.

In summary, these results confirm that the RC approached developed in Chapter 5.2 can suppress tremor more than the leading conventional approach. However the distortion

Table 6.6: Changes in the scaled measures with varied control variables of all controllers.

	Controller Type	Controller Parameters	Δy_v			Δy_t		
			T1⋆	no ZPHP‡	ZPHP‡	*T2*†	no ZPHP‡	ZPHP‡
Participant 1	FMI-RC	$\alpha = 30\ \beta = 28$	0.1827	0.2430	0.1792	0.1407	0.0167	0.0212
		$\alpha = 40\ \beta = 36$		0.2638	0.1773		0.0135	0.0322
		$\alpha = 65\ \beta = 51$		0.2495	0.1932		0.0128	0.0211
	GB-RC	$\gamma = 30$		0.2263	0.1994		0.0215	0.0224
		$\gamma = 60$		0.2230	0.1939		0.0188	0.0230
	HPF	$6^{th} order$		0.2089	0.2144		0.1016	0.1067
Participant 2	FMI-RC	$\alpha = \beta = 30$	0.1624	0.2567	0.1737	0.1790	0.0191	0.0205
		$\alpha = 61\ \beta = 51$		0.2919	0.1907		0.0119	0.0182
	GB-RC	$\gamma = 36.8$		0.2927	0.1968		0.0144	0.0205
	HPF	$6^{th} order$		0.3360	0.2174		0.0524	0.0442
Participant 3	FMI-RC	$\alpha = \beta = 40$	0.1867	0.2005	0.1659	0.1249	0.0166	0.0162
		$\alpha = \beta = 50$		0.2053	0.1752		0.0137	0.0167
	GB-RC	$\gamma = 136.5$		0.2825	0.1967		0.0279	0.0241
		$\gamma = 47.5$		0.2722	0.1902		0.0239	0.0203
	HPF	$6^{th} order$		0.1755	0.1709		0.0143	0.0206
Participant 4	FMI-RC	$\alpha = 35\ \beta = 30$	0.1827	0.1998	0.1844	0.2266	0.0588	0.0403
		$\alpha = \beta = 30$		0.1902	0.1620		0.0578	0.0333
		$\alpha = \beta = 25$		0.2020	0.1719		0.0545	0.0378
	GB-RC	$\gamma = 12.7$		0.2029	0.1815		0.0987	0.0727
		$\gamma = 38.8$		0.2043	0.1722		0.0836	0.0441
	HPF	$6^{th} order$		0.2075	0.2039		0.2018	0.1490

⋆ corresponds to Δy_v of tracking test *T1*.
† corresponds Δy_t of tracking test *T2*.
‡ These values are calculated from the data of tracking test *T3*.

in voluntary action is greater. The reason for this undesired effect is illustrated in Figure 6.23 and Figure 6.24, where the stimulation inputs(u_{fcr} and u_{ecr}) generated by FMI-RC and GB-RC approaches were respectively plotted. The corresponding wrist positions are plotted in Figure 6.22. As seen in Figure 6.23 and Figure 6.24, RC applies continuously the maximum stimulation input to the flexors. This high level stimulation impairs the voluntary motion of participants when they move their wrist from flexion (positive position) to extension (negative position). This can be clearly seen in results for the cases without the ZPHP filter, given in Appendix E. The ability of the ZPHP filter to reduce this distortion will now be examined.

6.4.5 Effects of ZPHP Filter on Voluntary Distortion

In this section, the second RC design of Section 6.4.2 employing the ZPHP filter F_H is evaluated to confirm the theoretical properties of Theorem 5.4. From the data in Table 6.6, it is apparent that adding the ZPHP filter contributes to a decrease in Δy_v in

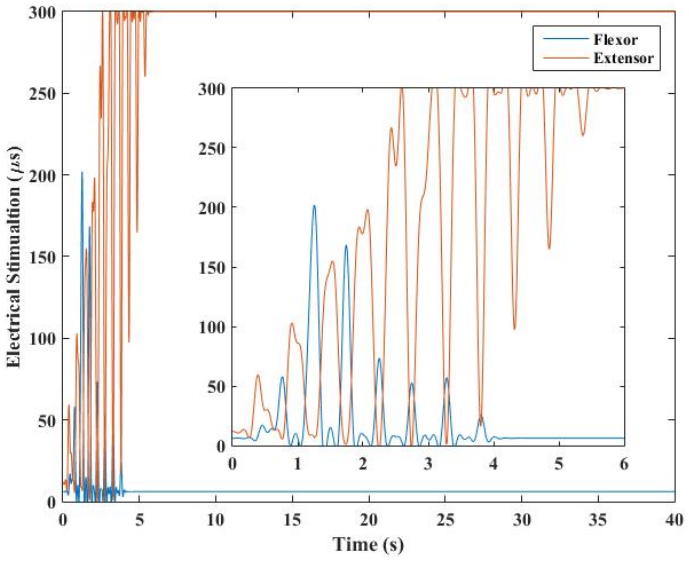

Figure 6.23: Control input applied by FMI-RC without ZPHP filter to muscles.

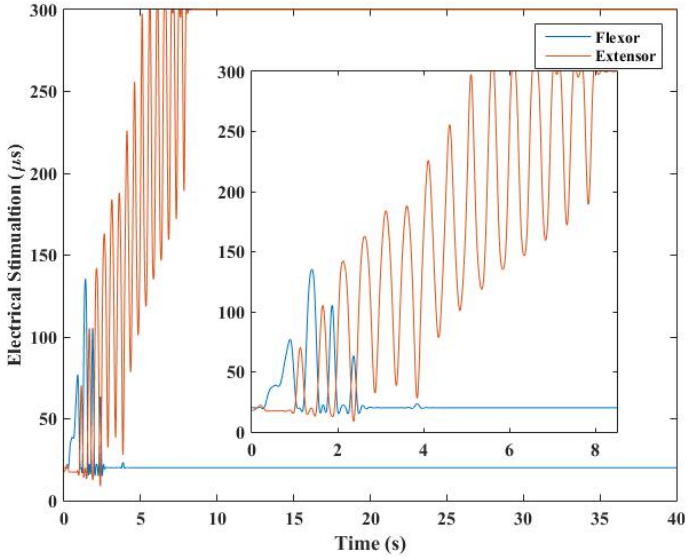

Figure 6.24: Control input applied by GB-RC without ZPHP filter to muscles.

all cases of RC and the average decreases in Δy_v are respectively calculated as 21.8% and 18.7% for FMI-RC and GB-RC. In contrast, the ZPHP filter is only capable of reducing Δy_v by 35.3% in Participant 2 for the cases of the HPF. On the other hand, the ZPHP filter also manages to produce the highest decrease in Δy_v for the RC approaches in Participant 2.

The results show that Δy_v is decreased by an average of 22.7% and 33.5% in Participant 1 and Participant 2 for FMI-RC cases. In addition, the ZPHP filter can produce a decrease of 32.8% and 30.4% in Δy_v in Participant 2 and Participant 3 for GB-RC cases. In Participant 4, the decrease in Δy_v ranges between 7.7% and 15.7% for various RC cases. Thus these results confirm that the ZPHP filter is able to reduce the interference of RC approaches with voluntary action. However the ZPHP filter may cause a slight

increase in Δy_t in some cases since adding the ZPHP filter shapes the frequency response of $S(q)$ and leads to a slight increase in the gain of $|S(q)|$ at the tremor frequency. In contrast, in several cases the ZPHP filter actually leads to a reduction in Δy_t (see e.g. the results of Participant 4). Figure 6.25 contains representative results showing that RC can suppress tremor effectively when the ZPHP filter is added.

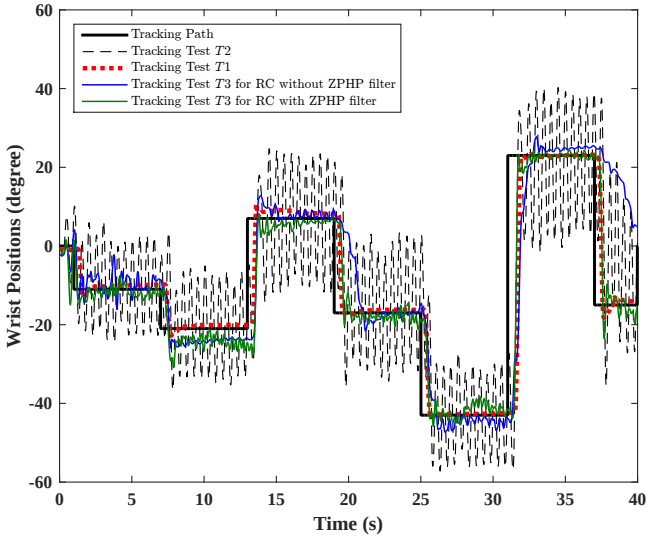

Figure 6.25: Wrist angular positions of the closed-loop RC system without and with ZPHP filter in Participant 1.

These results illustrate that adding a filter enables faster and more accurate tracking due to the lack of interference. In comparing to Figure 6.23 and Figure 6.24, Figure 6.26 and Figure 6.27 shows that RC only consider higher frequencies than the cutoff frequency of the ZPHP filter and do not attempt to control any low frequency movement. The further results corresponding to the cases with the ZPHP filter, shown in Appendix E, confirm that adding the ZPHP filter enables participants to follow the tracking path more satisfactorily.

6.5 Summary

In this chapter an experimental study is performed to validate the procedure developed in Chapter 4 to identify the wrist model and the RC approach developed in Chapter 5 to suppress tremor with minimal interference with voluntary action. Tests are conducted using a previously validated test platform with unimpaired participants. Since all participants recruited in the experiments are neurologically healthy, a mechanical system is designed and installed into the test platform to induce tremor artificially. This system is able to produce a tremulous motion at a desired frequency.

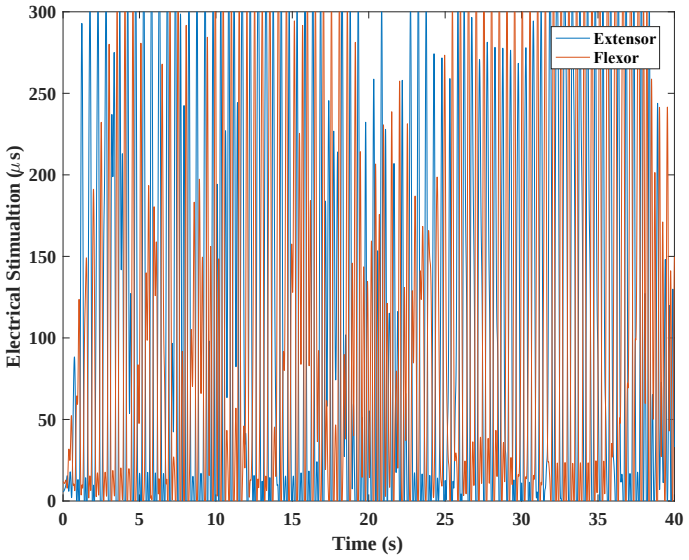

Figure 6.26: Control input applied by FMI-RC with ZPHP filter to muscles.

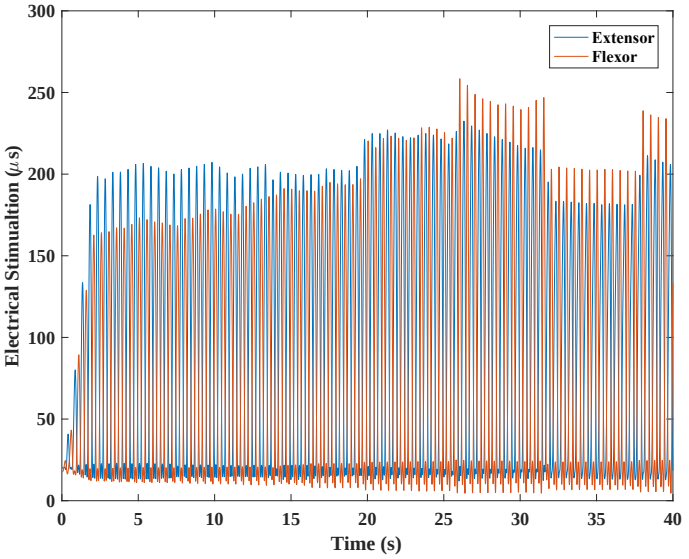

Figure 6.27: Control input applied by GB-RC with ZPHP filter to muscles.

Although the proposed model structure does not represent the fatigue of the flexor and extensor muscles during FES-induced muscle contractions, which can limit the performance of FES application, the experimental results have confirmed satisfactory modelling accuracy, with cross-validation tests giving rise to a fitting accuracy of over 60% in all participants tested. Moreover, they confirm that a prescribed parameter set can be fixed for all participants with only minor degradation in accuracy, further reducing the identification time required. This makes the system identification procedure appropriate for clinical deployment.

In control application, the test results corresponding to the case where ZPHP filter is not employed show that RC can suppress tremor by higher than 90%, although the simulation results of the RC approaches presented in Chapter 3 confirm that RC can

produce complete tremor suppression. In addition, the results also show that RC leads to an average increase of 32.5% in the voluntary distortion. This confirms that RC has a significant interference with voluntary motion, leading to impairment in voluntary wrist movement. Thus a ZPHP filter is designed and implemented such that it can reduce this distortion in the intended movement. The experiments confirm that the implementation of the ZPHP filter with RC approach reduces the distortion by an average of 20.2% and leads to minimal interference in voluntary motion but may cause a decrease in tremor suppression. The results indicate that RC can suppress tremor more efficiently than conventional filtering techniques. However, the performance of the RC approach is dependent on the accuracy of the model since the design of RC requires the knowledge of the responses of the model in either time or frequency domain. Based on the experiences gained from the experiments, a model with an accuracy of higher than 50% is sufficiently reliable to design an effective RC. However, there are also other limitations of RC mentioned previously in Chapter 3 due to a change in either model dynamics or tremor frequency over time. If the model is changed (due to, e.g., the effect of muscle fatigue), then the model should be re-identified and RC should also be re-designed using the new model to maintain its performance. Otherwise, the monotonic convergence criteria may not be satisfied or the performance of RC may be decreased. To examine this limitation, $F(q)$ of RC is designed based on the wrist dynamics $P_1(q)$ and then the wrist dynamics is considered to become $P_2(q)$ and $P_3(q)$. However, $F(q)$ is not re-designed using these new wrist dynamics. Figure 6.28 shows whether the monotonic convergence is satisfied using the same $F(q)$ with $P_2(q)$ and $P_3(q)$. For the case of $P_2(q)$, RC is able to suppress tremor more slowly. This means that the transient response becomes longer. However, the case of $P_3(q)$ is more troublesome than the previous case since the convergence criteria cannot be satisfied. This means that this case produces an unstable closed-loop system. In addition, RC, which has the structure of $F(q)(q^{N_p}-1)^{-1}$, is designed for a

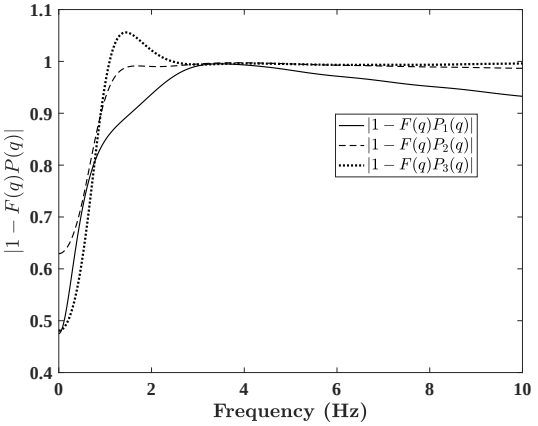

Figure 6.28: The change of RC convergence due to a change in $P(q)$.

constant N_p period to suppress a N_p-periodic tremor signal. However the performance of RC is limited if RC is designed based on a period which is different from the current period. To confirm this, a simulation is undertaken in which RC is designed based on

the tremor frequency of 2 Hz and then it is used to suppress tremor at the frequencies of 2, 2.002 and 2.02 Hz. From the results shown in Figure 6.29, it is apparent that RC can suppress tremor at 2 Hz completely but it is unable to achieve a complete tremor suppression at the other frequencies. Thus RC should be re-designed if N_p is changed. To address these limitations, a more robust RC approaches to varying tremor frequency and model uncertainties will be used for future research.

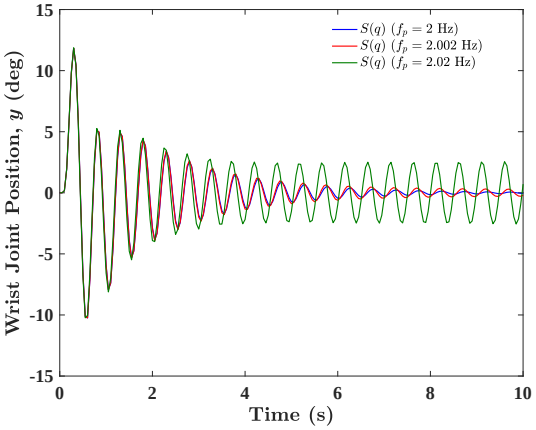

Figure 6.29: The effects of varying tremor frequency f_p of RC designed for $f_p = 2$ Hz on tremor suppression.

Chapter 7

Conclusions & Future Work

7.1 Conclusions

Tremor is a rapid, periodic involuntary movement often seen in patients with neurological conditions such as MS and Parkinson's disease. Different techniques have been developed for tremor suppression. However, each technique has its own drawbacks. An alternative method is to use functional electrical stimulation for tremor suppression. Previous studies on FES based tremor suppression system suggest that this debilitating oscillation can be suppressed by applying FES within a closed-loop control system. However, current implementations use classical control methods and have proved capable of only limited performance. They cause undesirable distortion below 1 Hz, thereby impairing the patient's voluntary motion, and produce large high-frequency stimulation transients, leading to significant discomfort (Prochazka et al., 1992a). Additionally, they are incapable of producing complete tremor suppression. To produce a complete disturbance rejection, a controller must include a model of the disturbance and RC scheme based on IMP.

To establish the feasibility of embedding RC for tremor suppression, Chapter 3 presents a rigorous comparison between a general RC scheme and the conventional filtering technique proposed by the leading study of Prochazka et al. (1992a). To obtain reliable results, the simulation study is conducted using a linear model of the electrically stimulated tremulous wrist based on experimental data. The simulation results show that the RC scheme can suppress tremor completely, significantly outperforming the filtering technique. However the RC scheme has also a significant effect on voluntary action, in the same way as filtering technique does. In addition, the underlying dynamics of the limb is required to design an effective RC scheme for tremor suppression.

To address these obstucles, Chapter 4 develops a nonlinear model structure with an identification procedure. The proposed model structure represents critical features of wrist

dynamics, together with identification procedure that can be easily applied to clinical application. The preliminary simulation results show that the developed system identification procedure is capable of identifying an accurate wrist model, thereby explicitly addressing the limitations of existing methodologies. In addition, this model structure can be linearised to enable the linear RC scheme proposed in the previous chapter to be employed within the closed-loop system for tremor suppression.

From the simulation results in Chapter 3 it is also apparent that the proposed RC scheme has a significant interference with voluntary action. To eliminate the interference of RC with voluntary action, Chapter 5 proposes a novel and rigorous framework for implementing RC based FES tremor suppression which combines the wrist model developed in Chapter 4 with the linear RC scheme proposed in Chapter 3. This framework includes a linearising procedure to enable a linear RC scheme, together with a mechanism to preserve the patient's voluntary motion. This mechanism employs a zero-phase high-pass filter implemented in series with the RC scheme. However the simulation results performed to test this mechanism show that there is a trade-off between the reduction in voluntary distortion and the monotonic convergence of the RC scheme. Thus the designer should maintain the balance between the conditions of satisfying monotonic convergence and allowing minimal interference with voluntary motion.

The closed-loop system proposed in this research is tested experimentally on unimpaired subjects using a wrist rig with a FES device linked to a computer using a dSpace 1103 control card which collects all data and performs the control action in the Matlab/Simulink environment. Since unimpaired participants are recruited, a mechanical system is installed within the test equipment to produce an artificial tremulous motion. This system employs a DC motor and a motor controller employing the torque control. The test results confirm that this mechanical system is able to produce a tremulous motion at a desired tremor frequency.

Experimental results in Chapter 6 confirm the accuracy of the proposed identification procedures, andshow that high levels of accuracy can be achieved in a short identification time using test procedures that are suitable for future transference to the clinical domain. Another experimental study is performed to test the performance of the RC scheme. The results are bench-marked against classical feedback control designs to establish the efficacy of the proposed RC approach in Chapter 5. The experimental results show that this novel RC approach can suppress tremor more efficiently than the traditional filtering technique and prevent the FES control action interfering with the patient's voluntary response. These findings confirm that the proposed RC based approach has great potential for tremor suppression and motivates this novel approach to be transferred to clinical practice.

7.2 Future Work

The experimental results confirm that the proposed technique in this research has great potential to suppress tremor and has important advantages over conventional techniques. Furthermore, the results presented in this research motivate a number of areas of further research as follows:

1. **Robust RC design**: In this research, the experiments were conducted with models that were assumed accurate at the time of identification. However there are uncertainties due to either the inaccuracy in model parameters or the unmodelled high frequency dynamics. To solve these issues would increase the robust performance of the repetitive controller. The latter can be handled by implementing a zero-phase low pass filter (Longman, 2010). To address the former, there are several methods to design a more robust repetitive controller in the presence of the modelling uncertainty.

   (a) Hatonen et al. (2004) states that if a multiplicative uncertainty is defined that reflects the uncertainties caused by modelling errors, then a robust closed-loop RC system can be designed using the approximation of the true plant and this multiplicative uncertainty.

   (b) An alternative method is developed by Freeman and French (2015) to design a robust iterative learning control framework. The same method can be applied to repetitive control scheme proposed in this research. The method is based on designing the controller using the plant model, which has the best performance amongst a set of plants whose uncertainty can be specified in advance. The performance of each plant candidate is evaluated using an optimisation based estimation process and then the best plant model is selected to design the controller. This is a form of switched adaptive control.

2. **Adaptation of RC scheme to a varying tremor frequency:** In this research study, it was considered, based on the results presented by the previous studies, that the tremor frequency was invariant. However it may change over time. If this is the case, then RC will suppress tremor less effectively. To address this issue, the following methods can be used:

   (a) Multiple internal models corresponding to the possible frequency range of the tremor can be employed in the RC scheme. The necessary range will be defined using an online tremor estimation method. This method is based on the study of Steinbuch (2002) which showed that satisfactory performance could be achieved over a wider range of disturbance frequencies.

   (b) Another alternative method is to adapt the repetitive controller according to a change in tremor frequency. To measure the tremor frequency, an online

frequency estimation method can be developed, and the repetitive controller can then be updated. However, issues related to initial conditions and the inclusion of time-delays to prevent instability will need to be addressed.

3. **Testing of the approach clinically:** Following successful evaluation with unimpaired subjects, testing can be undertaken with MS patients diagnosed with intention tremor to examine whether the proposed approach is able to produce significant tremor suppression in clinical application. To do it, the same testing procedure proposed in this research can be applied. To perform the experiments with MS patients, a research ethics application can be carried out, in collaboration with researchers from the School of Health Sciences at the University of Southampton.

4. **Home-based tremor suppression:** The current system is inapplicable to a home-based use since it employs a potentiometer to measure the movements of the wrist and an medium-sized immobile stimulator. In addition, the current system limits the wrist motion to flexion/extension. However participants need to use this system in their daily life. Thus this system should be upgraded such that it can meet the needs of patients in home-based use. This motivates design of a new system using new sensors and small sized stimulator suitable for home-based use.

5. **Location of electrodes:** Locating the accurate electrode position can be a very time-consuming process. The electrode employed in the current system is one of the smallest electrodes commercially available. However the other muscles adjacent to the targeted muscle can be also stimulated due to the large conducting surface of the electrode, and this undesired stimulation makes participants feel uncomfortable. This issue can be solved using a new type electrode, named an electrode array. This new invention is composed of a set of small conductive electrodes arrayed regularly on a wearable patch. Participants only need to wear the electrode array on their affected arm. Then a developed system can automatically select the electrodes amongst the others that enables the relevant muscles to produce the maximum torque.

Appendix A

Theorem and Property

A.1 Bode Sensitivity Integral (Waterbed Effect)

The *waterbed* effect is explained by Skogestad and Postlethwaite (1996) as follows:

If the loop transfer function $[L(s)]$ in that case, which can be found as $cH(s)G(s)$ from (3.1), has at least two more poles than zeros, then a trade-off between a reduction and an increase in sensitivity must be performed. The sensitivity function for the closed-loop system is $S = (I + L)^{-1}$ and must satisfy:

$$\int_0^\infty |S(jw)|\, dw = \pi \sum_{i=1}^{N_p} Re(p_i) \tag{A.1}$$

where $Re(p_i)$ denotes the real part of each right-half plane pole (RHP-pole) of $L(s)$ and N_p denotes the number of the RHP-poles of loop transfer function at locations p_i. Furthermore, if the loop transfer function has no poles in the RHP, then the right-hand side of the sensitivity function is equal to zero which means that the sensitivity function can be modified such as

$$\int_0^\infty |S(jw)|\, dw = 0. \tag{A.2}$$

So, if one wants to suppress the amplitude at one frequency for a stable system, then some increases in amplitudes at other frequencies should occur in order to provide the modified sensitivity function for the modified system, in other words, to keep the value of the left-hand side term of the modified function equal to zero.

A.2 Controllability of Discrete Time System

Controllability is defined as the ability of an external input to move the system state $x(k)$ from any initial state $x(0)$ to any desired final state $x(N)$ in a finite time $N < \infty$.

Theorem A.1. *The discrete time system given by*

$$\begin{aligned} x(k+1) &= \Xi x(k) + \Psi u(k) \\ y(k) &= \Theta x(k) \end{aligned}, \tag{A.3}$$

with a state matrix $\Xi \in \mathbb{R}^{n \times n}$ and a input vector $\Theta \in \mathbb{R}^{n \times m}$ is controllable if and only if the rank of the controllability matrix defined by

$$\mathcal{C}(\Xi, \Psi) \coloneqq [\ \Psi \ \vdots\ \Xi\Psi \ \vdots\ \dots \ \vdots\ \Xi^{n-1}\Psi\ ]$$

is equal to n.

A.3 Observability of Discrete Time System

Observability is used to examine how well the states of a system can only be determined from the measurements of its outputs.

Theorem A.2. *The discrete time system given by* (A.3) *with a state matrix $\Xi \in \mathbb{R}^{n \times n}$ and a output vector $\Theta \in \mathbb{R}^{r \times n}$ is observable if and only if the rank of the observability matrix defined by*

$$\mathcal{O}(\Xi, \Theta) \coloneqq [\ \Theta \ \vdots\ \Theta\Xi \ \vdots\ \dots \ \vdots\ \Theta\Xi^{n-1}\ ]^\top$$

is equal to n.

Appendix B

State Feedback Control

Recall the plant $P(q)$ with one input and one output from (4.12)

$$P(q) = \frac{B_P(q)}{A_P(q)} = \frac{b_0 q^{-m_P} + b_1 q^{-(m_P+1)} + \ldots + b_{n_P} q^{-(m_P+n_P)}}{1 + a_1 q^{-1} + \ldots + a_{l_P} q^{-l_P}} \tag{B.1}$$

can be represented in a state space form of

$$\begin{aligned} x(k+1) &= \Xi x(k) + \Psi u(k) \\ y(k) &= \Theta x(k) \end{aligned} \tag{B.2}$$

where

$$\Xi = \begin{bmatrix} -a_1 & -a_2 & \cdots & -a_{l_p-1} & -a_{l_p} \\ 1 & 0 & \cdots & 0 & 0 \\ 0 & 1 & \cdots & 0 & 0 \\ \vdots & \vdots & \ddots & \vdots & \vdots \\ 0 & 0 & \cdots & 1 & 0 \end{bmatrix},$$

$$\Psi = \begin{bmatrix} 1 & 0 & 0 & \cdots & 0 \end{bmatrix}^\top,$$

$$\Theta = \begin{bmatrix} b_0 & b_1 & \cdots & b_{n_P} \end{bmatrix}.$$

which define the system matrix, the input vector and the output vector, respectively. Then, the impulse response of the system $P(q)$ can be described as the solution of the following initial value problem

$$\begin{aligned} x(k+1) &= \Xi x \ , \ x(0) = \Psi \\ y(k) &= \Theta x(k) \end{aligned} . \tag{B.3}$$

which shows the impulse response of $P(q)$ depends on the eigenvalues of Ξ. To achieve an impulse response length of the plant $P(q)$ less than N_P, the eigenvalues of Ξ can be

relocated. To do this, a state feedback law with a gain of K, which has the form of

$$u = -Kx, \tag{B.4}$$

can be implemented if the plant $P(q)$ is controllable and observable (see Appendix A.2 and Appendix A.3).

B.1 Deadbeat Control

As mentioned above, one possible method is deadbeat control algorithm in which the control law (B.4) is determined such that all closed-loop system poles are placed at the origin with a suitable choice of K.This yields the desired characteristic polynomial of the closed loop system

$$\Upsilon^{\star}(q) = \det\left(qI_{l_P}\right). \tag{B.5}$$

Substituting (B.4) into (B.2), the characteristic polynomial of the closed-loop system becomes

$$\Upsilon_c(q) = \det\left(qI_{l_P} - (\Xi - \Psi K)\right). \tag{B.6}$$

Then with equating (B.5) to (B.6), the state feedback gain K can be found by solving $\Xi - \Psi K = 0$. This strategy has the property that it can drive the system outputs to zero in the smallest time step, which is usually equal to the system order l_P. If the number of the states l_P is less than the length of the period N_p, then deadbeat control can be applied to satisfy the assumption $h_i = 0$, $\forall i > N_p$. However Åström and Wittenmark (1997) states that deadbeat control produces a control input with higher magnitude if lower N_p is required.

B.2 Pole Placement

An alternative method is to use the control law (B.4) that can place the poles of the closed-loop system to the desired positions if the desired characteristic polynomial of the closed loop system is known. Assume the desired characteristic polynomial is

$$\Upsilon^{\star}(q) = q^{l_p} + a_1^{\star}q^{l_p-1} + \ldots + a_{l_P-1}^{\star}q + a_{l_P}^{\star} = \det\left(qI_{l_P} - \Xi^{\star}\right). \tag{B.7}$$

Similarly, K can be found by solving the problem given by

$$\det(qI_{l_P} - \Xi^{\star}) = \det(qI_{l_P} - (\Xi - \Psi K))$$

which arises from equating (B.7) to (B.5).

The control methods mentioned above require the information of the states. If all states are measurable, then these methods can directly be applied. If some states are measurable, then an state observer should be implemented to estimate the unmeasurable states.

Appendix C

Consent Form

Ethics reference number: **ERGO/**FPSE**/16530**	Version: 2	Date: 2016-09-23
Study Title: Can Functional Electrical Stimulation mediated by Repetitive Control dampen intention tremor in Multiple Sclerosis? – feasibility study		
Investigator: Engin Hasan Copur		

Please initial the box(es) if you agree with the statement(s):

I have read and understood the Participant Information (version 6.6c dated 2016-09-23) and have had the opportunity to ask questions about the study. ☐

I agree to take part in this study. ☐

I understand my participation is voluntary and I may withdraw at any time and for any reason. ☐

Data Protection

I understand that information collected during my participation in this study is will be stored on a password protected computer and that this information will only be used in accordance with the Data Protection Act (1998). The DPA (1998) requires data to be processed fairly and lawfully in accordance with the rights of participants and protected by appropriate security. In addition, the DPA (1998) makes provision for an appropriate authority, such as the Police, to access data held by the study for the purpose of the examination of the efficiency of the proposed tremor suppression strategy.

Name of participant (print name).....

Signature of participant.....

Date.....

Appendix D

Participant Information Form

Ethics reference number: **ERGO/**FPSE**/16530**	Version: 2	Date: 2015-07-28
Study Title: Can Functional Electrical Stimulation mediated by Repetitive Control dampen intention tremor in Multiple Sclerosis? – feasibility study		
Investigator: Engin Hasan Copur		

Please read this information carefully before deciding to take part in this research. If you are happy to participate you will be asked to sign a consent form. Your participation is completely voluntary.

Some definitions:

- **An intention tremor** at the wrist joint is an uncontrollable movement at the wrist which makes it harder to perform daily tasks, which include grasping.
- **Functional Electrical Stimulation** (FES) is when a small current from a FES device is applied to a muscle to make it contract. It gives a tingling feeling.
- **Repetitive control** are special computer programmes that have been written and included in the FES device that will learn and predict your intention tremor and so alter the electrical stimulation (tingling) to stop the intention tremor.

What is the research about? This research aims to ascertain whether an intention tremor at the wrist joint can be dampened by Functional Electrical Stimulation (FES). The study will look at how effective it is to place a few small electrical currents into the muscles around your wrist. This will cause them to contract. The electrical current gives you a tingling feeling and does not hurt. The study will look at mimicking a temporary intention tremor into healthy, unimpaired adults and identify whether this can be suppressed by FES. The long term aim, which is beyond the scope of this study, is to be able to control intention tremor of the wrist joint in MS people. This study has not been funded and is being undertaken as an academic requirement for me to attain a PhD qualification in Electronic and Electrical Engineering. It will also form part of a major collaborative research programme between The Faculty of Physical and Applied Sciences and the RHT Research Group in the Faculty of Health Science at the University of Southampton.

Why have I been chosen? You will be participating to establish whether FES can dampen a temporarily induced intention tremor. We are specifically asking you as you are healthy and we need to trial the FES device to control intention tremor on healthy adults.

Do I have to take part? Taking part in this study is completely voluntary. We will describe the study and go through this information sheet and give you a chance to ask any questions. If you agree to take part, we will then ask you to sign a consent form. You will also be able to leave the study at any time if you so wish.

Confidentiality All details relating to you will be kept completely confidential.

Benefit to you and others? There will be no direct benefit to you from this study nor will there be any monetary compensation. However, the study will provide the evidence needed to build a FES device to control intention tremor over more than one joint such as the elbow and the shoulder. This will ultimately benefit MS patients with intention tremor to help improve their quality of life. You will be eligible to receive details of the study's results. The results of this study will be published in an academic journal but your identity will be kept completely anonymous.

What will be required of you? You will be asked to provide informed consent to participate in the study but only if you are willing to participate in this study. The research requires you to attend a single sitting where we will collect data about the movement in your wrist. This will take place in the research laboratory (room 2045) at the University of Southampton's Building 16, University Rd. This is expected to be between 15/08/2015 and 15/12/2016 but we will confirm a date with you. The session should last no longer than one hour. However, you will be able to leave the study at any time if you so wish.

What will happen to you? You will be asked to sit in a chair. You will place one of your arms into the specialised padded armrest which we can adjust so that it is comfortable. There are some Velcro straps and an inflatable pouch (similar to a blood pressure cuff) which will hold your arm still so only your wrist can move. At the end of the arm rest is a measuring device called a wrist rig, which will be used to indicate to you where you will need to move your wrist to. This is linked to a computer so we can collect data about your wrist movement. The photo below, Figure 1., shows roughly what the wrist rig will look like.

You will be asked to move your wrist forwards and backwards for us to take some readings. This gives us information about the amount of force you have available in your wrist. This may be done a few times during the data collection. You will be asked to perform a tracking task where you move your wrist to specified positions that will be displayed on the wrist rig. Individual lights will illuminate on the rig to guide you to where you need to move your wrist joint to. We will place jelly electrodes onto your forearm. A small electrical stimulation (FES) will be applied to your forearm muscles through the jelly electrodes causing them to contract and mimic the intention tremor. We will ask you to perform another tracking task. We will then place jelly electrodes onto your forearm so that an electrical

stimulation from the FES device can be applied to your forearm muscles to try and dampen the intention tremor. You will then be asked to perform another tracking task. Figure 2. below is a photo of the FES device and the jelly electrodes that will be attached to your arm.

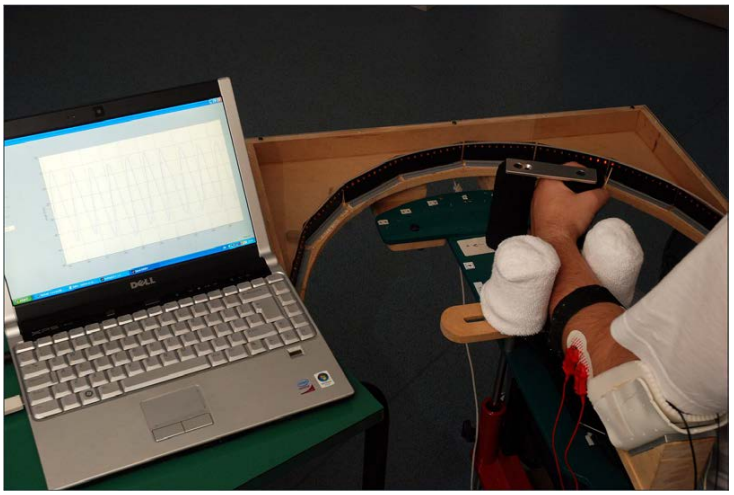

Figure 1. A photo of the wrist rig with the attached laptop.

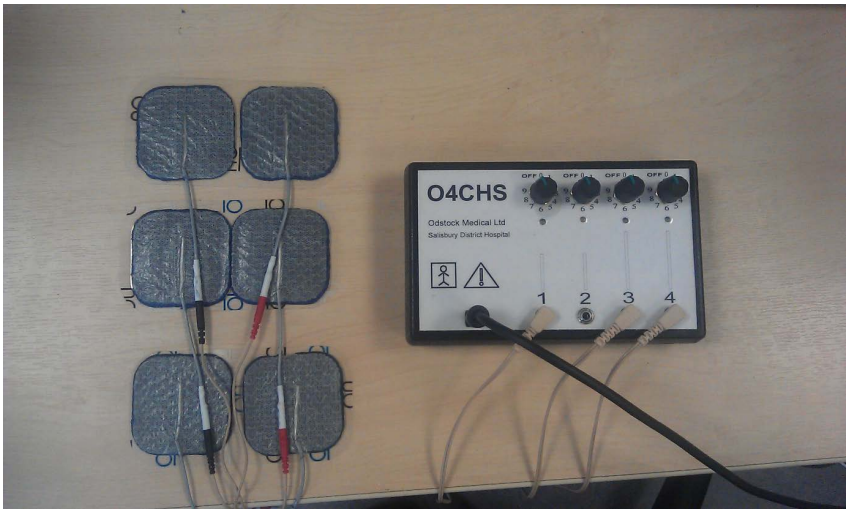

Figure 2. A photo of the jelly electrodes (left) and the FES device (right).

The FES device includes sophisticated technology called Repetitive Control that will try and predict the intention tremor's movements in your hand and thus produce the correct electrical stimulation to dampen it. FES technology is currently used commercially for people with foot drop to assist them to adequately lift their foot during walking. No harm will come to you during the test as we are using the same FES device currently used for foot drop.

Everything will be explained again at the time of data collection just before we start the process, so you do not need to worry.

If you agree to be included in this study you will be asked to perform the following actions.

- Contact the researcher at ehc1g12@ecs.soton.ac.uk so we can arrange a mutually convenient time for collecting data.
- Sign a written consent form just before we start the data collection.
- Move your wrist forward and backward when the rig is held stationary so that we can measure the force in your wrist.
- Perform a tracking task with your wrist.
- Allow jelly electrodes to be attached to your forearm.
- Allow the FES device to be attached to the jelly electrodes so we can try and dampen the intention tremor.
- Allow a temporary intention tremor to be artificially induced into your wrist joint using a motor driven system.
- Perform a tracking task with your wrist with an induced intention tremor.
- Allow the FES device to be used to dampen the intention tremor.
- Perform another tracking task with your wrist with the induced intention tremor and also with stimulation from the FES device.

What are the disadvantages or risks of taking part? There are no disadvantages or risks to taking part in this research. The only discomfort you may experience is the tingling sensation from the FES device but if you find this too uncomfortable we will stop the session.

What are the side effects of taking part? Any stimulation from the FES device is temporary and only lasts while the FES device is attached to the muscle. So there are no side effects of taking part.

What if I have a problem or a complaint? If you have a concern or a complaint about this study you should contact Cecilia Di Chio, RIS Officer (Address: University of Southampton, Building 60, Highfield, Southampton, SO17 1BJ ; Tel: +44 (0)23 8059 5686; Email: C.Di-Chio@soton.ac.uk) and/or Lester Gilbert (Address: University of Southampton, ECS, Highfield, Southampton, SO17 1BJ ; Tel: +44 (0)23 8059 3831; Email: lg11@soton.ac.uk). If you remain unhappy and wish to complain formally Martina can provide you with details of the University of Southampton Complaints Procedure.

Should you require further information or if you have any questions: Please contact me, Engin Hasan Copur the researcher, at ehc1g12@ecs.soton.ac.uk or my supervisors, Christopher Freeman, at cf@ecs.soton.ac.uk, Bing Chu, b.chu@ecs.soton.ac.uk, Dina Shona Laila, D.Laila@soton.ac.uk at the University of Southampton

Your help in this research is greatly appreciated and results from the research will be sent to you if you wish to receive them.

Yours sincerely

Engin Hasan Copur

The Investigator

Appendix E

Full Results

E.1 Participant 1

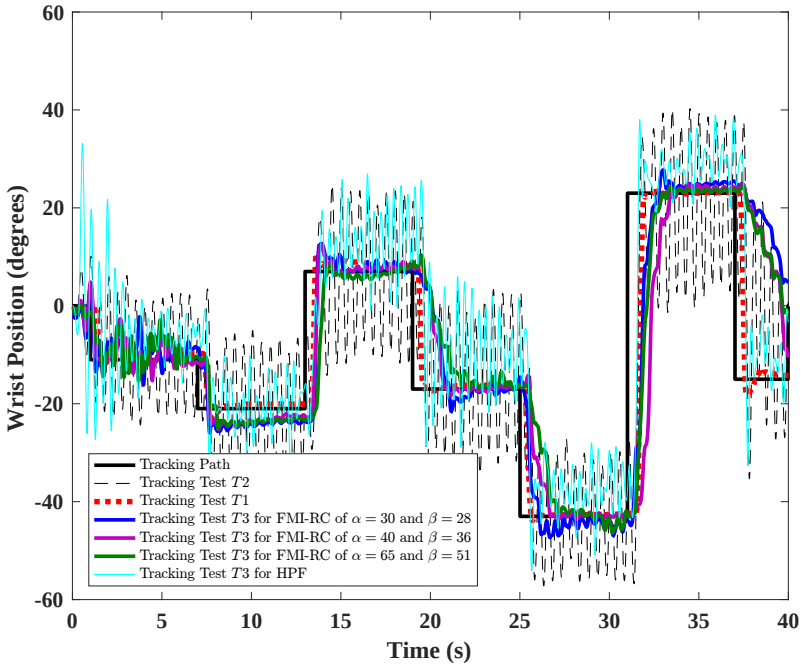

Figure E.1: Wrist positions from tracking tests of Participant 1 for FMI-RC without ZPHP filter.

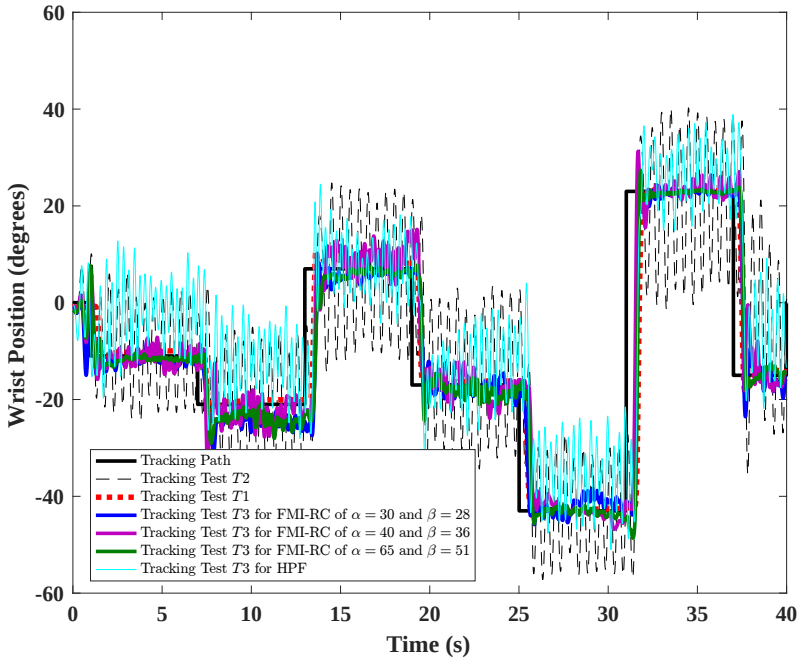

Figure E.2: Wrist positions from tracking tests of Participant 1 for FMI-RC with ZPHP filter.

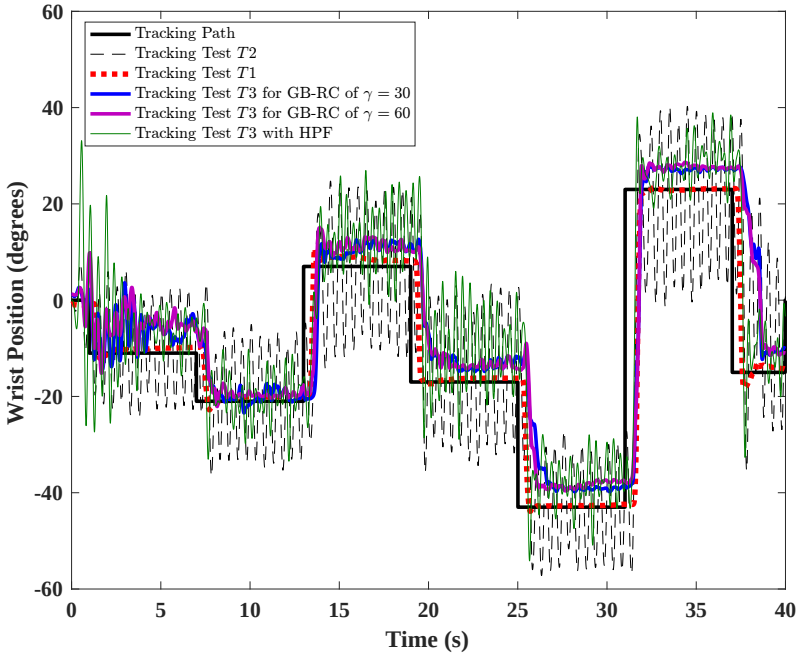

Figure E.3: Wrist positions from tracking tests of Participant 1 for GB-RC without ZPHP filter.

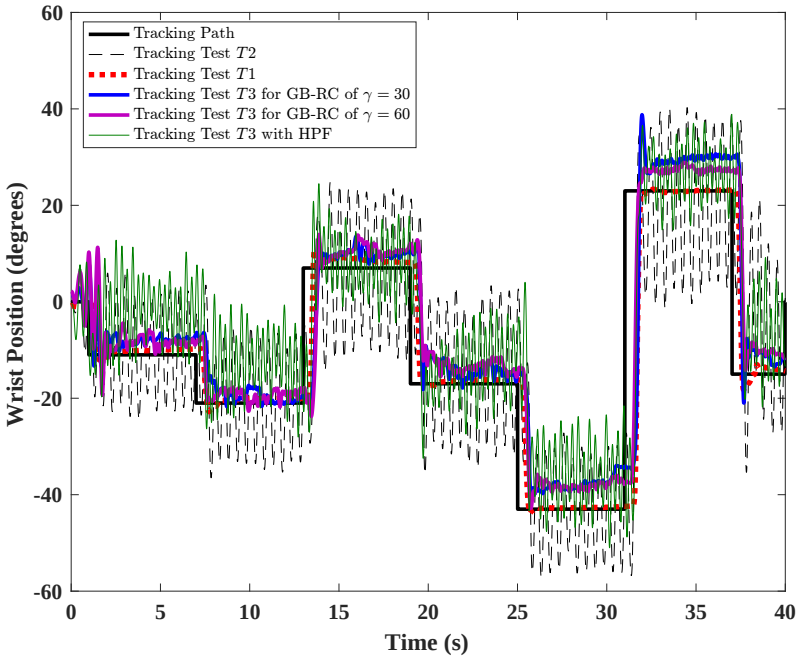

Figure E.4: Wrist positions from tracking tests of Participant 1 for GB-RC with ZPHP filter.

E.2 Participant 2

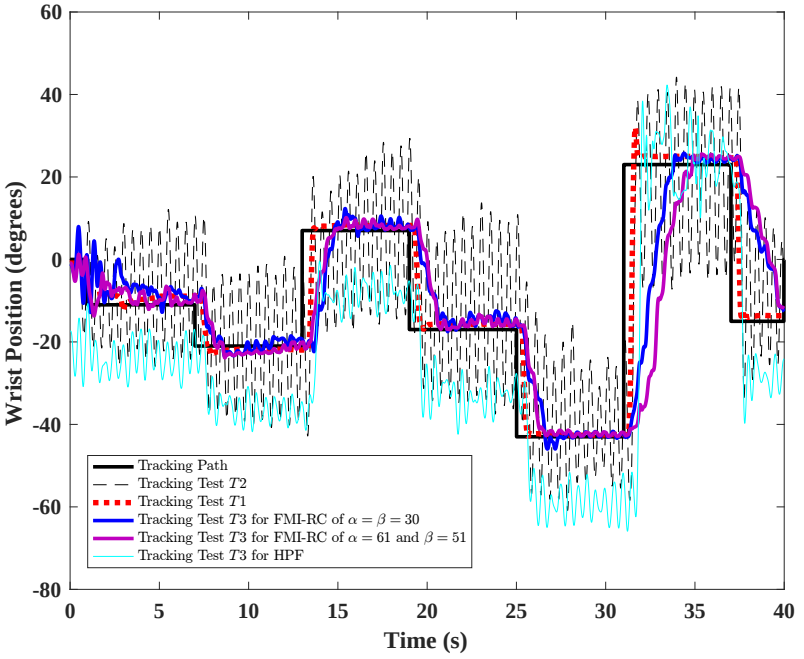

Figure E.5: Wrist positions from tracking tests of Participant 2 for FMI-RC without ZPHP filter.

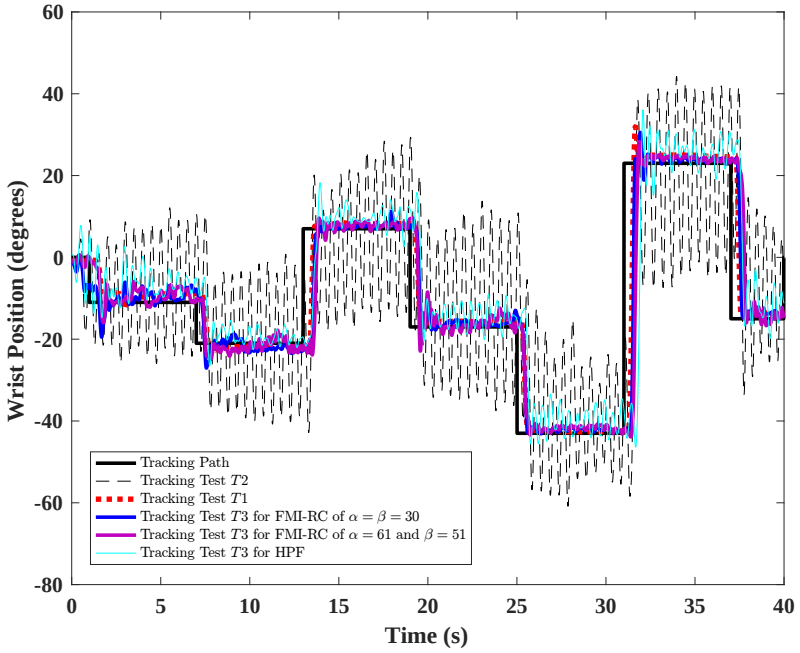

Figure E.6: Wrist positions from tracking tests of Participant 2 for FMI-RC with ZPHP filter.

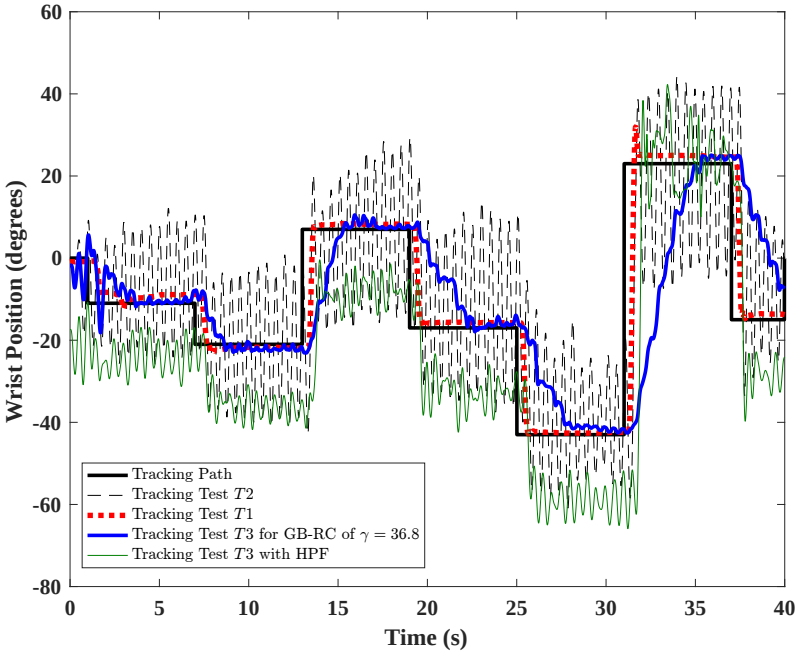

Figure E.7: Wrist positions from tracking tests of Participant 2 for GB-RC without ZPHP filter.

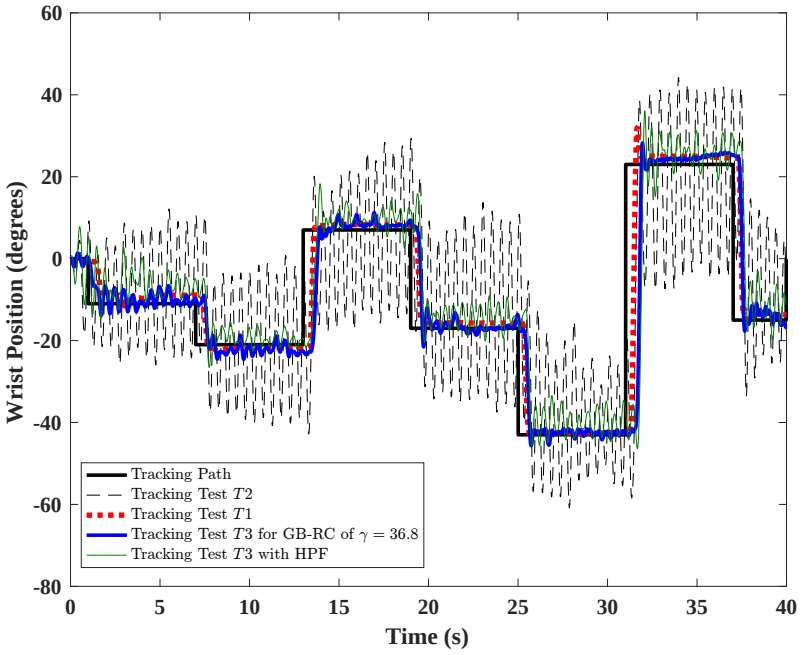

Figure E.8: Wrist positions from tracking tests of Participant 2 for GB-RC with ZPHP filter.

E.3 Participant 3

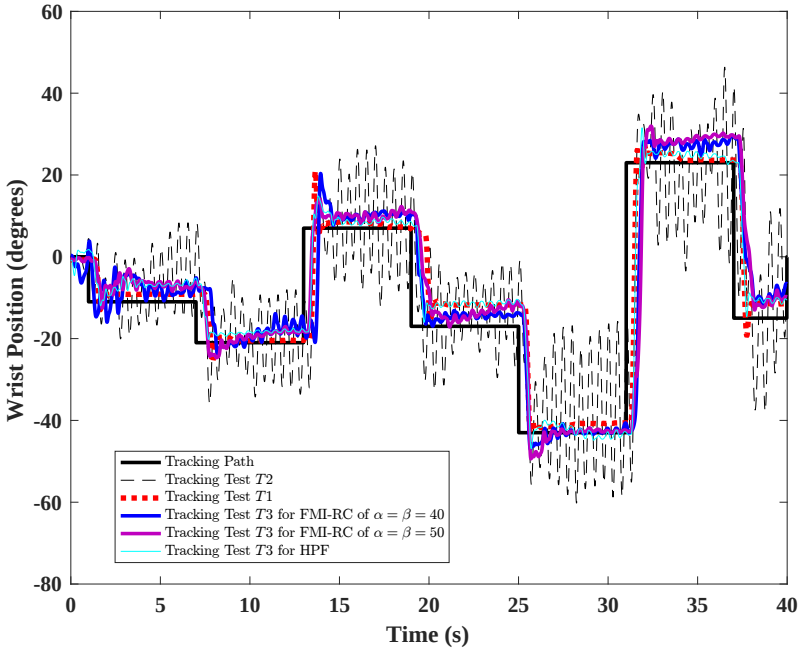

Figure E.9: Wrist positions from tracking tests of Participant 3 for FMI-RC without ZPHP filter.

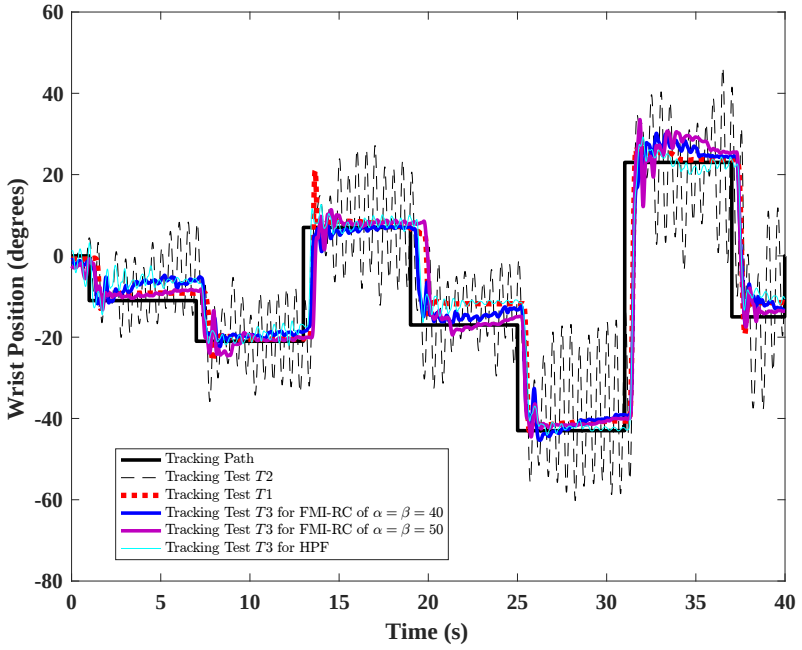

Figure E.10: Wrist positions from tracking tests of Participant 3 for FMI-RC with ZPHP filter.

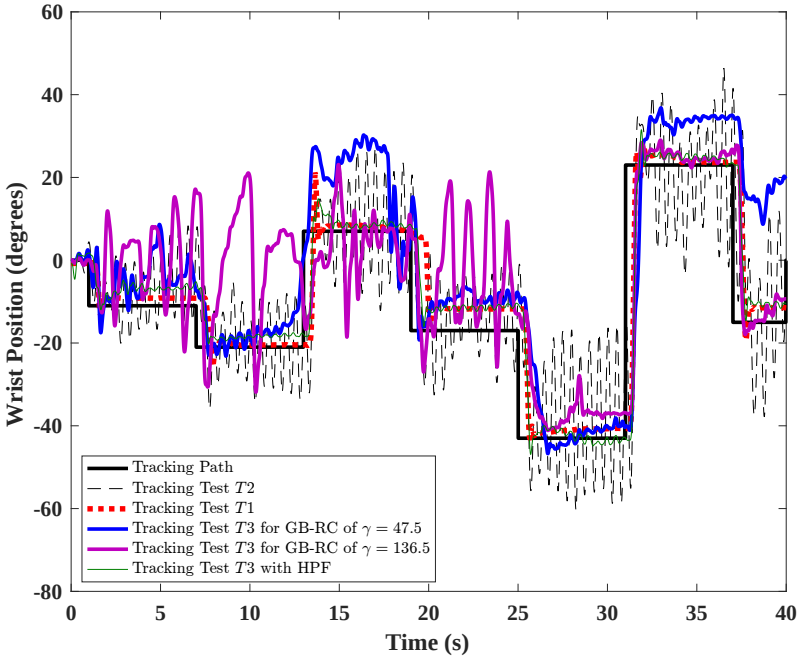

Figure E.11: Wrist positions from tracking tests of Participant 3 for GB-RC without ZPHP filter.

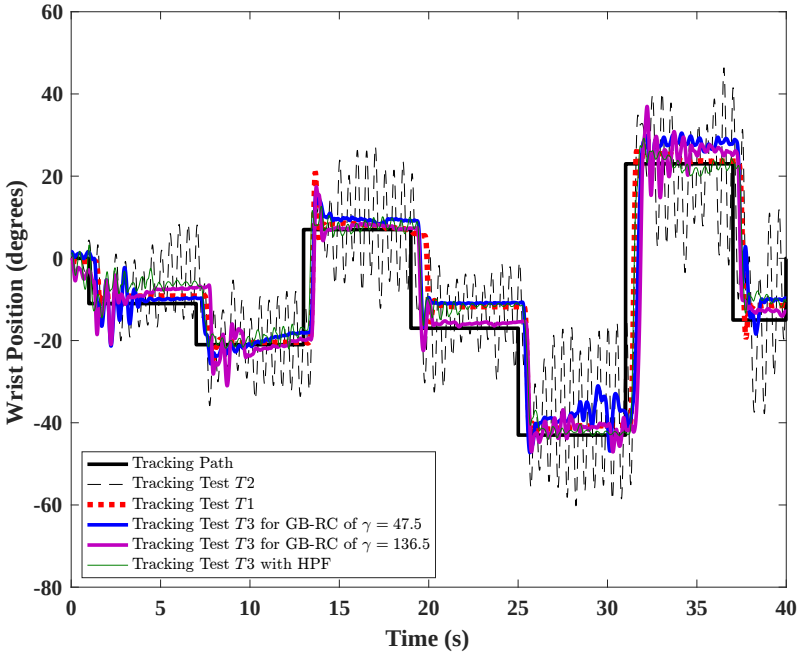

Figure E.12: Wrist positions from tracking tests of Participant 3 for GB-RC with ZPHP filter.

E.4 Participant 4

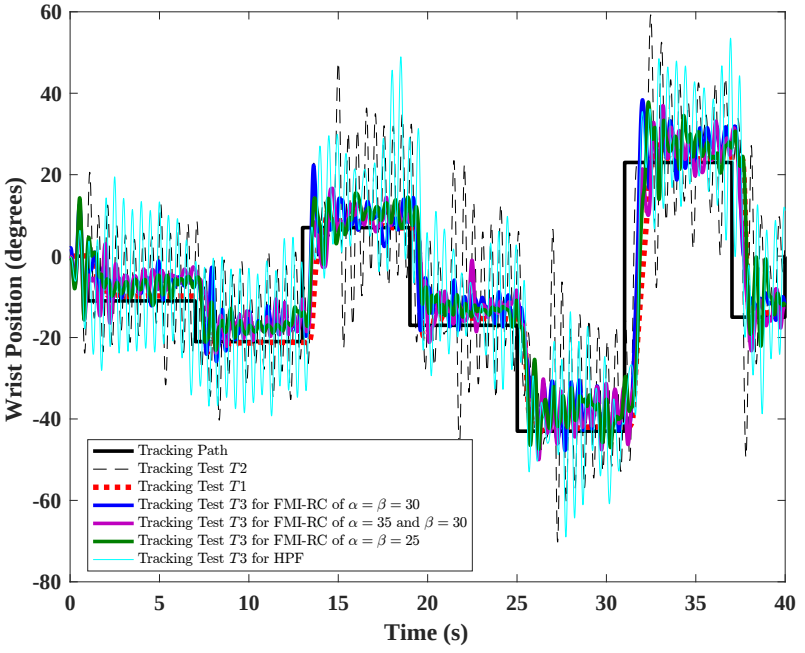

Figure E.13: Wrist positions from tracking tests of Participant 4 for FMI-RC without ZPHP filter.

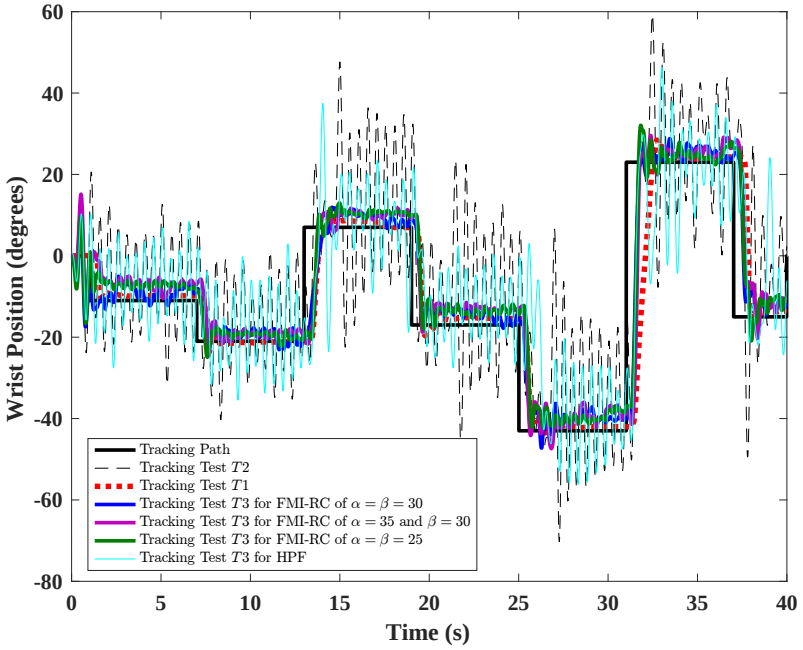

Figure E.14: Wrist positions from tracking tests of Participant 4 for FMI-RC with ZPHP filter.

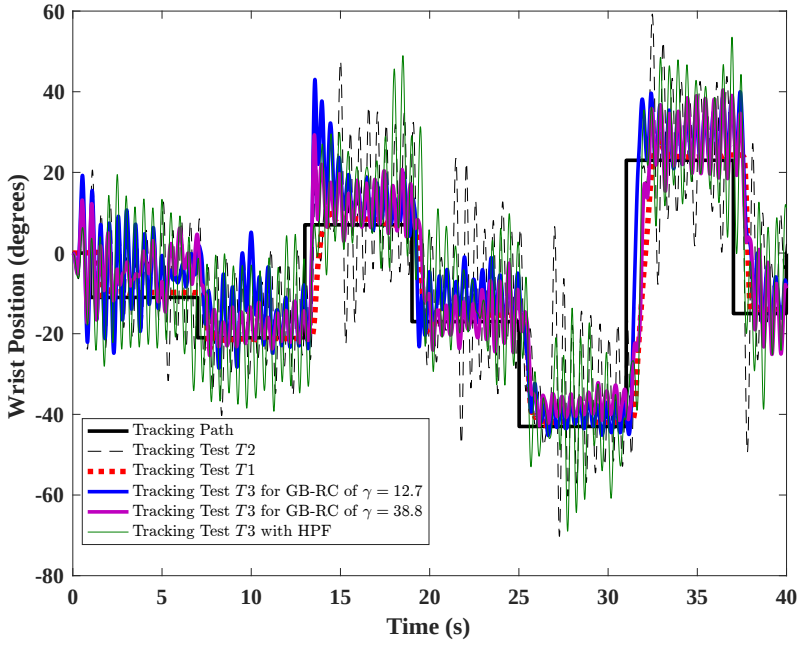

Figure E.15: Wrist positions from tracking tests of Participant 4 for GB-RC without ZPHP filter.

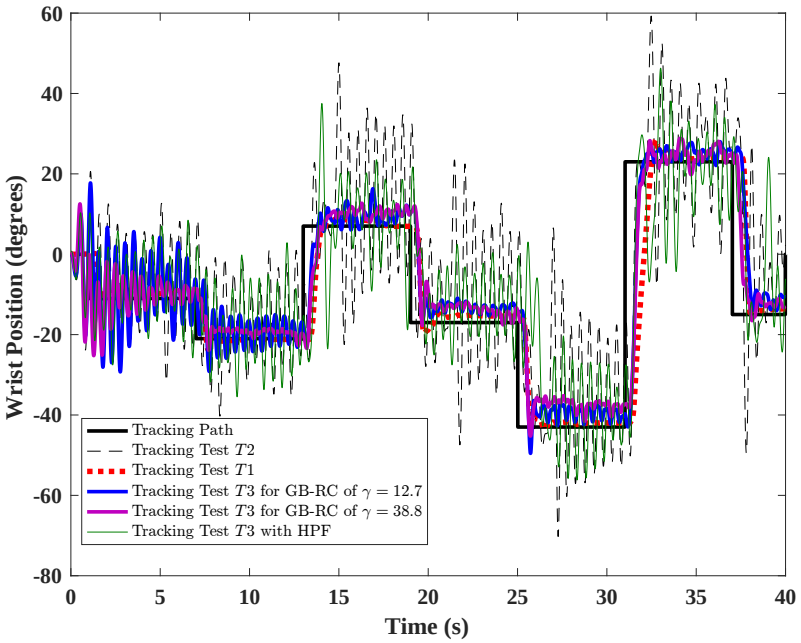

Figure E.16: Wrist positions from tracking tests of Participant 4 for GB-RC with ZPHP filter.

Bibliography

Adelstein, B. D. (1981). *Peripheral mechanical loading and the mechanism of abnormal intention tremor*. Phd thesis, Massachusetts Institute of Technology, USA.

Alusi, S. H., Worthington, J., Glickman, S., and Bain, P. G. (2001). A study of tremor in multiple sclerosis. *Brain*, 124:720–730.

Archer, D. (2014). Transcranial magnetic stimulation (TMS) treats depression. `https://www.psychologytoday.com/blog/reading-between-the-headlines/201401/transcranial-magnetic-stimulation-tms-treats-depression`.

Armutlu, K., Karabudak, R., and Nurlu, G. (2001). Physiotherapy approaches in the treatment of ataxic multiple sclerosis: a pilot study. *Neurorehabilitation and Neural Repair*, 15(3):203–211.

Bai, E.-W., Cai, Z., Dudley-Javoroskv, S., and Shields, R. K. (2009). Identification of a modified Wiener-Hammerstein system and its application in electrically stimulated paralyzed skeletal muscle modeling. *Automatica*, 45:736–743.

Bain, P. G. (2002). The management of tremor. *Journal of Neurology, Neurosurgery & Psychiatry*, 72(suppl 1):i3–i9.

Bo, A. P. L., Azevedo-Coste, C., Poignet, P., Geny, C., and Fattal, C. (2011a). On the use of FES to attenuate tremor by modulating joint impedance. In *50th IEEE Conference on Decision and Control and European Control Conference*, pages 6498–6503.

Bo, A. P. L. and Poignet, P. (2010). Tremor attenuation using FES-based joint stiffness control. In *2010 IEEE International Conference on Robotics and Automation (ICRA)*, pages 2928–2933.

Bo, A. P. L., Poignet, P., and Geny, C. (2011b). Pathological tremor and voluntary motion modeling and online estimation for active compensation. *Transactions on Neural Systems and Rehabilitation Engineering*, 19(2):177–185.

Bobet, J., Gossen, E., and Stein, R. (2005). A comparison of models of force production during stimulated isometric ankle dorsiflexion in humans. *IEEE Transactions on Neural Systems and Rehabilitation Engineering*, 13(4):444–451.

Bobet, J. and Stein, R. (1998). A simple model of force generation by skeletal muscle during dynamic isometric contractions. *IEEE Transactions on Biomedical Engineering*, 45(8):1010–1016.

Boutayeb, M. and Darouach, M. (1995). Recursive identification method for MISO Wiener-Hammerstein model. *IEEE Transactions on Automatic Control*, 40(2):287–291.

Chalah, M. A., Lefaucheur, J.-P., and Ayache, S. S. (2015). Non-invasive central and peripheral stimulation: New hope for essential tremor? *Frontiers in Neuroscience*, 9:440.

Colacino, F. M., Rustighi, E., and Mace, B. R. (2012). Subject-specific musculoskeletal parameters of wrist flexors and extensors estimated by an EMG-driven musculoskeletal model. *Medical Engineering and Physics*, 34(5):531–40.

Cooper, I. S. (1960). Neurosurgical relief of intention tremor due to cerebellar disease and multiple sclerosis. *Archives of Physical Medicine and Rehabilitation*, 41:1–4.

Copur, E. H., Freeman, C.T.and Chu, B., and Laila, D. (2014). Repetitive control based tremor suppression using electrical stimulation. In *UKACC 10th International Conference on Control*, pages 585–590.

Copur, E. H., Freeman, C., Chu, B., and Laila, D. S. (2015). FES based tremor suppression using repetitive control. In *54th IEEE Conference on Decision and Control*, pages 6023–6028.

Copur, E. H., Freeman, C. T., Chu, B., and Laila, D. S. (2016a). Repetitive control of electrical stimulation for tremor suppression. Submitted to IEEE Transactions on Control Systems Technology.

Copur, E. H., Freeman, C. T., Chu, B., and Laila, D. S. (2016b). System identification for FES-based tremor suppression. *European Journal of Control*, 27:45–59.

Curtin, M. and Lowery, M. M. (2014). Musculoskeletal modelling of muscle activation and applied external forces for the correction of scoliosis. *Journal of Neuroengineering and Rehabilitation*, 11(1):52.

Deuschl, G., Bain, P., Brin, M., and an Ad Hoc Scientific Committee (1998). Consensus statement of the movement disorder society on tremor. *Movement Disorders*, 13(3):2–23.

Deuschl, G., Herzog, J., and Fasano, A. (2009). Selecting appropriate tremor patients for DBS. In Bain, P., Aziz, T., Liu, X., and Nandi, D., editors, *Deep Brain Stimulation*, chapter 16, pages 139–156. Oxford University Press.

Dewey, C. W. (2013). *A Practical Guide to Canine and Feline Neurology*. Wiley.

Ding, J., Wexler, A. S., and Binder-Macleod, S. A. (2002). A mathematical model that predicts the force-frequency relationship of human skeletal muscle. *Muscle & Nerve*, 26(4):477–485.

Durfee, W. K. and Maclean, K. E. (1989). Methods for estimating isometric recruitment curves of electrically stimulated muscle. *IEEE Transactions on Biomedical Engineering*, 36(7):654–666.

Elble, R. J. (2009). Tremor: clinical features, pathophysiology, and treatment. *Neurologic Clinics*, 3:177–185.

Elble, R. J. and Koller, W. C. (1990). *Tremor*. The John Hopkins University Press.

Feys, P., D'hooghe, M. B., Nagels, G., and Helsen, W. F. (2009). The effect of levetiracetam on tremor severity and functionality in patients with multiple sclerosis. *Multiple Sclerosis Journal*, 15(3):371–378.

Feys, P., Helsen, W., Liu, X., Mooren, D., Albrecht, H., Nuttin, B., and Ketelaer, P. (2005). Effects of peripheral cooling on intention tremor in multiple sclerosis. *Journal of Neurology, Neurosurgery and Psychiatry*, 76(3):373–379.

Feys, P., Helsen, W. F., Verschueren, S., Swinnen, S. P., Klok, I., Lavrysen, A., Nuttin, B., Ketelaer, P., and Liu, X. (2006). Online movement control in multiple sclerosis patients with tremor: effects of tendon vibration. *Movement Disorders*, 21(8):1148–1153.

Francis, B. A. and Wonham, W. M. (1975). The internal model principle for linear multivariable regulators. *Applied Mathematics and Optimization*, 2(2):170–194.

Freeman, C. T. and French, M. (2015). Estimation based multiple model iterative learning control. In *54th IEEE Conference on Decision and Control*, pages 6070–6075.

Freeman, C. T., Hughes, A.-M., Burridge, J. H., Chappell, P. H., Lewin, P. L., and Rogers, E. (2009). A model of the upper extremity using FES for stroke rehabilitation. *Journal of Biomechanical Engineering*, 131(3):031011–12pp.

Freriks, B., Hermens, H. J., Disselhorst-Klug, C., and Rau, G. (1999). *SENIAM 8: European Recommendations for Surface ElectroMyoGraphy*, chapter 2: The Recommendations for Sensors and Sensor Placement Procedures for Surface ElectroMyoGraphy. Roessingh Research and Development.

Frey Law, L. A. and Shields, R. K. (2007). Mathematical models of human paralyzed muscle after long-term training. *Journal of Biomechanics*, 40(12):2587–2595.

Gallego, J. Á., Rocon, E., Belda-Lois, J. M., and Pons, J. L. (2013). A neuroprosthesis for tremor management through the control of muscle co-contraction. *Journal of NeuroEngineering and Rehabilitation*, 10(1):1–13.

Gillard, D. M., Cameron, T., Prochazka, A., and Gauthier, M. J. A. (1999). Tremor suppression using functional electrical stimulation: a comparison between digital and analog controllers. *IEEE Transactions on Rehabilitation Engineering*, 7(3):385–388.

Grimaldi, G. and Manto, M.-U. (2008). *Tremor: From Pathogenesis To Treatment.* Morgan & Claypool, San Rafael, California.

Hallett, M., Lindsey, J. W., Adelstein, B. D., and Riley, P. O. (1985). Controlled trial of isoniazid therapy for severe postural cerebellar tremor in multiple sclerosis. *Neurology*, 35(9):1374–1377.

Hara, S., Omata, T., and Nakano, M. (1985). Synthesis of repetitive control systems and its application. In *Proceedings of 24th conference on Decision and Control*, pages 1387–1392.

Hassan, A., Ahlskog, J. E., Rodriguez, M., and Matsumoto, J. Y. (2012). Surgical therapy for multiple sclerosis tremor: a 12-year follow-up study. *European Journal of Neurology*, 19(5):764–768.

Hatonen, J., Freeman, C., Owens, D. H., Lewin, P., and Rogers, E. (2004). Robustness analysis of a gradient-based repetitive algorithm for discrete-time systems. In *Decision and Control, 2004. CDC. 43rd IEEE Conference on*, volume 2, pages 1301–1306.

Hatonen, J. J., Freeman, C. T., Owens, D. H., Lewin, P. L., and Rogers, E. (2006a). A gradient-based repetitive control algorithm combining ILC and pole placement. *European Journal of Control*, 12(3):278–292.

Hatonen, J. J., Freeman, C. T., Owens, D. H., Lewin, P. L., and Rogers, E. (2006b). A gradient-based repetitive control algorithm combining ILC and pole placement. *European Journal of Control*, 12(3):278–292.

Hawes, F., Billups, C., and Forwell, S. (2010). Interventions for upper-limb intention tremor in multiple sclerosis. *International Journal of MS Care*, 12(3):122–132.

Heenan, M., Scheidt, R. A., Woo, D., and Beardsley, S. A. (2014). Intention tremor and deficits of sensory feedback control in multiple sclerosis: a pilot study. *Journal of NeuroEngineering and Rehabilitation*, 11(1):1–19.

Hogan, N. (1984). Adaptive control of mechanical impedance by coactivation of antagonist muscles. *IEEE Transactions on Automatic Control*, 29(8):681–690.

Houtzager, I., van Wingerden, J.-W., and Verhaegen, M. (2013). Rejection of periodic wind disturbances on a smart rotor test section using lifted repetitive control. *IEEE Transactions on Control Systems Technology*, 21(2):347–359.

Hunt, K. J., Munih, M., Donaldson, N. d., and Barr, F. M. D. (1998). Investigation of the hammerstein hypothesis in the modeling of electrically stimulated muscle. *IEEE Transactions on Biomedical Engineering*, 45(8):998–1009.

Iaquinto, J. M. and Wayne, J. S. (2010). Computational model of the lower leg and foot/ankle complex: application to arch stability. *Journal of Biomechanical Engineering*, 132(2):021009.

Inoue, T., Nakano, M., and Iwai, S. (1981a). High accuracy control of a proton synchrotron magnet power supply. In *Proceedings of 8th IFAC World Congress (Part 2)*, pages 3137–3142.

Inoue, T., Nakano, M., and Iwai, S. (1981b). High accuracy control of servomechanism for repeated contouring. In *Proceedings of 10th Annual Symposium Incremental Motion Control Systems and Devices*, pages 285–292.

Jones, L., Lewis, Y., Harrison, J., and Wiles, C. M. (1996). The effectiveness of occupational therapy and physiotherapy in multiple sclerosis patients with ataxia of the upper limb and trunk. *Clinical Rehabilitation*, 10(4):277–282.

Kalyanam, K. and Tsao, T.-C. (2012). Two-period repetitive and adaptive control for repeatable and nonrepeatable runout compensation in disk drive track following. *IEEE/ASME Transactions on Mechatronics*, 17(4):756–765.

Koch, M., Mostert, J., Heersema, D., and De Keyser, J. (2007). Tremor in multiple sclerosis. *Journal of Neurology*, 254(2):133–145.

Kortmann, M. and Unbehauen, H. (1987). Identification method for nonlinear MISO systems. In *IFAC 10th Triennial World Congress*, pages 233–238, Munich, Germany.

Kringelbach, M. L., Jenkinson, N., Owen, S. L. F., and Aziz, T. Z. (2007). Translational principles of deep brain stimulation. *Nature Reviews Neuroscience*, 8(8):623–625.

Le, F., Markovsky, I., Freeman, C. T., and Rogers, E. (2010). Identification of electrically stimulated muscle models of stroke patients. *Control Engineering Practice*, 18(4):396–407.

Le, F., Markovsky, I., Freeman, C. T., and Rogers, E. (2012). Recursive identification of hammerstein systems with application to electrically stimulated muscle. *Control Engineering Practice*, 20(4):386 – 396.

Lenz, F. A., Jaeger, C. J., Seike, M. S., Lin, Y. C., and Reich, S. G. (2002). Single-neuron analysis of human thalamus in patients with intention tremor and other clinical signs of cerebellar disease. *Journal of Neurophysiology*, 87(4):2084–2094.

Liberson, W. T., Holmquest, H. J., Scot, D., and Dow, M. (1961). Functional electrotherapy: stimulation of the peroneal nerve synchronized with the swing phase of the gait of hemiplegic patients. *Archives of Physical Medicine and Rehabilitation*, 42:101–105.

Liu, Z., Wu, Q., Zhang, Y., Wang, Y., and Chen, C. L. P. (2011). Adaptive fuzzy wavelet neural network filter for hand tremor canceling in microsurgery. *Applied Soft Computing*, 11(8):5315–5329.

Ljung, L. (1999). *Systen Identification Theory for the User*, chapter 3: Simulation and Prediction, pages 66–69. Prentice-Hall, second edition.

Long, C. I. and Masciarelli, V. D. (1963). An electrophysiologic splint for the hand. *Archives of Physical Medicine and Rehabilitation*, 44:499–503.

Longman, R. W. (2000). Iterative learning control and repetitive control for engineering practice. *International Journal of Control*, 73(10):930–954.

Longman, R. W. (2010). On the theory and design of linear repetitve control systems. *European Journal of Control*, 16(5):447–496.

Lynch, C. L. and Popovic, M. R. (2008). Functional electrical stimulation. *IEEE Control System Magazine*, 28(2):40–50.

Lyons, G. M., Leane, G. E., Clarke-Moloney, M., O'Brien, J. V., and Grace, P. A. (2004). An investigation of the effect of electrode size and electrode location on comfort during stimulation of the gastrocnemius muscle. *Medical Engineering and Physics*, 26(10):873 – 878.

Mann, K. A., Werner, F. W., and Palmer, A. K. (1989). Frequency spectrum analysis of wrist motion for activities of daily living. *Journal of Orthopedic Research*, 7(5):304–306.

Manto, M., Rocon, E., Pons, J., Belda, J. M., and Camut, S. (2007). Evaluation of a wearable orthosis and an associated algorithm for tremor suppression. *Physiological Measurement*, 28(4):415–425.

Matsumoto, J., Morrow, D., Kaufman, K., Davis, D., Ahlskog, J. E., Walker, A., Sneve, D., Noseworthy, J., and Rodriguez, M. (2001). Surgical therapy for tremor in multiple sclerosis: an evaluation of outcome measures. *Neurology*, 57(10):1876–1882.

McGruder, J., Cors, D., Tiernan, A. M., and Tomlin, G. (2003). Weighted wrist cuffs for tremor reduction during eating in adults with static brain lesions. *American Journal of Occupational Therapy*, 57(5):507–516.

Mckelvey, C. (2014). Deep brain stimulation helpful in some patients with MS tremor. `http://www.msdiscovery.org/news/news_synthesis/13214-deep-brain-stimulation-helpful-some-patients-ms-tremor`.

Mehanna, R. and Jankovic, J. (2013). Movement disorders in multiple sclerosis and other demyelinating diseases. *Journal of the Neurological Sciences*, 328(1-2):1 – 8.

Mellano, S., Palmerini, L., Cappello, A., and Chiari, L. (2011). Hilbert-huang-based tremor removal to assess postural properties from accelerometers. *Transactions on Boimedical Engineering*, 58(6):1752–1761.

MSIF (2013). Atlas of MS 2013. Technical report, Multiple Sclerosis International Federation.

Naderi, F., Javadi, S. A., Motamedi, M., and Sahraian, M. A. (2012). The efficacy of primidone in reducing severe cerebellar tremors in patients with multiple sclerosis. *Clinical Neuropharmacology*, 35(5):224–226.

Nakahara, J., Maeda, M., Aiso, S., and Suzuki, N. (2012). Current concepts in multiple sclerosis: Autoimmunity versus oligodendrogliopathy. *Clinical Reviews in Allergy and Immunology*, 42(1):26–34.

NCC-CC (2003). Multiple sclerosis national clinical guideline for diagnosis and management in primary and secondary care. Technical report, The National Collaborating Centre for Chronic Conditions.

Nekoukar, V. and Erfanian, A. (2011). An adaptive fuzzy sliding-mode controller design for walking control with functional electrical stimulation: A computer simulation study. *International Journal of Control, Automation and Systems*, 9(6):1124–1135.

Nicholson, T. and Milne, R. (1999). Pallidotomy, thalamotomy and deep brain stimulation for severe parkinson's disease. Technical report, Wessex Institute for Health Research and Development.

O'Connor, R. and Kini, M. U. (2011). Non-pharmacological and non-surgical interventions for tremor: a systematic review. *Parkinsonism Related Disorders*, 17(7):509–515.

Oliveri, M., Torriero, S., Koch, G., Salerno, S., Petrosini, L., and Caltagirone, C. (2007). The role of transcranial magnetic stimulation in the study of cerebellar cognitive function. *The Cerebellum*, 6(1):95–101.

Panomruttanarug, B. and Longman, R. W. (2004). Repetitive controller design using optimization in the frequency domain. In *Proceedings of the 2004 AIAA/AAS Astrodynamics Specialist Conference*, pages 1215–1236.

Pledgie, S. and Barner, K. E. (2000). Tremor suppression through impedance control. *IEEE Transactions on Rehabilitation Engineering*, 8(1):53–59.

Popovic, D., Stein, R. B., Oguztoreli, M. N., Lebiedowska, M., and Jonic, S. (1999). Optimal control of walking with functional electrical stimulation: A computer simulation study. *IEEE Transactions on Rehabilitation Engineering*, 7(1):69–79.

Prochazka, A., Elek, J., and Javidan, M. (1992a). Attenuation of pathological tremors by functional electrical stimulation. I: Method. *Annals of Biomedical Engineering*, 20(2):205–224.

Prochazka, A., Elek, J., and Javidan, M. (1992b). Attenuation of pathological tremors by functional electrical stimulation. II: Clinical evaluation. *Annals of Biomedical Engineering*, 20(2):225–236.

Riener, R. and Fuhr, T. (1998). Patient-driven control of fes-supported standing up: a simulation study. *IEEE Transactions on Rehabilitation Engineering*, 6(2):113–124.

Riviere, C. N., Reich, S. G., and Thakor, N. V. (1997). Adaptive fourier modeling for quantification of tremor. *Journal of Neuroscience Methods*, 74(1):77–87.

Rocon, E., Belda-Lois, J. M., Ruiz, A., Manto, M., Moreno, J. C., and Pons, J. (2007). Design and validation of a rehabilitation robotic exoskeleton for tremor assessment and suppression. *IEEE Transactions on Neural Systems and Rehabilitation Engineering*, 15(3):367–378.

Rocon, E., Gallego, J. A., M., B.-L. J., Benito-Leon, J., and J., L. P. (2012). Biomechanical loading as an alternative treatment for tremor: a review of two approaches. *Tremor and Other Hyperkinetic Movements*, 2:1–13.

Rocon, E., Ruiz, A. F., Brunetti, F., Pons, J. L., Belda-Lois, J. M., and Sanchez-Lacuesta, J. J. (2006). On the use of an active wearable exoskeleton for tremor suppression via biomechanical loading. In *Proceedings of the 2006 IEEE International Conference on Robotics and Automation*, pages 3140–3145.

Rogasch, N. C. and Todd, G. (2013). rTMS over human motor cortex can modulate tremor during movement. *European Journal of Neuroscience*, 37(2):323–329.

Samra, K., Waltz, J. M., Riklan, M., Koslow, M., and Cooper, I. S. (1970). Relief of intention tremor by thalamic surgery. *Journal of Neurology, Neurosurgery and Psychiatry*, 33(1):7–15.

Schniepp, R., Jakl, V., Wuehr, M., Havla, J., KÃŒmpfel, T., Dieterich, M., Strupp, M., and Jahn, K. (2012). Treatment with 4-aminopyridine improves upper limb tremor of a patient with multiple sclerosis: a video case report. *Multiple Sclerosis Journal*, 19(4):506–508.

Schuurman, P. R., Bosch, D. A., Bossuyt, P. M. M., Bonsel, G. J., Van Someren, E. J. W., De Bie, R. M. A., Merkus, M. P., and Speelman, J. D. (2000). A comparison of continuos thalamic stimulation and thalamotomy for suppression of severe tremor. *The New England Journal of Medicine*, 342(7):461–468.

Sechi, G., Agnetti, V., Sulas, F. M. I., Sau, G., Corda, D., Pitzolu, M. G., and Rosati, G. (2003). Effects of topiramate in patients with cerebellar tremor. *Progress in Neuro-Psychopharmacology and Biological Psychiatry*, 27(6):1023–1027.

Sechi, G., Zuddas, M., Piredda, M., Agnetti, V., Sau, G., Piras, M. L., Tanca, S., and Rosati, G. (1989). Treatment of cerebellar tremors with carbamazepine: a controlled trial with long-term follow-up. *Neurology*, 39(8):1113–1115.

Sheean, G. (2002). The pathophysiology of spasticity. *European Journal of Neurology*, 9(Supplement s1):3–9.

Simmons, R. W. and Richardson, C. (1988). Peripheral regulation of stiffness during arm movements by coactivation of the antagonist muscles. *Brain Research*, 473(1):134–140.

Skogestad, S. and Postlethwaite, I. (1996). *Multivariable feedback control : analysis and design*. John Wiley, Chichester.

Songchon, T. and Longman, R. (2000). Iterative learning control and the waterbed effect. In *AIAA/AAS Astrodynamics Specialist Conference*, pages 444–453.

Steinbuch, M. (2002). Repetitive control for systems with uncertain period-time. *Automatica*, 38(12):2103–2109.

Steinbuch, M., Weiland, S., and Singh, T. (2007). Design of noise and period-time robust high-order repetitive control, with application to optical storage. *Automatica*, 43(12):2086 – 2095.

Stiles, R. N. and Hahs, D. W. (1991). Muscle-Load Oscillations: Detection, Analysis, and Models. In *Bioinstrumentation and Biosensors*, pages 75–120. CRC Press.

Åström, K. J. and Wittenmark, B. (1997). *Computer-Controlled Systems: Theory and Design*, chapter Pole-Placement Design: A State-Space Approach, page 132. Prentice Hall.

Takehara, S., Murakami, M., and Hase, K. (2012). Biomechanical evaluation of an electric power-assisted bicycle by a musculoskeletal model. *Journal of System Design and Dynamics*, 6(3):343–350.

Tasker, R. R. (1998). Deep brain stimulation is preferable to thalamotomy for tremor suppression. *Surgical Neurology*, 49(2):143–153.

Thompson, A. K., Doran, B., and Stein, R. B. (2006). Short-term effects of functional electrical stimulation on spinal excitatory and inhibitory reflexes in ankle extensor and flexor muscles. *Experimental Brain Research*, 170(2):216–226.

Tomizuka, M., Tsao, T.-C., and Chew, K.-K. (1989). Analysis and synthesis of discrete-time repetitive controllers. *Journal of Dynamic Systems, Measurement, and Control*, 111(3):353–358.

Topka, H., Mescheriakov, S., Boose, A., Kuntz, R., Hertrich, I., Seydel, L., Dichgans, J., and Rothwell, J. (1999). A cerebellar-like terminal and postural tremor induced in normal man by transcranial magnetic stimulation. *Brain*, 122(8):1551–1562.

Turk, R., Notley, S. V., Pickering, R. M., Simpson, D. M., Wright, P. A., and Burridge, J. H. (2008). Reliability and sensitivity of a wrist rig to measure motor control and spasticity in post-stroke hemiplegia. *Neurorehabilitation and Neural Repair*, 22(6):684–696.

Van den Eerenbeemt, J. F. (2003). High order repetitive control application to a cd-player system. Master thesis, Eindhoven University of Technology, Netherlands.

Verstappen, R. J. L. M., Freeman, C. T., Rogers, E., Sampson, T., and Burridge, J. H. (2012). Robust higher order repetitive control applied to human tremor suppression. In *IEEE Multi-Conference on Systems and Control*, pages 1214–1219.

Vodovnik, L., Long, C., Reswick, J. B., Lippay, A., and Starbuck, D. (1965). Myoelectric control of paralyzed muscles. *IEEE Transactions on Biomedical Engineering*, BME-12(3 and 4):169–172.

Wang, L., Chai, S., Rogers, E., and Freeman, C. T. (2012). Multivariable repetitive-predictive controllers using frequency decomposition. *IEEE Transactions on Control system*, 20(6):1597–1604.

Westwick, D. T. and Kearney, R. E. (2001). Separable least squares identification of nonlinear hammerstein models: Application to stretch reflex dynamics. *Annals of Biomedical Engineering*, 29(8):707–718.

Yap, L., Kouyialis, A., and Varma, T. R. K. (2007). Stereotactic neurosurgery for disabling tremor in multiple sclerosis: thalamotomy or deep brain stimulation?. *British Journal of Neurosurgery*, 21(4):349–354.

Zeuner, K. E. and Deuschl, G. (2012). An update on tremors. *Current Opinion in Neurology*, 25(4):475–482.

Zhang, D. and Ang, W. T. (2006). Tremor suppression of elbow joint via functional electrical stimulation: a simulation study. In *Proceeding of the 2006 IEEE International Conference on Automation Science and Engineering*, pages 182–187.

Zhang, D. and Ang, W. T. (2012). *Mechanisms and Emerging Therapies in Tremor Disorders*, chapter 5: Musculoskeletal Models of Tremor, pages 79–107. Springer Science & Business Media.

Zhang, D., Poignet, P., Bo, A., and Ang, W.-T. (2009). Exploring peripheral mechanism of tremor on neuromusculoskeletal model: A general simulation study. *IEEE Transactions on Biomedical Engineering*, 56(10):2359–2369.

Zhang, D., Poignet, P., Widjaja, F., and Ang, W. T. (2011). Neural oscillator based control for pathological tremor suppression via functional electrical stimulation. *Control Engineering Practice*, 19(1):74–88.